Ph.D. Dissertation

Probabilistic Assessment of Structural Condition through Clustering-based Multiple FE Model Update

클러스터링에 기반한 다중 유한요소모델 업데이트를 통한 확률론적 구조성능 평가

February 2015

Graduate School of Engineering
Seoul National University
Department of Civil and Environmental Engineering

Hyun-Joong Kim

클러스터링에 기반한 다중 유한요소모델 업데이트를 통한 확률론적 구조성능 평가

Probabilistic Assessment of Structural Condition through Clustering-based Multiple FE Model Update

指導敎授 高 鉉 武

이 論文을 工學博士 學位論文으로 提出함

2015년 2월

서울大學校 大學院

建設環境工學部

金 顯 中

金顯中의 工學博士 學位論文을 認准함

2015년 2월

위 원 장 金 鎬 卿 印

부위원장 高 鉉 武 印

위 원 李 海 成 印

위 원 宋 準 鎬 印

위 원 金 哲 永 印

Abstract

This study proposes a new procedure for probabilistic assessment of structural condition through updating multiple FE models. Sets of measurement data are constructed in order to incorporate measurement uncertainties into the model updating process. Multiple updated FE models are obtained by performing optimization for each constructed set of measurement data. Each updated FE model is regarded as the most probable one that represents the state of the concerned structure for the given measurements. As a result, variability of possible structural conditions caused by the uncertainties in measurement data can be inferred from the statistical distribution of multiple FE models. In addition, machine learning techniques are employed for the purpose of probabilistic description and classification of the multiple updated FE models. The Principal Component Analysis (PCA) method is utilized to better understand the distribution feature of multiple FE models by transforming FE models onto principal subspace. The sensitivity of structural parameters to the uncertainty of data is also investigated by using the principal components. Moreover, overall variance characteristics can be described more efficiently using a subset of the principal components. The transformed models are further classified based on their similarity by using the *K*-means method. The probabilistic features of the FE models are then identified by fitting a Gaussian mixture model to the distribution. Finally, the statistical features of structural condition are obtained by using the identified classes of the updated FE models. The proposed procedure is demonstrated by the numerical example of the Yeondae Bridge, a 4-span continuous steel-box girder bridge in South Korea. The distribution of the rating factors is evaluated using the updated FE models. The probability of the bridge failure is also estimated by structural reliability analysis utilizing the identified Gaussian mixture models. The results show that the clustering-based model selection procedure can reduce the possibility of inaccurate condition assessment caused by a high level of measurement error, thus can provide more consistent rating factor and reliability index.

Keywords : Condition assessment, Model update, Measurement uncertainty, Clustering, Structural Reliability analysis
Student Number : 2009-30227

Table of Contents

List of Figures

List of Tables

Chapter 1. Introduction

This chapter provides research background, literature reviews on the FE model update incorporating measurement uncertainties. Research objective and scope of the proposed procedure for probabilistic assessment of structural condition are presented.

1.1 Research Background

The purpose of structural condition assessment is to diagnose its current state, predict upcoming performance degradation, and ultimately prevent gradual or sudden failure. Recent advances in structural health monitoring technology enable us to collect large amounts of measurement data of behavior of real life, full-scale structures. For example, Seohae Bridge, a cable-stayed bridge with 470m main span located in South Korea, has operated a total of 183 sensors, which are accelerometers, displacement transducers, and strain gauges, to provide valuable long-term information of the bridge since it was opened for traffic in the year 2000 (Koh *et al.,* 2009). Actually, many application examples have been reported all over the world thanks to the recent rapid development of sensor, communication, and related data processing technologies (Farrar and Worden, 2007). This plenty of data seems to give opportunities to identify the actual properties of what we built rather than the expected responses.

However, extracting valuable information from the long-term monitored data is a very challenging task. One of the prevailing usages of the measurement data is updating Finite Element (FE) models for the structure being monitored (Mottershead and Frisswell, 1995). Finite element models are very powerful for design purpose since we could estimate virtually any response of the structure within the model fidelity. However, finite element model, which is used for design purpose, is usually difficult to represent exact structural behavior for the constructed structure because of various uncertainties and limitation of information. Thus, further adjustment of the FE model based on measurement data is essential. The corrected FE models, which are typically

updated from a baseline model, then can be used to diagnose health status of the structure or evaluate future structural performance to expected events (Doebling *et al*., 1998).

The discrepancies between the observed and the analyzed behaviors are accounted for by assumptions in the design process, deterioration of the structures, and variability of material properties, which are generally regarded as *epistemic uncertainties* related to a lack of knowledge (Moens and Vandepitte, 2005). Limited resolution of the FE model and numerical errors in discretization using finite number of elements also prevent realization of the actual behavior of the concerned structures, which can be classified as *aleatoric uncertainties*. Modeling uncertainty comprises the two types of uncertainties, which need to be reduced through FE model update for better understanding and predicting structural performance. Causes and impacts of both type of uncertainties on structural identification of civil structures were well introduced by Moon and Aktan (2006).

The procedure of FE model update using measurement data mostly involves solving an optimization problem to find the most appropriate structural parameters (Park *et al*., 2012). The conventional updating procedure usually regards the measurement data as trustworthy and takes them as deterministic values, thus a single FE model is updated. Actually, the FE model update is ill-posed inverse problem, thus uniqueness of solution is not assured. It has been demonstrated that a large number of possible models may exist for full-scale civil structures such as bridges (Raphael and Smith, 1998). Furthermore, measurement data may exhibit considerable variability due to noise, non-stationary behavior of structure, and the effect of adverse environmental conditions. Moon and Aktan (2006) presented several examples of past monitoring studies regarding sources of epistemic uncertainty in making measurements on constructed system. Many studies have reported about 5-20% variation in modal frequencies and mode-shapes of typical bridges due to interactions with operating environment (Farrar *et al*., 1994; Cornwell *et al*., 1999; Lenett, 1998; Roberts and Pearson, 1998; Rohrmann *et al*., 2000; Fu and DeWolf, 2001; Peeters *et al*., 2001). Main source of the variation in modal property has been indicated as fluctuation of

temperature and moisture content. The effect of the temperature fluctuation is known as the most influencing among others to the variation of structural characteristics for highway bridges. In addition, varying operational conditions of structure also affect the variation of modal properties. Figueiredo *et al*. (2010) noted varying live loads, speed of operation, and changing excitation sources conditions as non-stationary sources of measured response variability.

1.2 Literature Survey

Because of the significance of the uncertainty in measurement data, necessity to incorporate uncertainties in both a numerical model and measurement data when performing model update has been proposed (Robert-Nicoud *et al.,* 2000; Schuëller *et al*., 2008). In this sense, the concept of a non-deterministic FE model update has been adopted to overcome limitation of the single updated model under the existence of data uncertainties. Moens and Vandepitte (2005) classified the approaches of uncertainty treatment in FE analysis into two categories; non-probabilistic and probabilistic approaches.

In general, probabilistic approaches deal with uncertainty in measurement data and FE model by implementing Probability Density Function (PDF). One relevant approach is employing a theory of Stochastic Finite Element Model (SFEM), in which probability model for the stochastic FE model is updated using an inverse Monte-Carlo procedure with multiple sets of experimental results (Mares *et al*., 2006; Govers and Link, 2009). Similarly, seasonal variation of bridge stiffness was described by using a PDF relating with the variation of modal properties (Soyoz and Feng, 2008). A non-parametric probabilistic method was also proposed to find an optimal stochastic FE model from a set of data (Soize *et al*., 2008). Another suitable approach is Bayesian model updating that utilizes measurement data as well as engineer's judgment to find a PDF for model variability. Posterior PDF for structural parameters are identified from a prior PDF using the sets of measurement data through the Bayes theorem, not by a conventional optimization process. In the Bayesian model updating, error of measurement data is usually represented by

employing the coefficient of the prediction error level in a likelihood function (Katafygiotis *et al*., 1998; Beck and Au, 2002; Park *et al*., 2010). Relatively simple methods based on random sampling from an assumed PDF values have also been proposed. Goulet *et al*. (2010) generated feasible FE models from the assumed prior PDF of a general FE model. The models were validated with respect to the discrepancy associated with measurement data, and the models for which errors are smaller than threshold are then included. The threshold indicates possible variability of FE models due to the effects of model uncertainty and data uncertainty. Similar approaches have also been utilized in papers written by a group of authors (Gokce *et al*., 2011; Catbas *et al*., 2012). In these papers, several parent FE models, each of which represents a different damage scenario, are found initially from a deterministic set of measurements. Offspring FE models are then generated from each parent FE model according to PDF assumed to represent the uncertainty of structural parameters. Some models with large errors over the threshold are rejected, and new ones are sampled again from the PDF.

Meanwhile, non-probabilistic approaches have drawn attention in terms of dealing with random quantities by using alternative methods. Erdogan *et al*. (2013) used the fuzzy number concept to take into account uncertainties in both a mathematical model and experimental data. As a result, multiple FE models were obtained and used to determine optimum sensor configuration. Steenackers and Guillaume (2006) attempted to represent the level of data uncertainty by weighting factors, by which various types of errors are combined into single objective function. The inverse of the standard deviation of measurement is taken to determine value of corresponding weighting factor.

Finding a number of local optimal solutions or Pareto solutions has also been proposed to incorporate data uncertainty into updating a FE model. Zarate and Caicedo (2008) proposed a methodology to find a family of possible solutions for the problem of model update. In the process, multiple local minimums are identified instead of the global minimum based on sequential optimization problems. As a result, physically different alternate solutions but with a similar

performance are identified for better representations of the physical properties of the structure in the presence of modeling and measurement uncertainty. A multi-objective optimization algorithm has also been used to deal with uncertainty in updating a FE model (Haralampidis *et al.,* 2005; Christodoulou *et al.,* 2008; Jung *et al.,* 2010). The authors recognized that multiple solutions have much better chance to capture the true solution in the presence of noise associated with data. Therefore, Pareto optimal solutions, which are equally good with respect to the considered component objectives, were identified and utilized for further analysis and assessments. In contrast, a methodology to find local optimal solution by a stochastic global search and random sampling, not based on optimization, was also presented in a series of papers (Robert-Nicoud *et al.*, 2005; Smith and Saitta, 2008; Saitta *et al*., 2008; Kripakaran and Smith, 2009).

Saitta *et al.* (2008) proposed system identification through multiple models using clustering technique. The authors used a technique that combines principal component analysis (PCA) and *K*-means clustering to group candidate models. The grouped models are utilized selectively for optimal sensor placement. Similar research was presented that overcome limitation of the *K*-means method to determine optimal number of clusters by calculating score functions (Smith and Saitta, 2008). Meanwhile, the *K*-means method assigns hard membership to models and cannot quantify plausibility that data points belong to specific cluster. As a result, all models are assigned to specific cluster deterministically even through their actual memberships are ambiguous. Furthermore, information about each cluster's characteristics provided by *K*-means is very limited in terms of cluster size, compactness and variance. However, statistical feature of model distribution density is not well represented. Considering the purpose of probabilistic bridge assessment, relative importance or plausibility of candidate FE models should be known.

Recognition of previous researches directed to just one FE model updated deterministically had obvious limitations. Therefore, a set of feasible models, or the statistical properties of structural parameters were estimated by incorporating measurement data uncertainty through various methodologies. However, the identified variability of structural parameters has not been

well reflected for the assessment of structural condition. In most cases, the multiple FE models are utilized simply for estimating feasible distribution or feasible range of responses and evaluation. If the probability model that account for the distribution of FE models can be obtained and is utilized with an appropriate probabilistic assessment procedure, structural condition can be evaluated effectively considering the effect of measurement data uncertainty. Meanwhile, the distribution of the updated models may be expected to be multimodal in nature due to identifiability issues (Mukhopadhyay *et al*., 2014). In such cases, a unimodal PDF may not be appropriate to describe variability of structural parameters that may be separated. In case that PDF for structural parameters is not associated, utilizing all updated models of which distribution is not unimodal includes extreme conditions and may render excessive variation in evaluated structural condition. On the contrary, selecting the appropriate subset of multiple FE models according to desired structural characteristics can achieve assessment that is more refined. Therefore, procedures of feature extraction, dimension reduction and clustering can be used to utilize updated models efficiently for the assessment.

1.3 Research Objective and Scope

This study proposes a new procedure for probabilistic assessment of structural condition through updating multiple FE models. Sets of measurement data are constructed in order to incorporate measurement uncertainties into the model updating process. Multiple updated FE models are obtained by performing optimization for each constructed set of measurement data. Each updated FE model is regarded as the most probable one that represents the state of the concerned structure for the given measurements. As a result, variability of possible structural conditions caused by the uncertainties in measurement data can be inferred from the statistical distribution of multiple FE models. In addition, machine learning techniques are employed for the purpose of probabilistic description and classification of the multiple updated FE models. The Principal Component Analysis (PCA) method is utilized to better understand the distribution feature of multiple FE

models by transforming FE models onto principal subspace. The sensitivity of structural parameters to the uncertainty of data is also investigated by using the principal components. Moreover, overall variance characteristics can be described more efficiently using a subset of the principal components. The transformed models are further classified based on their similarity by using the *K*-means method. The probabilistic features of the FE models are then identified by fitting a Gaussian mixture model to the distribution. Finally, the statistical features of structural condition are obtained by using the identified classes of the updated FE models.

The proposed procedure is demonstrated by the numerical example of the Yeondae Bridge, a 4-span continuous steel-box girder bridge in South Korea. The distribution of the rating factors is evaluated using the updated FE models. The probability of the bridge failure is also estimated by structural reliability analysis utilizing the identified Gaussian mixture models. The results show that the clustering-based model selection procedure can reduce the possibility of inaccurate condition assessment caused by a high level of measurement error, thus can provide more consistent rating factor and reliability index.

1.4 Overview of Dissertation

This dissertation consists of five chapters. The outline is summarized as follows:

Chapter 1 provides research background, literature reviews on related topics, research objective and scope, and the overview of this dissertation. Chapter 2 describes the basic algorithms for updating multiple FE models. Sets of feasible FE models are updated using Probability Density Function (PDF) for the uncertainty of measurement data is represented through successive optimization. Validity of optimization algorithm to update FE models is discussed with respect to numerical instability of inverse problem and necessity of regularization. An idealized numerical example is accompanied to help understanding. Chapter 3 introduces machine learning techniques for feature extraction, clustering and probabilistic representation of the multiple FE models. Using the obtained information, structural condition is expressed as

reliability index and distribution of performance index. The idealized numerical example is also taken to prove the importance and effectiveness of the procedure. Chapter 4 shows numerical application to Yeondae bridge, a steel box girder bridge in South Korea. Advantage of the clustering-based assessment is verified by varying degree of uncertainty of measurement data. Chapter 5 concludes this study with a suggestion for future studies.

Chapter 2. Updating Multiple Finite Element Models

This chapter describes a procedure of updating multiple FE models to incorporate uncertainty of measurement data. Comparing to conventional single FE model, the successive optimization technique can deal with the uncertainty of measurement data, then, it provides probabilistic information about the structural condition effectively. Validity of the updated FE models is discussed regarding numerical instability and necessity regularization with an idealized numerical example.

2.1 Representation of Measurement Data Uncertainty

In this procedure, multiple Finite Element (FE) models are identified through successive optimization to incorporate uncertainty of measurement data. As a first step, we need to describe numerically the uncertainty of measurement data. In this study, Probability Density Function (PDF) is employed to describe uncertainty of measurement data. The plenty of data collected by long-term monitoring or repetitive instrumentation can be used to identify the PDF for measured responses. Multivariate Gaussian PDF has been widely used to describe the uncertainty of measurement. Then, sets of measurement data are sampled from the obtained PDF, and utilized for the successive updating of FE models. In case N sets of measurement data with M variables are generated, M-by-N matrix of sampled data is constructed as Eq. (2.1).

$$\mathbf{D}^m = \begin{bmatrix} \mathbf{D}_1^m & \mathbf{D}_2^m & \cdots & \mathbf{D}_N^m \end{bmatrix} = \begin{bmatrix} d_{11}^m & d_{12}^m & \cdots & d_{1N}^m \\ d_{21}^m & \ddots & & \vdots \\ \vdots & & \ddots & \vdots \\ d_{M1}^m & \cdots & \cdots & d_{MN}^m \end{bmatrix} \tag{2.1}$$

where superscript m denotes measured response, M the total number of considered response types, and N the number of generated sets of data. The sets of sampled responses indicate variation of

structural behavior associated to the concerned uncertainty.

On the other hand, equipment of operational monitoring system have been restricted to small portion of total bridges such as long-span bridges, historical structures, and several deteriorated bridges that hold high socio-economic value. In other words, the long-term monitoring data is not always available, especially for the typical bridges in use. In that case, uncertainty of data can be represented by assuming proper probability model. In this study, uniform distribution is taken to generate sufficient sets of measurement data from a single set of data. The perturbed responses are obtained within maximum amplitude using the Eq. (2.2).

$$\hat{d}_{ik}^{m} = \left(d_i^{m}\right)\left(1 + \eta_{ik}\right) \tag{2.2}$$

where d_i^m represents the i-th type of measured response, $\hat{d}_{ik}^{m}$ the sampled response for k-th sets of data, and η_{ik} a random number of the i-th type of measured response for the k-th sets of data. The random number is generated independently for each component of measurement data from a uniform distribution between maximum perturbation amplitude, $P_{\max}$. In the present study, the maximum perturbation amplitude is taken as average error between analyzed response and unperturbed response as proposed by Yeo *et al*. (2000).

$$P_{i,\max} = \frac{1}{N_i}\sum_{n=1}^{N_i}\left(\frac{d_n^{a} - d_n^{m}}{d_n^{m}}\right)^2 \tag{2.3}$$

where d is the concerned responses such as displacement and natural frequency, subscript n represents the n-the measurement within the total N_i measurements, superscript a and m represent the analyzed and measured values, respectively. The sets of perturbed responses compose the matrix of measurement data $\mathbf{D}^m$. Figure 2.1 shows the example of measurements sampled from for both of uniform distribution and multivariate Gaussian PDF. Every dot represents the each of sampled measurements, and each axis indicates different type of responses such as natural frequency, displacement, and so on.

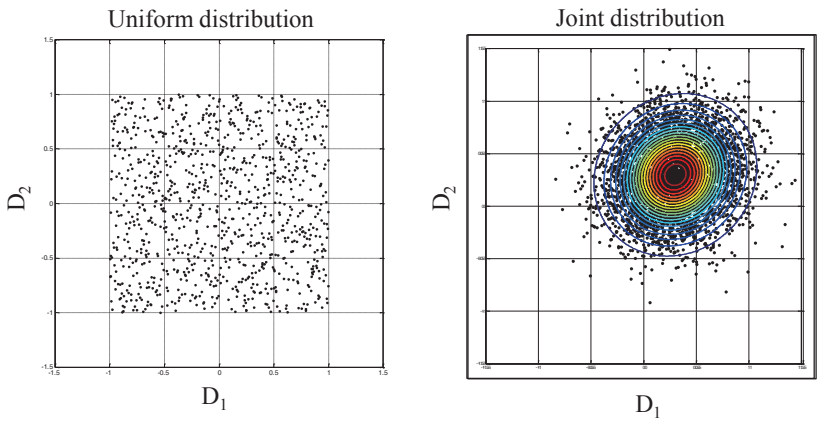

Figure 2.1 Schematic representation of measurement data uncertainty by two types of PDFs

2.2 Successive optimization to Update Multiple FE Models

A procedure for updating a FE model involves different types of measurement data, e.g. natural frequencies, mode-shapes, damping ratios, displacement, strain, and so on, in order to avoid obtaining under-fitted solutions. This represents the multi-objectivity nature of FE model update problems. However, the multi-objective optimization of more than three objectives would be computationally too expensive, and may converge to the wrong solution (Jung *et al*., 2010). The problem of convergence and the credibility of a solution may be worsened especially in case of the large-scale structure examples, because sufficient number of structural parameters and target responses should be considered. As an alternative, the problem of finding an optimal FE model satisfying various types of responses can be formulated as an aggregated single-objective function by assigning a weighting factor for each residual. Typically, a single FE model is updated from the objective function through optimization procedure. The single updated model can reflect specific structural condition, but is not suitable to represent probabilistic condition of the structure incorporating measurement uncertainty.

In this study, successive optimization is proposed to overcome the limitation of conventional

single model update to deal with the uncertainty of measurement data, and to estimate probabilistic information about the structural condition. Sets of optimization problems are formulated with the generated measurement data, each of which is expressed as Eq. (2.4), in order to find multiple FE models considering data uncertainty.

$$\min \ J_i(\boldsymbol{\theta}_i) = \mathbf{W}^T \mathbf{r}_i(\boldsymbol{\theta}_i) \ \text{ subjected to } \ \boldsymbol{\theta}_{lb} \le \boldsymbol{\theta}_i \le \boldsymbol{\theta}_{ub} \tag{2.4}$$

The objective function J_i, denoted by the index i, is a component in the sets of optimization problems corresponding to each column the measurement data matrix, $\mathbf{D}_i^m$. A column vector $\mathbf{W}$ is weighting vector, of which components imply weighting for different type of concerned response. The residual vector $\mathbf{r}_i$ is the discrepancy between the measurement data and the analysed value. The $\boldsymbol{\theta}_i$ for i-th updated FE model corresponds to rate of changes of P updated structural parameter values from the initial value with the entries $\boldsymbol{\theta}_i = [\theta_{1i}, \theta_{2i}, \ldots, \theta_{Pi}]^T$. The definition of $\boldsymbol{\theta}_i$ is to consider structural parameters of diverse dimensions and magnitudes effectively. The optimal value of $\boldsymbol{\theta}_i$ that can minimize the objective function is identified within a reasonable range defined by $\boldsymbol{\theta}_{lb}$ and $\boldsymbol{\theta}_{ub}$, a lower and upper bound vector, respectively.

In case N sets of measurement data are generated, N multiple FE models are finally updated by N successive optimization. The identified structural parameters compose a matrix $\boldsymbol{\Theta}_{\text{opt}}$ as Eq. (2.5). Each of the N columns represents a different updated FE model, and each of the p rows gives a change rate for a structural parameter. Accordingly, the distribution of structural parameters of multiple FE models is described by the matrix $\boldsymbol{\Theta}_{\text{opt}}$.

$$\boldsymbol{\Theta}_{\text{opt}} = [\boldsymbol{\theta}_1, \boldsymbol{\theta}_2, \ldots, \boldsymbol{\theta}_N] = \begin{bmatrix} \theta_{11} & \theta_{12} & \cdots & \theta_{1N} \\ \theta_{21} & \ddots & & \vdots \\ \vdots & & \ddots & \vdots \\ \theta_{p1} & \cdots & \cdots & \theta_{pN} \end{bmatrix} \tag{2.5}$$

Figure 2.2 shows schematically the procedure of multiple FE model update through successive optimization incorporating measurement uncertainty.

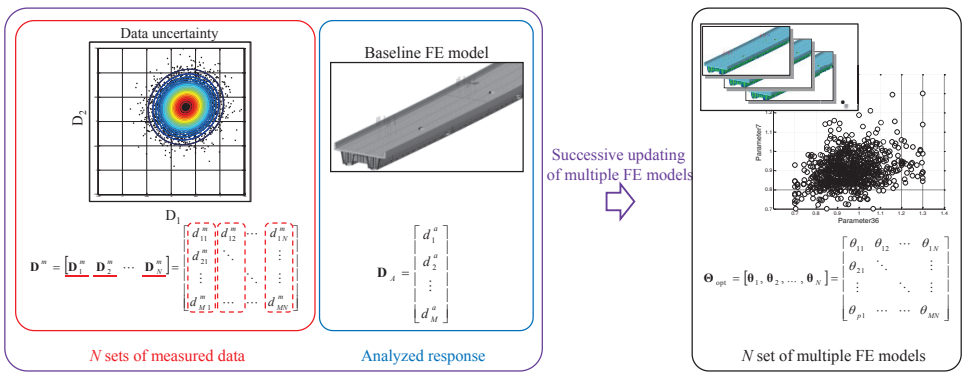

Figure 2.2 Multiple FE models updated by using sets of measurement data

2.3 Optimization Algorithm

The problem of updating FE models is expressed as constrained nonlinear multivariable optimization problem considering the objective function in Eq. (2.4) and the constraints. The optimization for FE model update generally encounters problems of numerical instability due to ill-posedness and rank-deficiency. Limitation of numerical model and irreducible uncertainty of measurement data account for the ill-posedness. In addition, rank-deficiency is aroused when the number of measurement is less than the number of optimization parameters. The rank-deficiency is easily occurred especially in updating of FE model of the civil structures, for which number of sensors are restricted generally.

One of the most successful remedies for the numerical instability is regularization of the objective function (Neuman and Yakowitz, 1979; Becks and Murio, 1984; Schnur and Zabaras 1990; Lee *et al*., 1999). The objective function in Eq. (2.4) is then modified as Eq. (2.6) by adding a regularization function.

$$\min\ J_i(\boldsymbol{\theta}_i) = \mathbf{W}^T \mathbf{r}_i(\boldsymbol{\theta}_i) + \beta \|\boldsymbol{\theta}_i\| \quad \text{subjected to} \quad \boldsymbol{\theta}_{lb} \le \boldsymbol{\theta}_i \le \boldsymbol{\theta}_{ub} \tag{2.6}$$

The first term in Eq. (6) denotes an error function to define discrepancy between analysed and measured behavior, and the latter term is a regularization function to reduce solution space reasonably. The regularization factor β determine the regularization effect in the optimization. If too small regularization factor is considered, the regularization effect is negligible and may fail to assure numerical stability. On the other hand, too large regularization factor results in a poorly optimized solution. In this study, Variable Regularization Factor Scheme (VRFS) method is implemented (Lee *et al*., 1999). In the VRFS, the regularization factor is modified at each step of iteration so that the error function is always equal to or larger than the regularization function, which is expressed as

$$\mathbf{W}^T \mathbf{r}_i\left(\boldsymbol{\theta}_i^k\right) \geq \beta^k \left\|\boldsymbol{\theta}_i^k\right\| \tag{2,7}$$

where the superscript k denotes the step of iteration for the optimization process. If the error function is smaller than regularization function at k-th step, the regularization factor β is modified by multiplying a reduction factor γ, ranging from 0 to 1.

The regularized objective function is solved by using the Sequential Quadratic Programming (SQP), which is a gradient-based optimization method. The SQP method approximates the objective function to a quadratic function as Eq. (2.8)

$$\min_{\mathbf{s}} \ \frac{1}{2}\mathbf{s}^T H_k \mathbf{s} + \nabla J\left(\boldsymbol{\theta}_k\right)^T \mathbf{s} \tag{2.8}$$

where $\mathbf{s}$ is a vector of search direction, and H_k is a Hessian matrix of Lagrangian function for k-th iteration. The H_k is a matrix of second-order partial derivatives of the objective function, and equated by

$$H_k = \nabla^2 L\left(\boldsymbol{\theta}, \boldsymbol{\lambda}\right) = \nabla^2 \left[J\left(\boldsymbol{\theta}\right) + \sum_{i=1}^{m} \lambda_i \cdot g_i\left(\boldsymbol{\theta}\right) \right] \tag{2.9}$$

where g_i denotes non-linear constraint, λ_i the Lagrangian multiplier for the i-th constraint. The

SQP method solves a sequence of optimization sub problems iteratively until convergence is obtained. The Gauss-Newton and relative algorithms calculate H_k through second order differentiation of Lagrangian function and rely inversion of matrix to update the Hessian matrix. The algorithms need quite a lot of regularizations in order to stabilize the ill-posed inverse problem character. Another prevailing method is quasi-Newton method for which the most popular algorithms are BFGS, DFP and Broyden methods and so on. The methods use first-order gradient for updating of the Hessian matrix, thus are much less sensitive to the ill-posed character and require the cost of a lower computational effort (Dubot *et al*., 2013). Consequently, regularization may be not compulsory, although its use may enhance regularity of the solutions. In this study, modified BFGS is adopted in order to pursue numerical stability in FE model update process. In the procedure, the H_k is taken initially as the identity matrix for numerical stability, and updated as:

$$H_{k+1} = H_k + \frac{\mathbf{q}_k \mathbf{q}_k^T}{\mathbf{q}_k^T \mathbf{s}_k} - \frac{H_k \mathbf{s}_k \mathbf{s}_k^T H_k^T}{\mathbf{s}_k^T H_k \mathbf{s}_k} \tag{2.10}$$

where $\mathbf{s}_k = \boldsymbol{\theta}_{k+1} - \boldsymbol{\theta}_k$ and $\mathbf{q}_k = \nabla_{\boldsymbol{\theta}} L(\boldsymbol{\theta}_{k+1}, \boldsymbol{\lambda}_k) - \nabla_{\boldsymbol{\theta}} L(\boldsymbol{\theta}_k, \boldsymbol{\lambda}_k)$. The quasi-Newton approximated Hessian matrix may differ from the exact one. In addition, the Hessian matrix is maintained as positive-definite by modifying $\mathbf{q}_k^T \mathbf{s}_k$ positive at each iteration in order to enhance stability of optimal solution. The modification can be understood as finding more stable step-size and search direction. The numerical instability issue of FE model update problem can be handled by using the regularization technique and modified-BFGS.

The SQP method also have advantage in its superliner convergent to global optimal solution for unconstrained convex problem. In case of FE model update problem, the solution space is restricted by constraints and the feasible space is not always convex. Therefore, a local optimal solution, which is not unique but may be one of the several possible solutions, is found near the initial value. Thus, intrinsic weakness of gradient-based optimization in finding global optimum

solution is generally recognized. However, global optimum solution does not necessarily mean the most plausible solution in the problem of updating FE model (Zarate and Caicedo, 2008). Especially if a baseline FE model secures sufficient credibility, the local optimal solution that is not deviated too much from the initial value may be more appropriate to represent physical properties of the real structure. Therefore, the SQP method is utilized to identify non-linear relationship between sets of measurement data and corresponding multiple FE models. Karush-Kuhn-Tucker (KKT) conditions and change rate of structural parameters are measures for convergency check. The algorithm performs well in terms of efficiency, accuracy, and percentage of successful solutions. As results of successive optimization using the SQP, a set of updated FE models are identified.

The employed optimization process can clarify meaning of the updated multiple FE models. Each of the multiple FE models represents the most probable physical properties of structure for the considered measurement data by the optimization process. Thus, distribution of multiple FE models can give the probabilistic information explicitly about the structural condition considering data uncertainty, which cannot be provided by previous non-probabilistic methods. The meaning of updated FE models is related to the nature of measurement data uncertainty. If the considered measurement uncertainty accounts for the noise or numerical error, the variability of multiple models simply indicates possibilities of structural properties, rather than actual variation of the structural behaviors. On the other hand, if the data uncertainty includes the effect of environmental effects such as temperature fluctuations, the variability of multiple models can be associated with actual variation of structural properties. For both cases, a likelihood that the structure exhibits specific behavior can be inferred from the distribution of multiple FE models. Consequently, the probabilistic information about the structural condition can be estimated from the identified distribution of multiple models in terms of distribution of structural performance index, such as load rating factor, seismic fragility and safety index, or probability of failure.

2.4 Illustrative Example: 3-span Continuous Bridge

2.4.1 Definition of true model

An idealized numerical example is considered to verify effectiveness of proposed method. Stiffness and mass properties of three spans are perturbed from nominal values to define virtual true model, as summarized in Table 2.1.

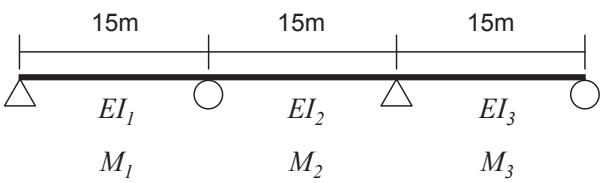

Figure 2.3 3-span continuous bridge for illustrative example

Table 2.1 Perturbation of structural parameters compared to nominal values

	EI_1	EI_2	EI_3	M_1	M_2	M_3
Ratio to nominal value	0.90	1.10	0.85	1.02	1.05	1.02

The first three natural frequencies and vertical displacements of three spans by three load cases are obtained through simulation with the 'true model' to define 'measurement data'. The three load cases for static displacements are defined using design truck model (MLTM, 2012), of which locations are determined as maximum displacement is induced at each span. Figures (2.4) - (2.6) illustrate the employed modal properties, three load cases and static displacements.

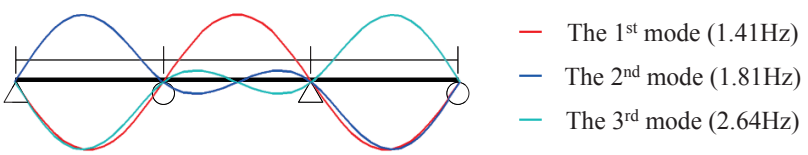

Figure 2.4 Mode-shape and natural frequency of first three modes

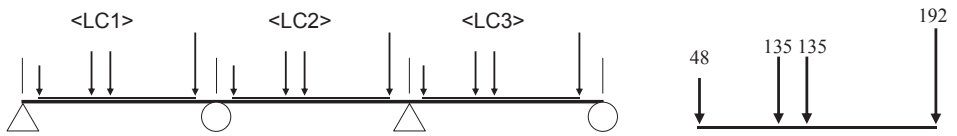

(a) Location of design trucks for three load cases (b) Design truck model (KL-510)

Figure 2.5 Three load cases for static displacements

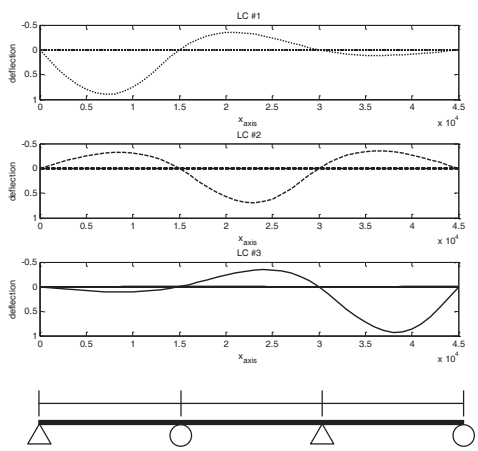

Figure 2.6 Deflected shape of the bridge for three load cases

2.4.2 Case study 1: Measurement data without noise

Since the true model is given, sufficient number of measurement data to represent uncertainty of measurement data can be obtained. As a first case study, probability models for the stiffness and mass of the true model are assumed (Table 2.2). The probability models are purposed to represent actual variation of structural properties due to environmental effect, rather than the effect of noise.

Table 2.2 Probability models for structural parameters of true model

	Bias factor (λ)	C.O.V (c_V)	Distribution type
Stiffness (EI)	1.00	0.08	Lognormal
Mass (M)	1.00	0.08	Normal

Feasible models are generated by sampling structural parameters from the probability models. Numerical simulation with the feasible models render 10,000 sets of 12 responses, and the matrix of measurement data, $\mathbf{D}_{sample}$, is obtained.

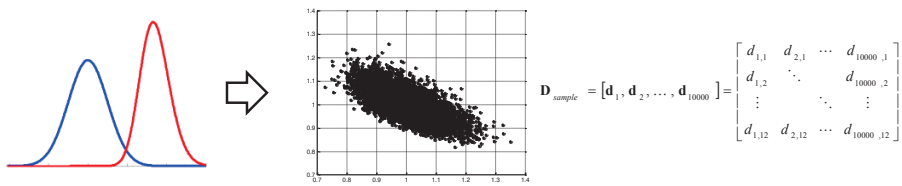

<Probability model of structural parameters> <Artificially generated sets of long-term measurement data>

Figure 2.7 Schematic illustration of measurement data generation

Multiple FE models are identified by updating a baseline model with nominal values using the sets of measurement data. An objective function for i-th updated model is formulated as:

$$\begin{aligned} J_i(\boldsymbol{\theta}_i) &= [r_f(\boldsymbol{\theta}_i) + r_\delta(\boldsymbol{\theta}_i)] + \Pi_R \\ &= \left[\frac{1}{N_f} \sum_{j=1}^{N_f} \left(\frac{f_j^a(\boldsymbol{\theta}_i) - f_j^m}{f_j^m} \right)^2 + \frac{1}{N_\delta M} \sum_j^{N_\delta} \sum_k^M \left(\frac{\delta_{kj}^a(\boldsymbol{\theta}_i) - \delta_{kj}^m}{\delta_{kj}^m} \right)^2 \right] + \beta \|\boldsymbol{\theta}_i\|^2 \end{aligned} \tag{2.11}$$

where r_f is a residual of natural frequency, r_δ a residual of displacement, Π_R the regularization function. The residual of natural frequency is equated with f_i the i-th natural frequency ($i = 1,\ldots,N_f$; $N_f = 3$), and the superscript a and m represent the analyzed and measured values, respectively. The residual of static displacement calculated similarly with δ_{kj} the vertical displacement value at the k-th span ($k = 1,\ldots,M$, $M = 3$), owing to the j-th load case ($j = 1,\ldots,N_\delta$, $N_\delta = 3$). The superscripts a and m are the same as before. The regularization factor β is taken 1.0 initially, and adjusted during each step of the optimization process by VRFS. Another case that β=0 is also considered to analyse the effect of regularization on the multiple FE models.

Consequently, 10,000 updated models are found for both cases of regularization factors. For comparison, the values of structural parameters of feasible models, which are utilized to obtain $\mathbf{D}_{sample}$, is also taken. Figure 2.8 shows the mean values of the structural parameters of generated

and updated models. The updated models for both regularized and unregularized cases accurately predict the actual variation of structural parameters in terms of mean value.

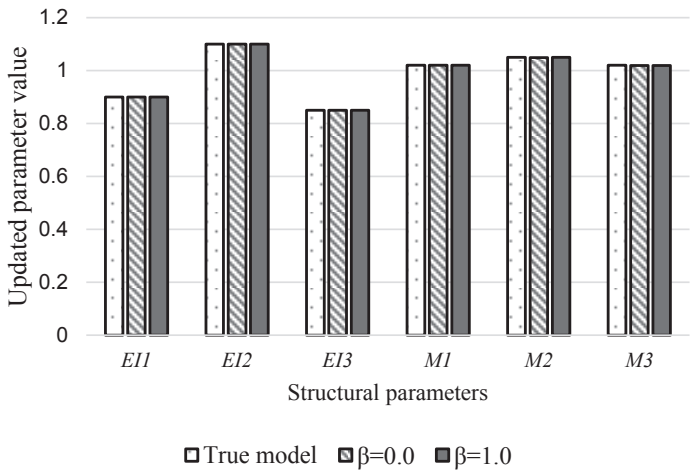

Figure 2.8 Mean values of the structural parameters

Accuracy of the updated models are also verified by estimating error of the updated structural parameters by

$$e_i = \frac{1}{6}\sqrt{\sum_{j=1}^{6}\left(\frac{\hat{\theta}_{ij} - \theta_{ij}}{\theta_{ij}}\right)^2} \tag{2.12}$$

where e_i denotes average error of the i-th updated model, subscript j type of structural parameters, θ the actual value of structural parameter sampled from true model, and $\hat{\theta}$ the estimated value of structural parameters for the updated model. As shown in Figure 2.9, most of the updated models showed negligible error lower than 0.1%.

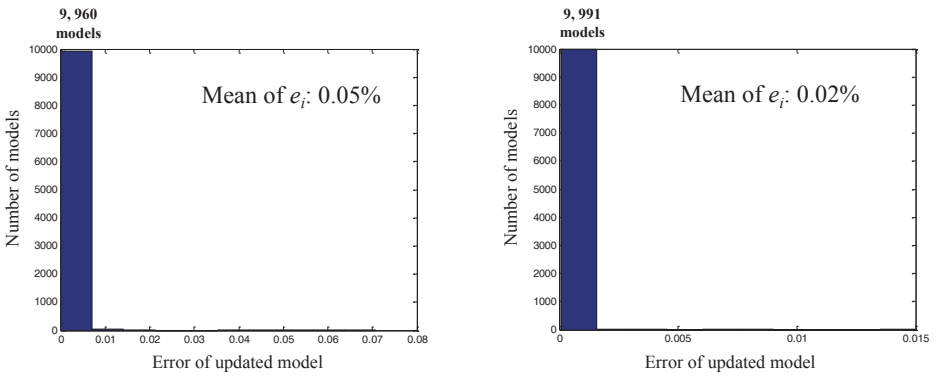

(a) $\beta = 1.0$ (b) $\beta = 0.0$

Figure 2.9 Histogram of average error of the updated models

In this case study, rank-deficiency is avoided by more measurement than optimization parameters. In addition, the ill-posed properties may be negligible because numerical model and the measurement data contain no uncertainty. Accordingly, the optimization process predicts the variation of structural parameters accurately regardless of regularization.

2.4.3 Case study 2: Measurement data with artificial noise

The objective of case study 2 is to verify whether the implemented method can update FE models reliably in the presence of random noise in measurement data. For the purpose, we mimic actually obtainable measurement data by adding artificial noise as Eq. (2.13).

$$\mathbf{D}_{noise} = \mathbf{D}_{sample} \times (1 + \eta) \tag{2.13}$$

where $\mathbf{D}_{sample}$ is sets of measurement data generated by using probability models for the true model, $\mathbf{D}_{noise}$ is a noised data, and η is a random number to represent effect of the noise. The random numbers for the sets of measurement data are sampled independently from uniform distribution, of which bound indicates noise level. Figure 2.10 shows the example of noised measurement data.

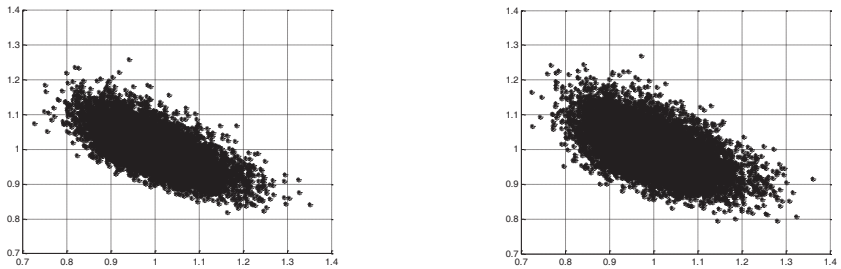

(a) Measurement data without noise (b) Noised measurement data

Figure 2.10 Generation of measurement data by adding noise

The level of noise that determine perturbation range of η is varied from 1% to 10%. For each case of noise level, the baseline model is updated with β=1.0 to obtain multiple FE models and the effect of noise level on distribution of the updated multiple FE models is investigated.

In Figure 2.11, every point represents each of multiple FE models in terms of updated stiffness and mass of the first span. Scatter and separation of the multiple FE models became definite according to the increase of noise level, and several clusters are also observed. The employed measurement data may not be reproducible by the numerical model due to the effect of noise, thus wide dispersions of the updated FE models are obtained. Nevertheless, all the updated models converge to local optimal solutions by using the optimization process without violating constraints.

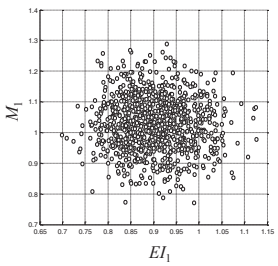

(a) Noise level: 1%

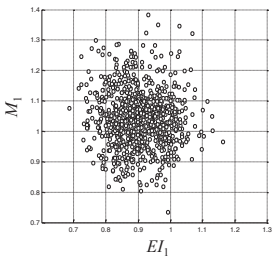

(b) Noise level: 2%

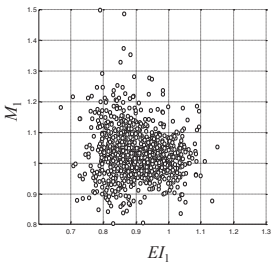

(c) Noise level: 3%

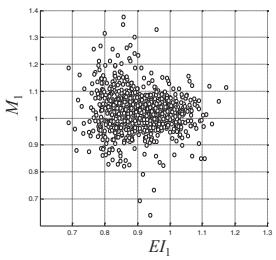

(d) Noise level: 4%

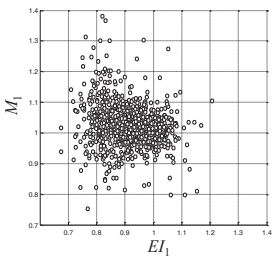

(e) Noise level: 5%

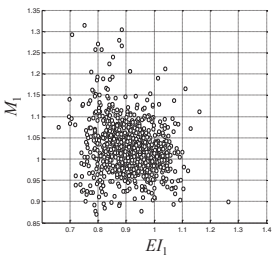

(f) Noise level: 6%

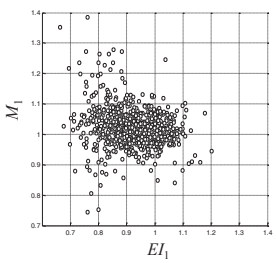

(g) Noise level: 7%

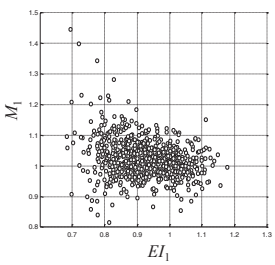

(h) Noise level: 8%

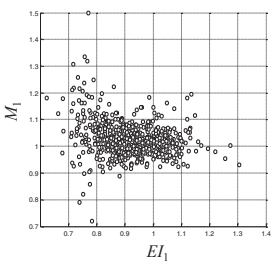

(i) Noise level: 9%

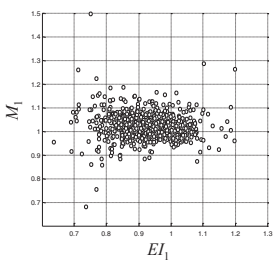

(j) Noise level: 10%

Figure 2.11 Distribution of multiple FE models according to increase of noise level

2.5 Summary

In this chapter, a procedure of updating multiple FE models by successive optimization is presented with the associated mathematical issues. Uncertainty of measurement data is described

by Probability Density Function (PDF) by either uniform distribution or specific type of joint PDF according to availability of sufficient data. Multiple FE models are updated from a baseline model through successive optimization using sets of measurement data sampled from the PDF. Numerical stability of the optimization process could be assured by employing regularization function and modified BFGS method. An idealized numerical example shows that the proposed method successfully update multiple FE models, which can predict variation of structural condition accurately. Especially, if uncertainties of modeling and measurement are not included, the errors of updated models are negligible. Even though when specific level of noise is added to the measurement data, well converged FE models could be obtained by using the implemented optimization algorithm.

Chapter 3. Probabilistic Assessment of Structural Conditions

The identified distribution of multiple FE models can predict physical properties of the structure in the presence of measurement uncertainty, and can be used for probabilistic assessment of structural condition. However, as shown in the previous chapter, the updated models could be separated and compose several clusters. Therefore, numerical algorithms are required to classify the updated models and describe their distribution probabilistically. This chapter introduces the procedures of feature extraction, dimension reduction, and clustering of updated FE models for more efficient probabilistic assessment. Principal component analysis (PCA) help to better reveal the distribution feature of multiple FE models. Other adopted techniques are *K*-means and Gaussian mixture model to group similar models, and describe their composition. Effectiveness of the grouping process is enhanced by the application of PCA. The analyzed results are utilized for probabilistic assessment of structure. Especially, the model selection based on clustering can refine the assessment results in spite of high uncertainty level.

3.1 Feature Extraction of Multiple FE Models by Applying PCA

The Principal Component Analysis (PCA) is applied to the updated values of multiple FE models for the purposes of dimension reduction, feature extraction, and visualization of the multiple models. The application of PCA is the orthogonal projection of the distributed FE models onto a lower dimensional linear space, known as the *principal subspace*, such that the variance of the projected models is maximized (Bishop, 2006). Equivalently, it aims to find orthonormal set of principal components and the coordinate of multiple FE models in the principal subspace. Since the principal components are orthogonal to each other and maximize the variance of multiple models, independent key factors affecting the distribution of multiple models are likely to be revealed in the principal subspace. Thus, the effect of uncertainty of diverse measurement data can be investigated by a few largest principal components. Applying PCA is also beneficial to

improve the clustering accuracy (Ding and He 2004). In addition, the PCA enables to visualize multiple FE models of high-dimension in reduced dimension effectively, thus analysis on the classified models became more efficient.

As a first step, the covariance matrix **S** of *P*-dimensional structural parameters of *N* updated FE models is computed as

$$\mathbf{S} = \mathrm{cov}(\boldsymbol{\Theta}) = E\left[(\boldsymbol{\Theta} - E[\boldsymbol{\Theta}])(\boldsymbol{\Theta} - E[\boldsymbol{\Theta}])^T\right] \tag{3.1}$$

Each entry of the covariance matris **S** is calculated as

$$S_{pq} = \frac{1}{N}\sum_{i=1}^{N}\left(\theta_{pi} - \bar{\theta}_p\right)\left(\theta_{qi} - \bar{\theta}_q\right) \tag{3.2}$$

where θ_{pi} is *p*-th component of optimal structural parameter vector $\boldsymbol{\theta}_i$. $\bar{\theta}_p$ is a mean value given by Eq. (3.3).

$$\bar{\theta}_p = \frac{1}{N}\sum_{i=1}^{N}\theta_{pi} \tag{3.3}$$

By applying eigenvector decomposition on **S**, eigenvector matrix **u** and eigenvalue matrix $\boldsymbol{\Lambda}$ are obtained.

$$\mathbf{S} = \mathbf{u}\boldsymbol{\Lambda}\mathbf{u}^T \tag{3.4}$$

The eigenvector matrix **u** contains principal components in its column vectors, which are bases of transformed space. The contribution of principal components to explain the variance of the distribution of structural parameters is calculated from diagonal components of $\boldsymbol{\Lambda}$. Finally, the coordinate of each model in the orthogonal space is calculated as

$$\hat{\boldsymbol{\theta}}_i = \mathbf{u}^T\left(\boldsymbol{\theta}_i - \bar{\boldsymbol{\theta}}\right) \tag{3.5}$$

where $\bar{\boldsymbol{\theta}} = [\bar{\theta}_1, \bar{\theta}_2, \ldots, \bar{\theta}_p]^T$.

The updated multiple FE models of numerical example in section 2.4.2 are taken to explain the procedure and outcomes of PCA application. Figure 3.1 (a) shows the distribution of multiple FE models by plotting the matrix $\boldsymbol{\Theta}_{\text{opt}} = [\boldsymbol{\theta}_1, \boldsymbol{\theta}_2, \ldots, \boldsymbol{\theta}_{10000}]$, which is the assemble of updated values of structural parameters in case of 1% level of noise. By applying the Eqs. (3.1) - (3.5), $\hat{\boldsymbol{\Theta}}_{\text{opt}} = [\hat{\boldsymbol{\theta}}_1, \hat{\boldsymbol{\theta}}_2, \ldots, \hat{\boldsymbol{\theta}}_{10000}]$, the matrix of multiple FE models projected to the principal subspace, can be estimated. By using $\hat{\boldsymbol{\Theta}}_{\text{opt}}$, distribution of the updated FE models are also plotted in the principal space, of which two axes correspond the first and third principal components (Figure 3.1 (b)). Compared to the distribution in the original space, separation of models into two distinct clusters is better observed in the principal subspace. The result indicates that distribution feature is well represented by the application of PCA.

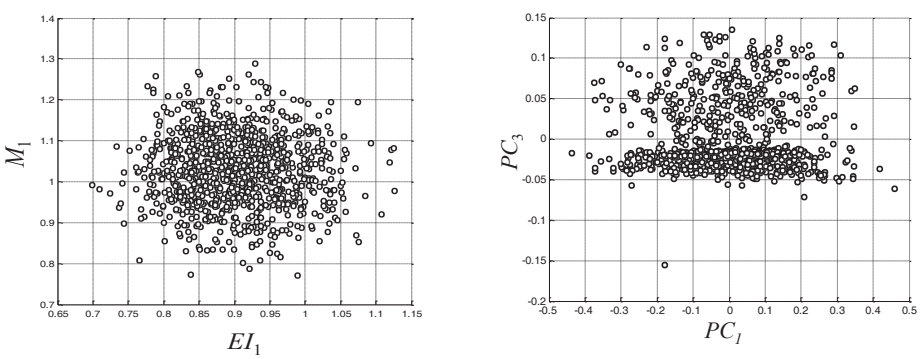

(a) Original space composed of two structural parameters of the largest variances

(b) The principal subspace composed of the first two largest principal components

Figure 3.1 Distribution of updated multiple FE models

We can investigate the effect of measurement uncertainty onto model distribution by using the principal components. The principal components are orthogonal to each other, and are likely to imply independent key factors affecting the distribution of multiple models. The more influencing the factor, it is likely to be observed in the first few principal components that contain

large portion of the information about the variability of multiple models. In this example, the uncertainty conditions of the measurement data are investigated by the first two principal components (Figure 3.2). The two figures present the variation of displacement and natural frequency, which are expected as two major factors for distribution of multiple FE models, by color legend. Color legend of each dot visualizes the perturbation of measurement data, which is normalized to the mean value using Eq. (3.6), for each updated FE models, respectively.

$$Change \quad rate \quad of \quad d_i = \frac{d_i - \mu_d}{\mu_d} \tag{3.6}$$

The variation of the displacement is observed along the 2nd principal component (Figure 3.2 (a)). On the other hand, variation of natural frequency is closely related to the 1st principal component (Figure 3.2 (b)). The observation proves that applying PCA can identify the principal subspace where distribution feature and influencing factors are well explained.

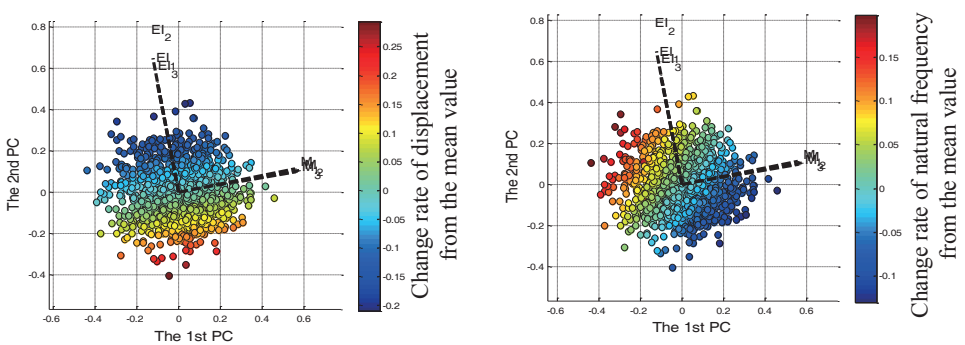

(a) Variation of displacement (b) Variation of natural frequency

Figure 3.2 Change rate of measurement data for updated FE models

Figure 3.2 also shows contributions and sensitivities of the structural parameters to the distribution of multiple FE models. Black vectors represent the principal component coefficients, which are row vectors of eigenvector matrix **u**, for six structural parameters. Direction and length of the vectors indicate how the each structural parameter contributes to the principal subspace. For example, the first principal component, the horizontal axis, has positive coefficient for M_1,

M_2 and M_3, which are directed into the right half of the plot. Therefore, variation of natural frequency can be associated to the mass properties. Similarly, stiffness properties of three spans have positive contribution to the second principal component, and can be related to the variation of the displacement. The observation shows that contributions of stiffness and mass properties contrast each other.

In the meantime, principal component coefficients for the same type of structural parameters almost coincide. They are represented in Figure 3.2 by black vectors that are overlapped almost. We can conclude that effects of stiffness properties are similar each other even though they are for different spans. Same conclusion can also be made for the mass properties. In this way, sensitivities and contributions of structural parameters can be identified with respect to the uncertainty of measurement data. The identified information is helpful to understand properties of clusters and select appropriate ones, in the following procedure.

3.2 Grouping of Multiple FE Models

3.2.1 Deterministic clustering by using *K*-means method

The *K*-means method is further implemented (Bishop, 2006) in order to classify the multiple FE models into several groups according to the similarity that is now revealed by the application of PCA. Combined use of PCA and *K*-means clustering can group the multiple models, and reduce subjectivity in the interpretations and assessments. The objective function is given by

$$J = \sum_{k=1}^{K} \sum_{i=1}^{N} r_{ik} \left\| \hat{\boldsymbol{\theta}}_i - \boldsymbol{\mu}_k \right\|^2 \tag{3.7}$$

where $\boldsymbol{\mu}_k$ is the centroid of the k-th cluster and r_{ik} indicates membership of the i-th model in the k-th cluster. If the i-th model is assigned to cluster k then $r_{ik} = 1$, otherwise $r_{ik} = 0$. Term inside Σ measures the sum of the inner-distances of data points that are assigned to the k-th cluster. The

algorithm iteratively finds centroids of clusters $\boldsymbol{\mu}_k$ and r_{ik} of each model by which the objective function is minimized.

The number of clusters K is determined by calculating score function which evaluates the quality of clustering by two quantities: the Between Cluster Distance (*BCD*) and the Within Cluster Distance (*WCD*). The former one indicates the degree of separation of clusters from each other, whereas the second term indicates the degree of compactness of each cluster. The score function is thus defined as follows:

$$S.F. = BCD \,/ WCD \tag{3.8}$$

$$BCD = \frac{1}{NK} \sum_{k=1}^{K} \left\| \overline{\boldsymbol{\mu}} - \boldsymbol{\mu}_k \right\|^2 n_k \tag{3.9}$$

$$WCD = \frac{1}{K} \sum_{k=1}^{K} \sqrt{\frac{1}{n_k} \sum_{i=1}^{N} r_{ik} \left\| \hat{\boldsymbol{\theta}}_i - \boldsymbol{\mu}_k \right\|^2} \tag{3.10}$$

Here, n_k is the number of FE models in the k-th cluster, and $\overline{\boldsymbol{\mu}}$ is the mean of centroids of all K clusters. Score function values are calculated for different number of clusters, and optimal number of clusters for the maximum score is chosen.

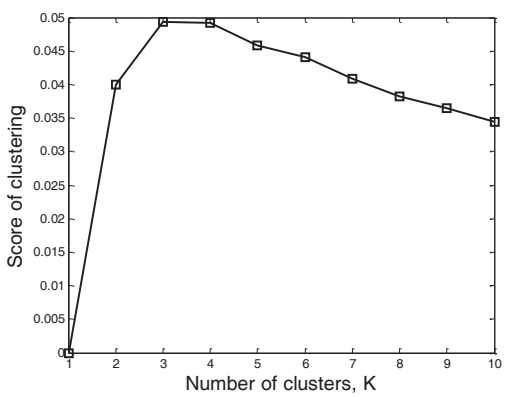

Figure 3.3 Scores of clustering for different number of clusters

Figure 3.3 shows the scores of clustering calculated for the updated FE models in the previous numerical example. The number of clusters is varied from one to ten. According to the maximum score, the multiple FE models are classified into three groups (Figure 3.4).

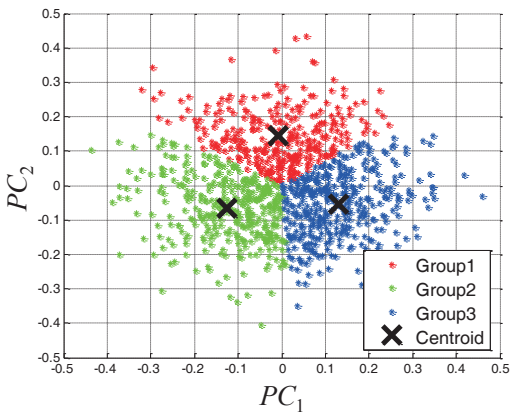

Figure 3.4 Classification of multiple FE models into three groups

The FE models in each classified group may be characterized by similar property of measurement uncertainty. Thus, depending on the features of the groups and characteristic of concerned assessment, a specific group of FE models is selected to assess the condition of structures probabilistically. In Figure 3.4, dots at the right part have the large scores for the first principal component, which corresponds to the natural frequency that is reduced from the mean value. At the same time, dots at the lower part are featured by displacements larger than mean value. Thus, FE models in Group 3 represent flexible condition of the bridge. Similarly, Group 1 can be associated with stiffer condition of the bridge, and Group 2 is close to average performance.

In this way, we can obtain information about the properties of each group, and select proper subset of FE models. In addition, we can identify which type of data and structural parameters affect significantly to the distribution of FE models can be identified, which is a useful information for maintenance.

3.2.2 Fitting of Gaussian mixture model

The *K*-means method has advantage with respect to easy implementation and definite classification even when complex distribution is concerned. However, relative plausibility of identified clusters cannot be estimated. Furthermore, membership of the each FE model is assigned deterministically even when their actual membership is ambiguous. On the other hand, utilizing mixture of distribution models have the advantage over *K*-means by its ability to deal with the problems probabilistically. Data distribution is described by superposition of several PDFs, and a better characterization of the distribution is given. Moreover, relative probability of each component PDF is calculated. Therefore, the approach is more suitable to classify FE models for the purposes of probabilistic assessment. In this study, Gaussian mixture model is implemented to take advantage its flexibility and ability to capture multimodal feature of distribution (Kurtz and Song, 2013). The distribution of the updated FE models are expressed in the form

$$p(\boldsymbol{\theta}) = \sum_{k=1}^{K} \pi_k N\left(\boldsymbol{\theta} \middle| \boldsymbol{\mu}_k, \Sigma_k\right) \tag{3.11}$$

The expression is superposition of K different Gaussian distributions. Through the process of fitting mixture model to the data, mixing probability coefficients π_k, mean vectors $\boldsymbol{\mu}_k$ and covariance matrices Σ_k of K component Gaussian distributions are found. Mean vectors and covariance matrices represent distribution feature of each clump. In addition, the mixing coefficient π_k evaluates the responsibility that k-th Gaussian density takes for explaining the individual model $\boldsymbol{\theta}_i$. Thus, relative plausibility of identified PDFs is obtained quantitatively.

The fitting of mixture model is carried out using the projected value of structural parameters in the PCA subspace to take advantage of feature extraction. Gaussian mixture models fitted using a couple of dominant principal components can exhibit good performance for the identification of distinctive groups, while considerable loss of information may be occurred. On the other hand,

the better explanation of variance of multiple FE models can be achieved by considering more principal components during the fitting. At the same time, inclusion of all principal components may provoke the problem of overfitting. In that case, the algorithm may fail to find distinctive groups and credibility of mixture model may be worsened. In this study, fitting of Gaussian mixture model is began with using the first two principal components. And then, fitting is carried out again considering one more principal component. The mean vectors, covariance matrices, and mixing coefficients identified in the previous step are taken as initial values in the next step of fitting. This sequential fitting of Gaussian mixture model is repeated until sufficient numbers of principal components are included, which is determined as more than 99% variance of FE models can be explained. The approach prevents under or overfitting, and enhance the identifiability of distinctive groups.

The proposed procedure is verified through application to the previous numerical example. Regularization parameter, determined as 0.001, is added to the diagonal components of covariance matrices in order to avoid getting ill-conditioned covariance matrices. Figure 3.5 illustrates mixture of three Gaussian component PDFs, which are fitted the distribution of the updated FE models considering different number of principal components. The three Gaussian models are denoted as component PDF 1, 2 and 3 from top to bottom of the figure. Mean vectors of three component PDFs are represented by yellow diamond markers. Contour of each component PDF describes covariance and density of component PDFs. Contour of component PDF 2 located at the right side of each figure are not observable, which is accounted for by relative smaller probability of the PDF as 4.76%. The component PDF 3 takes the largest portion to expalin distribution multiple FE models with 66.32% of mixing coefficient. The component PDF 2 also plays an important role in expalining the information of distribution with 28.92% of mixing coefficient. One can assess the structuarl condition using the 3rd and the 1st component PDFs with assumption that the 2nd componet PDF describe scatter of outliers rather than distribution of meaningful physical properties.

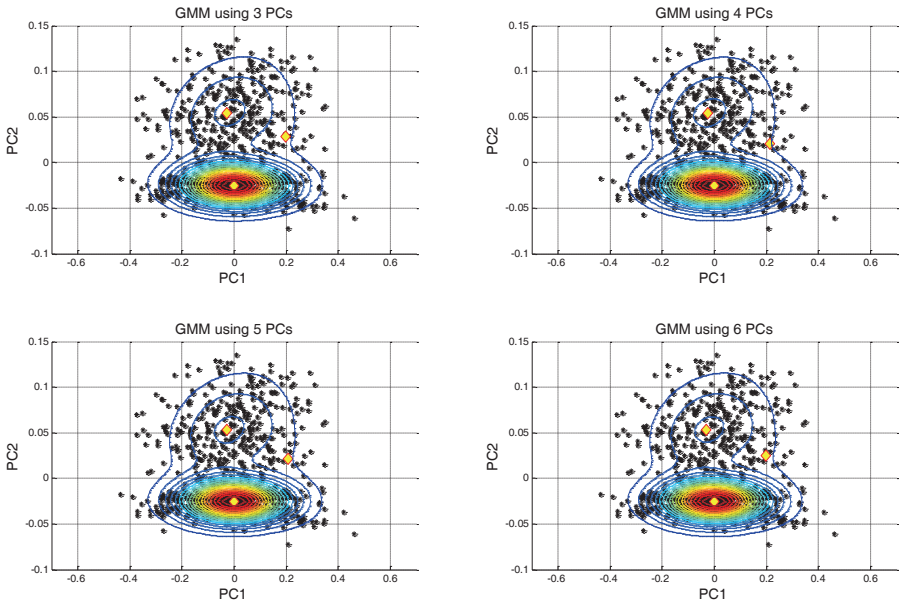

Figure 3.5 Sequential fitting of Gaussian mixture model by utilizing more principal components

3.3 Probabilistic Assessment of Structural Condition

A set of FE models, which are equally capable of representing the probable physical properties of structure, gives the probabilistic information about the structural condition considering data uncertainty. The condition of structure can be expressed as distribution of any types of performance index, such as load rating factor, seismic fragility and safety index using the estimated multiple FE models. Statistical parameters such as mean value and variance regarding the structural condition can be provided from the distribution of performance indices. In this study, distribution of load rating factors is calculated using the updated FE models. Another approach is estimating probability that the structure does not meet the required performance with respect to safety, serviceability, and so on. In this study, reliability index is calculated through structural reliability analysis using the Gaussian mixture model for the distribution of multiple FE models.

For both type of assessments, if the uncertainty of measurement data accounts for the noise or numerical error, the variability of multiple models indicates a likelihood of physical properties

that the structure may exhibit due to the existence of data uncertainty. Whereas, the effect of environmental condition may also be included to the uncertainty model, of which variance must be larger than before. In that case, accordingly, the estimated variability of multiple FE models may be related to actual variation of physical properties. Therefore, the meaning of probabilistic assessment should be associated with the philosophy regarding the employed measurement uncertainty.

3.3.1 Load rating factor evaluation

Load Rating Factor (RF) quantifies vehicle load carrying capacity of girder bridges (AASHTO, 2011; Moses, 2001). The RF lower than 1 indicates insufficient capacity of the concerned bridge, rather than actual collapse of the bridge. In this study, distribution of the RF is estimated by using the updated FE models, which cannot be estimated by a single deterministic FE model. As a result, statistical information about vehicle load carrying capacity of bridge is obtained in terms of mean value and variance of RF. The two statistical parameters can be used to determine current condition of girder bridges.

The RF for an updated FE model shall be computed as:

$$RF = \frac{\varphi_{cond}\ \varphi_m C_m - (\alpha_{DC})(DC) - (\alpha_{DW})(DW)}{(\alpha_L)(LL)(1 + IM)} \tag{3.12}$$

where DC is the dead load effect due to structural components and nonstructural attachments, DW the dead load effect due to wearing surfaces and utilities, LL the effect of the vehicular live load, and IM the vehicular dynamic load allowance. The condition factor φ_{cond} is related to the soundness of the bridge structure. C_m and φ_m are the strength of structural members and associated resistance factor, respectively. Load factors α_{DC}, α_{DW} and α_L are for the structural components and nonstructural attachments, for the wearing surface and utilities and for the vehicular live load, respectively. The formula is referred from the Korean Highway Bridge Design Code (MLTM,

2012). The load effects *DC*, *DW* and *LL* are estimated differently due to updated values of mass, stiffness, and boundary characteristics of multiple FE models. In addition, the modified structural parameters also result in different strengths of structural components C_m. As a result, the distribution of rating factors reflecting uncertainty is estimated.

When all the updated models are used, the assessment result can account for overall variability of multiple FE models caused by the employed measurement data uncertainty. On the other hand, several groups of similar models can also be selected to consider specific physical properties of structure according to the classified conditions of measurement uncertainty. In this case, the distribution of RF represents structural condition restrictively for specific measurement uncertainty condition, with reduced variance.

If the statistical information is not necessary, models representing each of the groups can be selected from the centroids of clusters by Eq. (3.13).

$$\boldsymbol{\theta}_c = \left[\mathbf{u}^T\right]^{-1} \boldsymbol{\mu}_c + \overline{\boldsymbol{\theta}} \tag{3.13}$$

where $\boldsymbol{\theta}_c$ is the structural parameters of representative FE model and $\boldsymbol{\mu}_c$ is coordinate of centroids or mean vector of selected group in the orthogonal space. Structural assessment using the representative model can represent the average condition of the structure, rather than rigorous probabilistic information.

The procedure of probabilistic load rating is applied to the previous numerical example. The equation for RF is expressed as Eq. (3.14) with respect to maximum bending stress.

$$RF = \frac{\sigma_{allow} - \sigma_{DC}}{\sigma_{LL}\left(1 + IM\right)} \tag{3.14}$$

where σ_{allow} is allowable stress, σ_{DC} bending stress by self-weight, σ_{LL} bending stress by live-load, and *IM* a dynamic impact factor. The RF is equated at three spans for three load cases, and the lowest rating is taken to represent overall condition of the bridge.

As a first case, the multiple FE models identified in the section 2.4.1 are considered. The models were updated from the measurement data without noise, thus actual variations of the structural parameters were predicted accurately already. Consequently, rating factors estimated by using the updated models are also almost identical to the actual values obtained from the idealized true model. Mean value and standard deviation of RFs are summarized in Table 3.1. The variation ranges of rating factors between $\mu_{RF}\pm 1\sigma_{RF}$ are also depicted in Figure 3.6.

Table 3.1 Mean value and standard deviation of RF

	True model	Updated (β=0)	Updated (β=1)
Mean value (μ_{RF})	19.61	19.58	19.65
Standard deviation (σ_{RF})	5.09	5.09	5.11

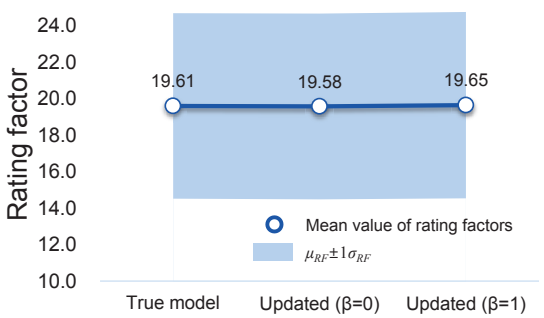

Figure 3.6 Range of RF between $\mu_{RF}\pm 1\sigma_{RF}$

Next, the multiple FE models updated using measurement data with noise are considered, which are identified in section 2.4.3. Since the models are affected by the measurement noise, exact realization of structural parameters was not achievable. Figure 3.7 shows variation of RF according to increase in noise level. Mean value of RFs increases according to the higher noise level with larger discrepancy to the exact mean RF. It indicates that the existence of noise in measurement data result in overestimated RF.

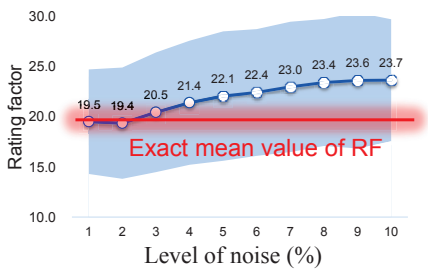

Figure 3.7 Variation of RF according to increase of noise level

3.3.2 Structural reliability analysis

Evaluating rating factors using the multiple FE models provides probabilistic information about the structural condition, which cannot be estimated by a single deterministic FE model. The influence of uncertainty level to the evaluation can also be investigated. However, the probabilistic feature of the updated FE models is not fully reflected by the distribution of rating factors. Furthermore, making a decision with the mean and variance of the rating factor has a certain limit. Therefore, structural reliability analysis is conducted using the identified Gaussian mixture model for rigorous reflection of the data uncertainty to probabilistic assessment. Reliability index β corresponding to the distribution of all updated FE models is calculated by a total probability theorem using Eqs. (3.15) and (3.16).

$$p_{f,tot} = \int_{G\le 0} p(\boldsymbol{\theta})\,d\boldsymbol{\theta} = \int_{G\le 0} \sum_{k=1}^{K} \pi_k N\left(\boldsymbol{\theta}\middle|\boldsymbol{\mu}_k, \Sigma_k\right) d\boldsymbol{\theta} = \sum_{k=1}^{K}\left[\pi_k \int_{G\le 0} N\left(\boldsymbol{\theta}\middle|\boldsymbol{\mu}_k, \Sigma_k\right) d\boldsymbol{\theta}\right] \tag{3.15}$$

$$\beta_{tot} = -\Phi^{-1}\left(p_{f,tot}\right) \tag{3.16}$$

where $p_{f,tot}$ and β_{tot} are probability of structural failure and associated reliability index when the total K component PDFs are included. A limit state function G is associated with the safety criteria. The mixing coefficient π_k can quantify relative plausibility of the k-th component PDF, and assign weightage for the related probability of failure. The reliability index and probability of failure are calculated by using First-Order Reliability Method (FORM) (Der Kiureghian, 2005) .

Meanwhile, structural reliability analysis can also be conducted by selecting several component PDFs through the Eqs. (3.17) and (3.18).

$$p_{f,select} = \frac{\int_{G \le 0} \sum_{k=1}^{K_s} \pi_k N\left(\boldsymbol{\theta} \middle| \boldsymbol{\mu}_k, \Sigma_k\right) d\boldsymbol{\theta}}{\sum_{k=1}^{K_s} \pi_k} = \frac{\sum_{k=1}^{K_s} \left[\pi_k \int_{G \le 0} N\left(\boldsymbol{\theta} \middle| \boldsymbol{\mu}_k, \Sigma_k\right) d\boldsymbol{\theta} \right]}{\sum_{k=1}^{K_s} \pi_k} \tag{3.17}$$

$$\beta_{select} = -\Phi^{-1}\left(p_{f,select}\right) \tag{3.18}$$

where $p_{f,\ select}$ and β_{select} are probability of structural failure and reliability index calculated using only K_s component PDFs. The denominator in Eq. (3.17) normalizes the probability failure according to smaller portion of FE models are included.

Selecting component PDFs for the structural reliability analysis can be made based on various information with respect to physical properties, associated measurement uncertainty condition, statistical properties of the PDF. In this study, mixing coefficient, which indicates relative probability of component PDF, is considered to select several component PDFs. Component PDFs with π_k lower than specific criteria are assumed to indicate group of outliers caused by noise, and neglected. On the other hand, component PDFs with mixing coefficients higher than the criteria are expected to represent structural condition properly, and are selected for structural reliability analysis.

The procedure of structural reliability is applied to the multiple FE models identified in section 2.4.1. In this case, clustering of the updated FE models is not observed. Therefore, conventional multivariate Gaussian PDF is fitted to the distribution of multiple FE models in the principal subspace, and utilized for structural reliability analysis. Failure of the bridge is defined as the combined bending stress due to live-load and dead-load exceeds allowable stress. The limit state function G for the failure is expressed as:

$$G = \sigma_{allow} - \sigma_{LL}(1 + IM) - \sigma_{DC} \tag{3.19}$$

In the idealized example, probability model for the variability of the true model is given in Table 2. Thus, reliability index of the true model is also calculated by using the probability models. The estimated reliability indices and probabilities are depicted in Figure 3.8. Error of reliability index estimated by using updated FE models is about 0.3%, while the error of probability of failure is about 3%. Similar to the evaluated rating factors, reliability index is also very close to the actual value. The small discrepancy may be caused in the fitting of Gaussian PDF, by which distributions of all structural parameters are described by normal distribution while the true probability model for stiffness was defined as lognormal distribution.

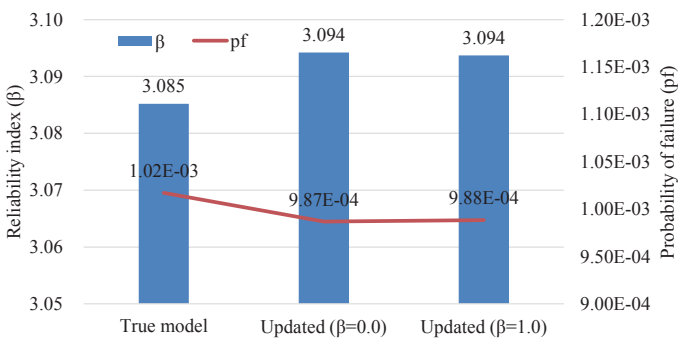

Figure 3.8 Reliability index and probability of failure by the updated models and true model

Next, multiple FE models that are affected by noise in measurement data are considered. The distributions of the updated models had multimodal properties, thus, they were described by using Gaussian mixture model in section 3.2.2 (Figure 3.5). Variation of the reliability indices is estimated with the identified Gaussian mixture models for the 10 noise level cases using Eq. (3.16). Figure 3.9 (a) shows the variation of reliability indices in case that all component PDFs are considered along with the actual value. Discrepancy between the estimated reliability index and the correct value increases mostly according to the higher noise level. Average error of the estimated reliability index is about 12%. Reliability index is also calculated by using several component PDFs with mixing coefficient higher than 10%, and the results are depicted in Figure

3.9 (b). It is observed that discrepancy between the estimated reliability index and the exact one is decreased in most cases of noise level. Average error of reliability index is reduced to 7% by the model selection. The results are also shown regarding probability of failure (Figure 3.10). Clustering process distinguishes the FE models highly affected by noise in measurement data, and thus selecting several groups of FE models that are appropriate to represent structural condition became feasible. Consequently, structural condition can be assessed more accurately in spite of the presence of high measurement uncertainty.

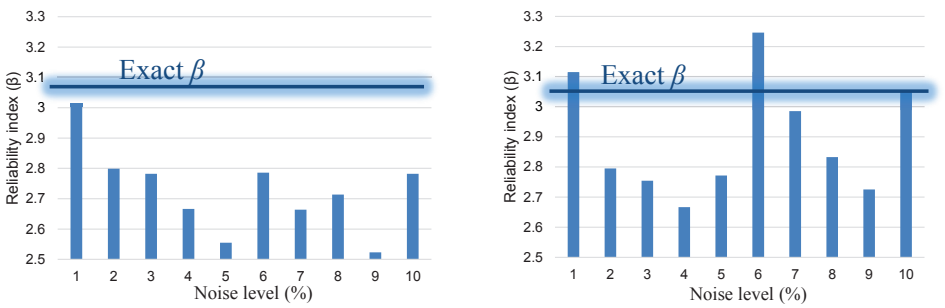

(a) Using all updated FE models

(b) Selective use of component PDF with higher mixing coefficient

Figure 3.9 Effect of clustering-based model selection to variation of reliability index

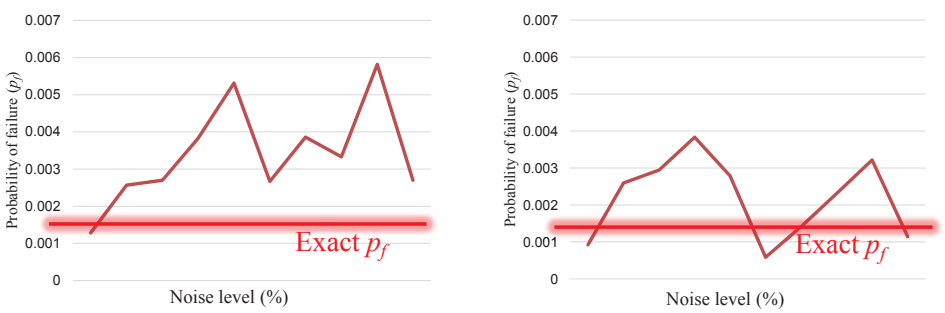

(a) Using all updated FE models

(b) Selective use of component PDF with higher mixing coefficient

Figure 3.10 Effect of clustering-based model selection to variation of probability of failure

Finally, sensitivities of the rating factor and reliability index to the variation of measurement uncertainty are investigated. As a first step, a multivariate normal distribution of fitted to the $\mathbf{D}_{noise}$, measurement data with noise. Then, the standard deviations for the probability model are varied

from -20% to +20%, and sets of measurement data are generated from the each of the varied probability models, respectively. Multiple FE models are obtained for each case, and utilized for RF evaluation and structural reliability analysis based on the proposed method.

Mean values of RFs obtained by using all updated FE models is plotted in Figure 3.11 according to variation of standard deviation. The horizontal axes of two figures represent proportion of the adjusted standard deviation to the initial value, for the natural frequency and displacement, respectively. The legends for two figures also indicate variation of standard deviation for the responses, vice versa. The mean RF varies sensitively to the variance of natural frequency (Figure 3.11 (a)), but variance of displacement is less effective (Figure 3.11 (b)). In this case, mean values of RF ranges from 20.99 to 23.16 of which average error compared to the actual value is about 12.77%. Next, clusters with mixing coefficients larger than 10% are selected. As shown in Figure 3.12, the influences of variance of natural frequency and displacement are similar as before. By the virtue of clustering and model selection, range of mean values of RF reduced from 22.76 to 21.35, and average error decreases as 12.54%.

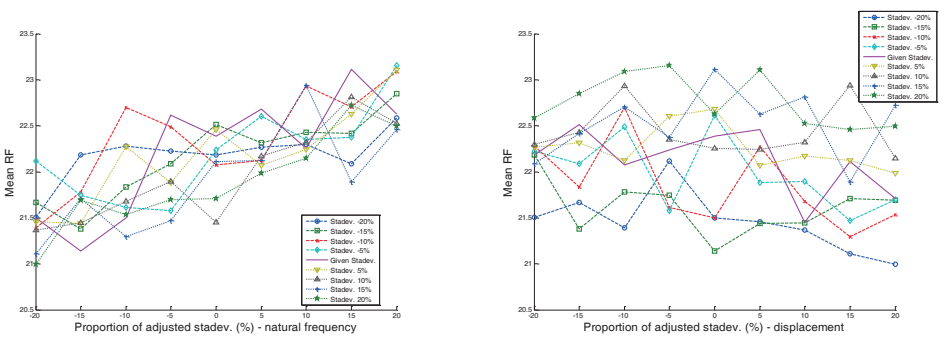

(a) Modifying standard deviation of natural frequency (horizontal axis)

(b) Modifying standard deviation of displacement (horizontal axis)

Figure 3.11 Variation of mean RF by using all models

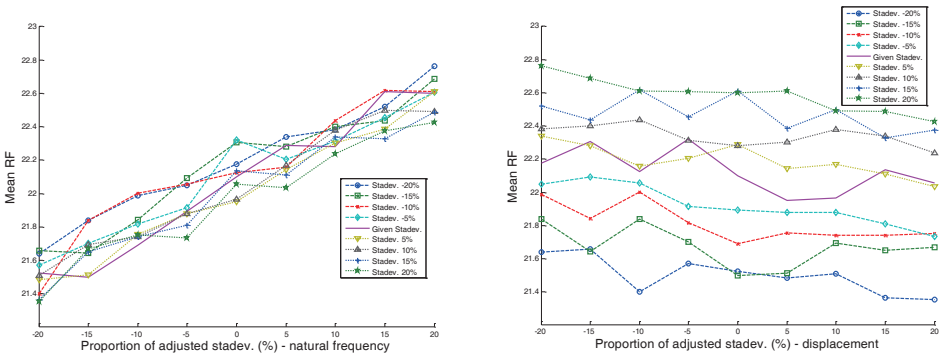

(a) Modifying standard deviation of natural frequency (horizontal axis)

(b) Modifying standard deviation of displacement (horizontal axis)

Figure 3.12 Variation of mean RF by selective model use through clustering

Variation of reliability index is also investigated. Figure 3.13 shows the variation of reliability index when all models are included. In contrary to rating factor evaluation, variation of reliability index is sensitive to the variance of displacement. The reliability index ranges from 2.16 to 3.10, and average error is 16.55%. The error could be reduced as 14.18% by selecting component PDFs with higher mixing coefficients. The variation of reliability index by clustering-based model selection is depicted in Figure 3.14.

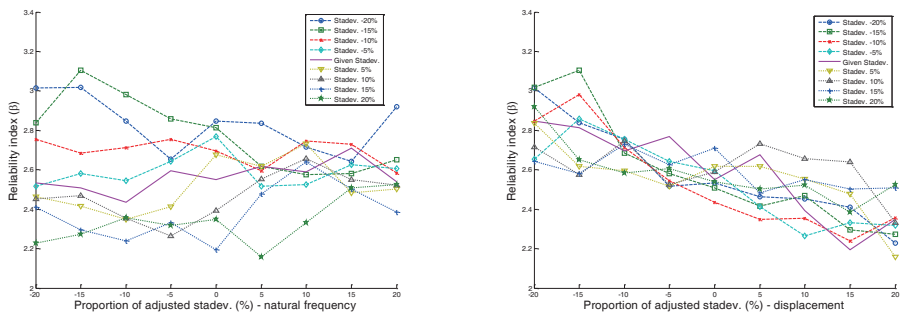

(a) Modifying standard deviation of natural frequency (horizontal axis)

(b) Modifying standard deviation of displacement (horizontal axis)

Figure 3.13 Variation of reliability index by using all models

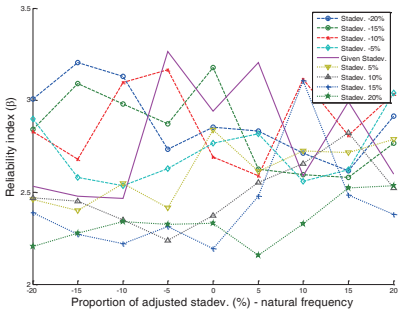

(a) Modifying standard deviation of natural frequency (horizontal axis)

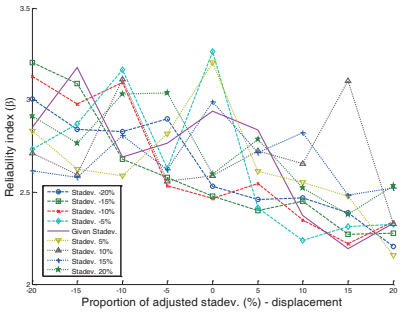

(b) Modifying standard deviation of displacement (horizontal axis)

Figure 3.14 Variation of reliability index by selective model use through clustering

3.4 Summary

In chapter 3, a procedure of probabilistic assessment using the updated FE models is presented. Combined use of Principal Component Analysis (PCA), *K*-means method and Gaussian mixture model can extract distribution feature of multiple FE models, cluster similar models and describe them probabilistically. The procedure is verified by applying to the 3-span continuous bridge example. The proposed procedure estimates structural condition exactly in terms of rating factor and reliability index when noise in measurement data is not associated. According to the increase of noise level, wider dispersion of FE models and existence of several clusters are observed. The multiple FE models are projected to principal subspace, from which variance of models are better revealed, and also utilized to evaluate structural condition in terms of rating factor and reliability index. Discrepancy between the evaluated structural condition and the actual value also show proportional relationship to the noise level. Clustering-based model selection via Gaussian mixture model and *K*-means clustering is able to evaluate structural condition more accurately. Finally, sensitivities of the rating factor and reliability index to the variation of measurement uncertainty are investigated. Clustering process contributes to refine evaluation in the existence of high measurement uncertainty, and the structural condition is assessed more accurately.

The overall flow of multiple FE model update, grouping, and the probabilistic assessment of structural condition is represented as a flow chart in Figure 3.15.

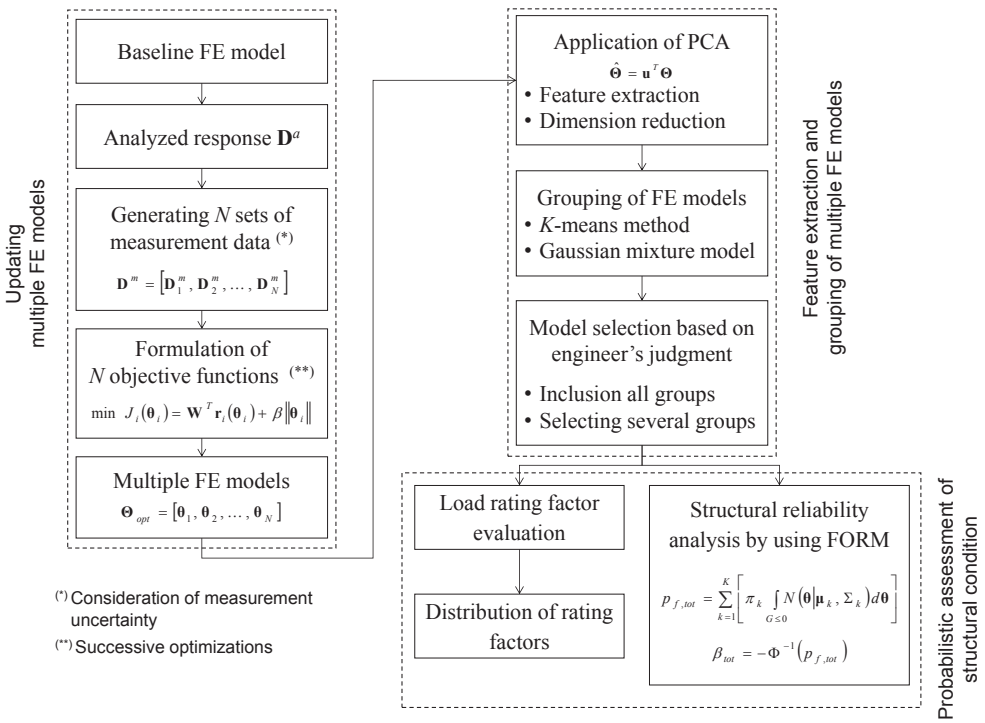

Figure 3.15 Flow chart: Proposed procedure of multiple FE model update, grouping, and probabilistic assessment of structural condition incorporating measurement data uncertainty

Chapter 4. Numerical Example: Yeondae Bridge

This chapter presents numerical verification through application to Yeondae bridge. The bridge is located in a test road section of the expressway 45 in South Korea. Thus, it has no thoroughfare for vehicles except for the purpose of vehicle loading tests. Unlike the idealized example, actual value of present structural condition is unknown. In addition, long-term accumulated data is not available. Therefore, various probability models for the measurement data uncertainty are assumed properly. Effectiveness of the proposed method is verified by investigating effects of the various probability models upon distribution of multiple FE models and following assessments.

4.1 Field Measurement

4.1.1 General description

Yeondae Bridge is comprised of composite steel box girders with two cells (Figure 4.1 (a)). The bridge consists of four continuous spans that are 45m in length. The concrete deck is made up of two lanes in only one direction with a net width of 11.7m between two side barriers. The Ultimate Strength Design (USD) was applied in the design of the concrete deck, while the Allowable Stress Design (ASD) was used for the steel box. Skewed abutments and internal piers support the bridge superstructure.

4.1.2 Field loading tests

Field tests were carried out on March, 2013, to identify structural characteristics for external loadings that were two test trucks shown in Figure 4.2. In this study, two types of measurement data are employed for updating FE models: the first three natural frequencies and the vertical displacements of box girders obtained by three static load cases. Static loading tests were performed to estimate the load effects in terms of the displacements of the box girders. Four displacement transducers were installed under the web plates of each box girder at the middle of

the first span (Figure 4.3). Displacements measured during three static load cases are considered for updating the FE model. Details on the load cases and the measured displacements are presented in Figure 4.4 and Table 4.1. The implemented information is sufficient to represent meaningful structural behavior.

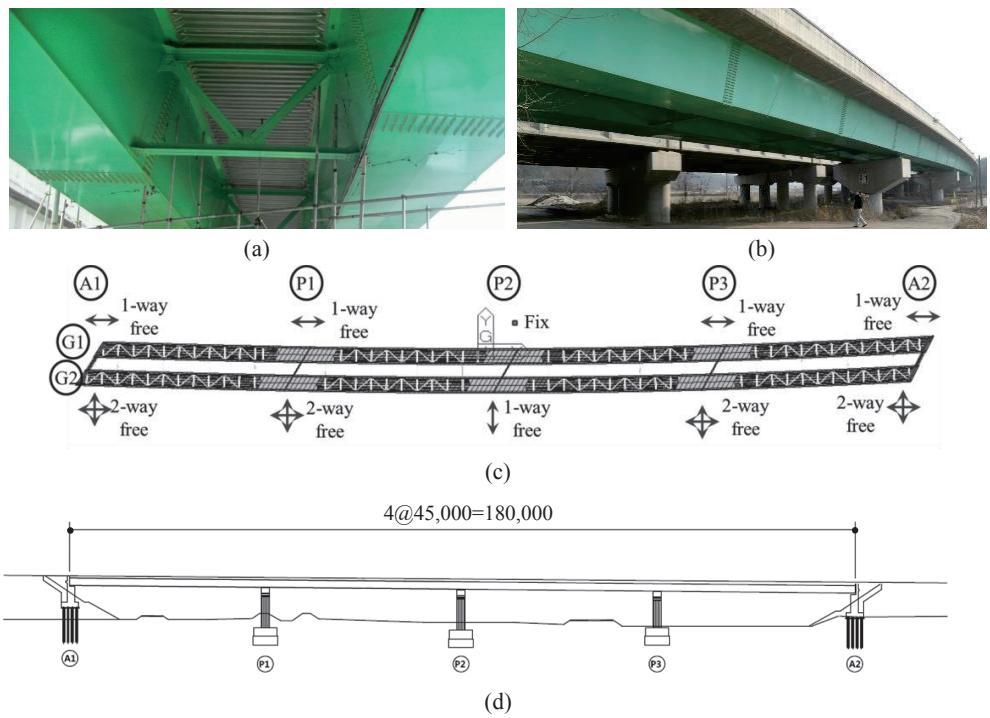

Figure 4.1 Description of Yeondae bridge: (a) a picture taken from beneath the box-girders and (b) from the side, (c) plan view, and (d) side view

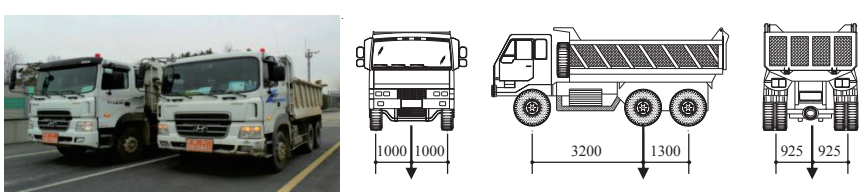

Figure 4.2 Dimension of test trucks (unit: mm)

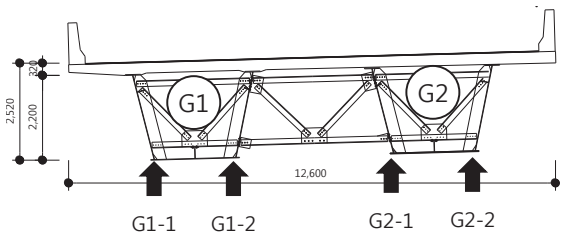

Figure 4.3 Location of four displacement transducers in the first span and their notations

Table 4.1 Measured displacements for three load cases (mm)

	Load case 1	Load case 2	Load case 3
G1-1	6.215	4.670	3.560
G1-2	5.730	5.315	4.570
G2-1	4.440	5.635	6.430
G2-2	3.700	5.205	6.990

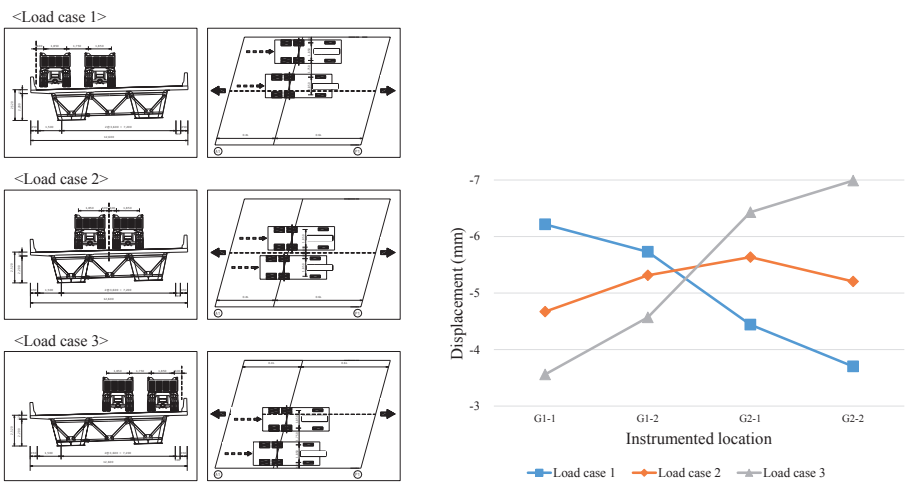

Figure 4.4 Three load cases for the static loading tests and the measured displacements (mm)

Dynamic loading tests were also carried out by changing the truck speed as 10km/h, 60km/h and 100km/h to identify modal properties such as natural frequency and mode-shape. Both static and dynamic test were repeated three times in order to obtain reliable test results. The mode-shapes and associated natural frequencies for the first three modes are depicted in Figure 4.5 with the mode-shape obtained from an analytic model. Details about the experiments and findings have been summarized in Kim *et al*. (2013).

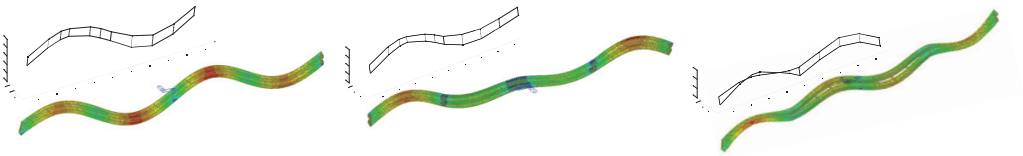

(a) The 1st mode (2.32Hz) (b) The 2nd mode (2.61Hz) (c) The 3rd mode (3.42Hz)

Figure 4.5 Mode-shape identified from the measured acceleration and a baseline FE model

4.2 Updating Multiple FE Models by Successive optimization

4.2.1 Development of a baseline FE model

A baseline FE model has been developed based on design documents. Each box girder is simulated with three-dimensional frame elements, of which equivalent sectional properties were calculated considering the composite concrete deck. Cross frames and bracings between two girders were also modeled by frame elements based on their design values, and they are attached to the box girders using rigid link elements. Figure 4.6 shows the plan view of the baseline FE model. The girder supporting bearings are modeled using elastic spring support elements of which coefficients are taken from commonly used specifications. The baseline FE model was refined manually in order to reduce modeling uncertainty caused by a simple modeling concept. Initial values for structural parameters were adjusted by taking into account the curing and aging of concrete. Some virtual beam elements were also included between two girders to reflect the lateral stiffness of RC slab. In this way, the baseline FE model constituted a better representation of actual behavior. The baseline model was validated as to have good accuracy through comparisons with the measured responses as well as analyzed responses by using a more sophisticated FE model (Kim *et al*., 2013).

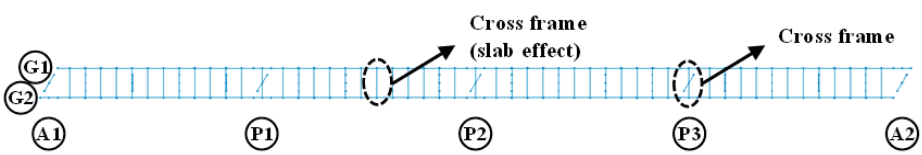

Figure 4.6 Baseline FE model

4.2.2 Formulation of objective function

An objective function to update the baseline FE model is comprised of error function and regularization function. Firstly, the discrepancy between measured and analyzed natural frequencies are equated as Eq. (4.1)

$$e_f(\boldsymbol{\theta}) = \frac{1}{N_f}\sum_{j=1}^{N_f}\left(\frac{f_j^a(\boldsymbol{\theta}) - f_j^m}{f_j^m}\right)^2 \tag{4.1}$$

where e_f is the residual of natural frequency, f_i is i-th natural frequency (i = 1,…,N, N = 3), and the superscripts a and m represent the analyzed and measured values, respectively. The residual of static displacement e_δ is also calculated similarly

$$e_\delta(\boldsymbol{\theta}) = \frac{1}{N_\delta M}\sum_{j}^{N_\delta}\sum_{k}^{M}\left(\frac{\delta_{kj}^a(\boldsymbol{\theta}) - \delta_{kj}^m}{\delta_{kj}^m}\right)^2 \tag{4.2}$$

where δ_{ji} is the vertical displacement value at the j-th displacement transducer (j = 1,…,M, M = 2) in the first span, owing to the i-th load case (i = 1,…,N, N = 3). The superscripts a and m are the same as before. The unregularizad objective function is formulated considering two types of residuals.

$$J(\boldsymbol{\theta}) = e_f(\boldsymbol{\theta}) + e_\delta(\boldsymbol{\theta}) = \left[\frac{1}{N_f}\sum_{i=1}^{N_f}\left(\frac{f_i^a(\boldsymbol{\theta}) - f_{ki}^m}{f_{ki}^m}\right)^2\right] + \left[\frac{1}{N_\delta M}\sum_{i}^{N_\delta}\sum_{j}^{M}\left(\frac{\delta_{ji}^a(\boldsymbol{\theta}) - \delta_{kji}^m}{\delta_{kji}^m}\right)^2\right] \tag{4.3}$$

By adding a regularization function, the n-th regularized objective to obtain n-th updated FE model is expressed as

$$\begin{aligned} J_n(\boldsymbol{\theta}_n) &= [e_{n,f}(\boldsymbol{\theta}_n) + e_{n,\delta}(\boldsymbol{\theta}_n)] + \Pi_R \\ &= \left[\frac{1}{N_f}\sum_{j=1}^{N_f}\left(\frac{f_j^a(\boldsymbol{\theta}_n) - f_j^m}{f_j^m}\right)^2 + \frac{1}{N_\delta M}\sum_{j}^{N_\delta}\sum_{k}^{M}\left(\frac{\delta_{kj}^a(\boldsymbol{\theta}_n) - \delta_{kj}^m}{\delta_{kj}^m}\right)^2\right] + \beta\|\boldsymbol{\theta}_n\|^2 \end{aligned} \tag{4.4}$$

The regularization factor β is taken as 1.0 initially, and modified during each step of optimization if the error function is smaller than regularization function.

4.2.3 Selection of optimization parameters

Prior to solving the optimization problems, appropriate structural parameters for optimization and step-size for Finite Difference Method (FDM) should be determined. The optimization parameters should include key structural parameters. At the same time, the number of total parameters is recommended to be equal or smaller than the number of measurement data to avoid rank-deficiency. For that purpose, total 61 structural parameters are selected preliminarily, which includes density, elastic modulus, moment of inertia, torsional stiffness, and spring coefficient for supports. Structural parameters for two girders at each span are considered as independent variables. The preliminary parameters will be refined and grouped considering their importance and relevancy in the following analysis.

Before finalize the selection of optimization parameters, a proper step-size is determined by using the preliminary optimization parameters. The step-size is used to calculate gradient of objective function as Eq. (4.5) during optimization process.

$$\Delta J_i = \frac{J(\boldsymbol{\theta} + \Delta\theta \cdot \mathbf{e}_i) - J(\boldsymbol{\theta})}{\Delta\theta} \tag{4.5}$$

where $\mathbf{e}_i$ is a unit vector of which only the i-th component is one and others are zero. Considering too small step-size may cause numerical instability, while too large step-size also render incorrect gradient. To find proper step-size that can calculate the gradient for all parameters stably, sensitivity of the ΔJ_i to the variation of step-size is examined. The ΔJ_i is calculated for the preliminary parameters using the unregularized objective function by varying the step-size $\Delta\theta$ from 0.0001 to 0.01. The gradient of objective function is stabilized when step-size larger than 0.005 is employed (Figure 4.7). Therefore, 0.01 is accepted as step-size to calculate gradient of

objective function by using FDM.

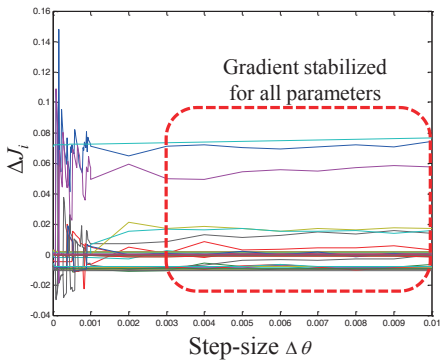

Figure 4.7 Sensitivity of gradient of objective function to step-size variation for preliminary parameters

Next, the importance and relationship of preliminary parameters are analyzed for final selection of optimization parameters. Hundred models are generated by sampling feasible values of the preliminary parameters randomly in the space of structural parameters. For each model, sensitivity of the unregularized objective function is estimated using the step-size. As a result, we obtain sensitivity matrix of objective function with respect to 61 structural parameters of 100 models. The PCA is applied to the sensitivity matrix, and we obtain principal component coefficients that are represented by red vectors in Figure 4.8. As discussed in the section 3.1, principal component coefficients inform degree and direction of structural parameters' contribution to the sensitivity of objective function. In other words, parameters featured by large principal component coefficients are sensitive to the objective function, and important to update FE models. Moreover, parameters with principal component coefficients of same direction can be grouped as a representative parameter. Therefore, nine parameters are determined by selecting effective parameters and grouping similar parameters based on the identified principal component coefficients. Table 4.2 summarizes the structural parameters and their allowable bounds considered in the optimization. An interesting finding is that Young's modulus and moment of inertia are grouped as single parameter for all girders according to the procedure, which is reasonable because multiplication of two parameters determine bending stiffness of girders. Another finding is that the stiffness properties of different girders are contrasted each other even

though they are at the same span. Thus, stiffness of girders are treated as independent parameters in most cases. Through the selecting the nine effective parameters, rank-deficiency problem can be avoided and numerical stability can be enhanced.

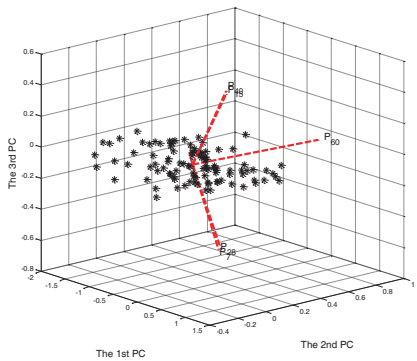

Figure 4.8 Applying PCA to investigate importance and relevancy of structural parameters

Table 4.2 Structural parameters and their allowable bounds considered in the optimization

# of parameter	Structural parameters	Allowable bounds (%)
1	Mass of structural member (vertical direction)	±40
2	Stiffness (*EI*) of girder 1 at span 1	±30
3	Stiffness (*EI*) of girder 2 at span 1	±30
4	Stiffness (*EI*) of girder 2 at span 2	±30
5	Stiffness (*EI*) of girder 1 & 2 at span 4	±30
6	Stiffness (*EI*) of girder 2 at span 3	±30
7	Stiffness (*EI*) of girder 1 at span 3	±30
8	Stiffness (*EI*) of girder 1 at span 2	±30
9	Coefficients of spring support elements (rotational direction)	±40

Before updating multiple FE models, the formulated objective function and optimization parameters need to be verified whether the updated FE model converges to local optimal solution properly or not. For that purpose, prior to multiple FE model update, the baseline FE model is updated by using the single set of measurement data. Numerical stability of the employed method is examined by applying three values of regularization factor that are β=1.0, 0.1 and 0.0. As shown in Figure 4.9, the updated values of structural parameters are almost similar in spite of variation

of regularization factor. Maximum discrepancy between the updated values is about 10%. More importantly, none of the parameters violates the constraints. The convergence of updated FE model to local optimal solution and numerical stability of the optimization procedure can be concluded.

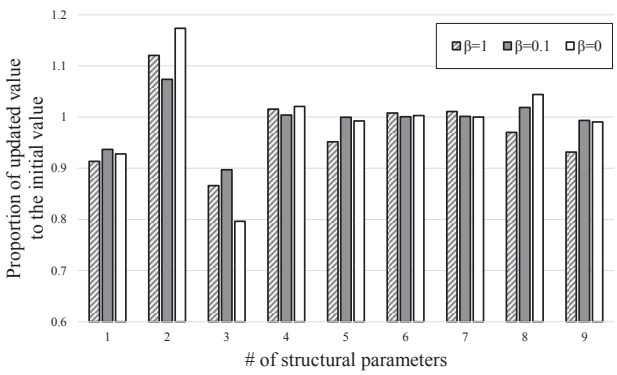

Figure 4.9 Updated values of structural parameters for different regularization factors

For further verification, updating a single FE model is repeated for doubled allowable ranges and unconstrained case. Change rate of the updated values compared to the previously obtained values is calculated, respectively (Figure 4.10). The discrepancies between the updated values are negligible no matter which regularization factors and constraints are applied. This proves that the implemented algorithm successfully finds local optimal solution.

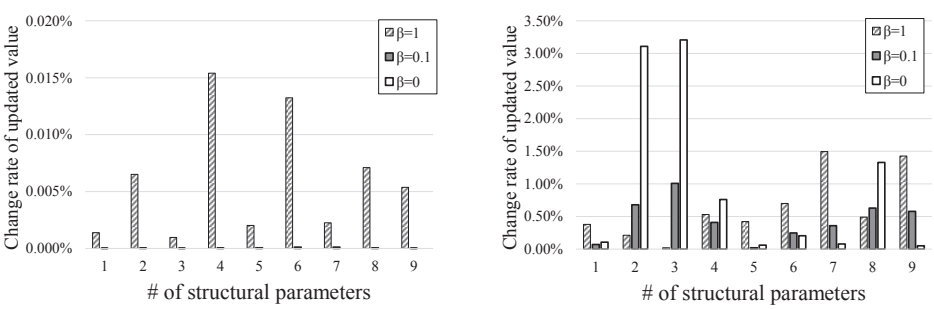

(a) Applying double range of constraints (b) Unconstrained case

Figure 4.10 Change rate of updated values of structural parameters for different constraints

4.2.4 Generating sets of measurement data

In case of Yeondae bridge, only a single set of measurement data is available. Thus, probability models for the measurement uncertainty need to be assumed properly. The single set of measurement data is taken as mean values, and several probability models are considered for case studies.

In the first case study, measurement uncertainty is modeled with uniform distribution. Perturbation amplitudes for displacement and natural frequency are equated as 3% and 1%, respectively, by using Eq. (2.3). The three natural frequencies and displacements by three load cases are sampled independently from the uniform distribution. Next, jointly normal distribution is taken to represent measurement uncertainty. The mean vector is the same as before. A correlation matrix should be appropriate to represent feasible relationship between different or same type of responses. The baseline FE model is utilized to identify the relationship. Numerical simulations with randomly generated models estimate sets of responses, from which the correlation matrix can be inferred (Figure 4.11).

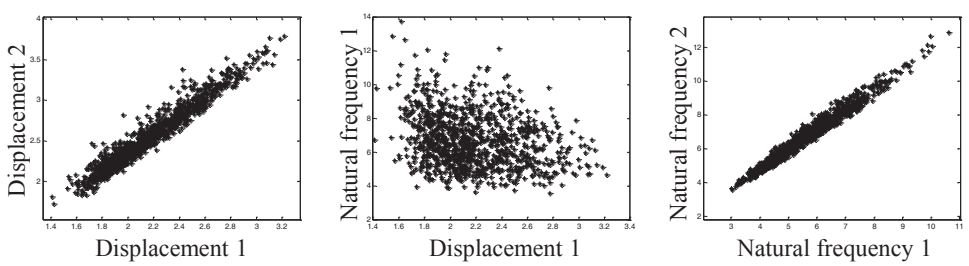

Figure 4.11 Correlation between the simulated responses

The correlation between the natural frequencies is about 0.98 that implies strong positive correlation. The displacements by the same load case are also strongly correlated with each other, while the displacements by different load cases are identified as less strong correlation. Finally, negative and weaker correlation is identified between displacement and natural frequency as about -0.3. Correlation between the nine responses are represented in Table 4.3, where f_i denotes

i-th natural frequency, δ_{ij} denotes the i-th displacement by j-th load case.

Table 4.3 Correlation between the employed responses

	f_1	f_2	f_3	δ_{11}	δ_{21}	δ_{12}	δ_{22}	δ_{13}	δ_{23}
f_1	1	0.97	0.98	-0.29	-0.29	-0.29	-0.29	-0.27	-0.26
f_2	0.97	1	0.98	-0.31	-0.31	-0.31	-0.30	-0.29	-0.27
f_3	0.98	0.98	1	-0.28	-0.28	-0.28	-0.28	-0.27	-0.25
δ_{11}	-0.29	-0.31	-0.28	1	0.99	0.93	0.90	0.84	0.77
δ_{21}	-0.29	-0.31	-0.28	0.99	1	0.98	0.96	0.91	0.84
δ_{12}	-0.29	-0.31	-0.28	0.93	0.98	1	0.99	0.95	0.88
δ_{22}	-0.29	-0.30	-0.28	0.90	0.96	0.99	1	0.97	0.92
δ_{13}	-0.27	-0.29	-0.27	0.84	0.91	0.95	0.97	1	0.98
δ_{23}	-0.26	-0.27	-0.25	0.77	0.84	0.88	0.92	0.98	1

In the meantime, coefficient of variation (C.O.V) of the natural frequencies and displacements for jointly normal distribution also should be defined. The larger variance of associated measurement is represented with larger C.O.V, and in turn, account for higher level of uncertainty. The values of C.O.V are varied, the effects of various level of measurement uncertainty onto the distribution of multiple FE models and assessments are investigated. Distribution types and the statistical parameters for the considered case studies are summarized in Table 4.4. The considered C.O.V values can be related to the perturbation range roughly. In the Table 4.4, the perturbation range means that 95% of sampled data would be located in the interval around the mean values, in case of standard normal distribution with each C.O.V value. Therefore, Case 1 and case 2 may cover similar range of measurement data perturbation even though distribution feature is somewhat different.

For seven case studies, 1,000 sets of measurement data are sampled from associated probability models. Latin Hypercube Sampling (LHS) is implemented for efficient sampling. The method divides the hyperspace of 9 responses into 1,000 intervals equally, and select 1,000 different pairs of data set from each divided sub-domains. In this way, distribution feature of data uncertainty can be described more efficiently using less samples. Finally, 1,000 updated FE

models are obtained by successive optimization using the sets of measurement data for each case study. Each of the multiple FE models can be regarded as the most probable one to represent the behavior of the targeted bridge for the sampled data.

Table 4.4 Distribution types and the statistical parameters for the 7 case studies

	Distribution type	Natural frequency		Static displacement	
		C.O.V	Perturbation	C.O.V	Perturbation
Case 1	Uniform	-	±1%	-	±3%
Case 2	Jointly normal	0.01	±2%	0.01	±2%
Case 3	Jointly normal	0.05	±10%	0.01	±2%
Case 4	Jointly normal	0.05	±10%	0.05	±10%
Case 5	Jointly normal	0.10	±20%	0.01	±2%
Case 6	Jointly normal	0.10	±20%	0.05	±10%
Case 7	Jointly normal	0.10	±20%	0.10	±20%

4.3 Distribution Feature of Multiple FE Models

4.3.1 Case 1: Representation of measurement data uncertainty by the uniform distribution

The 1,000 FE models updated by using measurement data from the uniform distribution are represented in Figure 4.12. In the left figure, distribution of the multiple FE models is plotted regarding updated values of two parameters of which variances are larger than others. The right figure shows the distribution of multiple FE models in the projected principal subspace. Separation and clustering of updated FE models are better revealed by applying PCA. Eigenvector matrix $\mathbf{u}$ and eigenvalue matrix $\mathbf{\Lambda}$ are also obtained as consequence of PCA application to the $\mathbf{\Theta}_{opt}$ of 1,000 updated FE models. The contributions of principal components for the variance of the FE models are identified from the diagonal components of the eigenvalue matrix $\mathbf{\Lambda}$ (Figure 4.13). The figure indicates that more than 95% of the variance of the multiple FE models can be explained by using the 6 largest principal components.

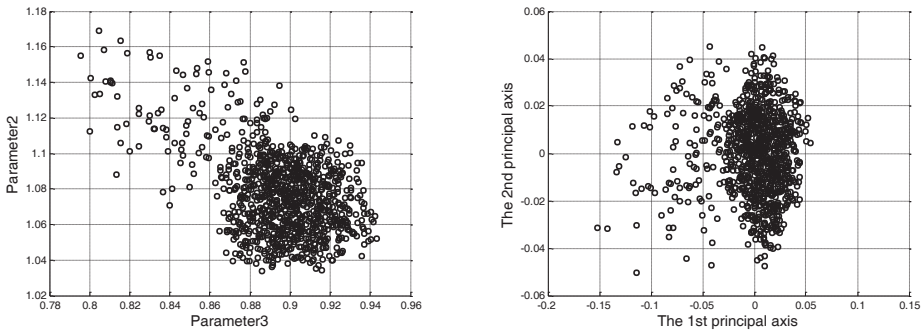

(a) The space of structural parameters (b) Principal subspace

Figure 4.12 Distribution of the updated multiple FE models

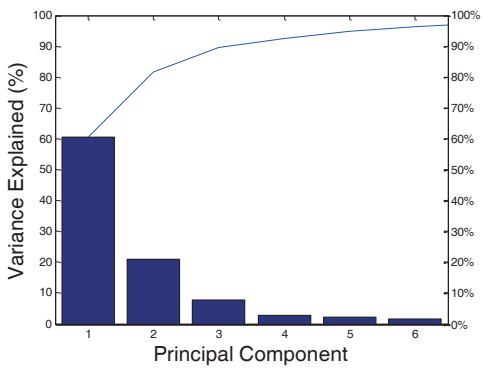

Figure 4.13 Contribution of each principal component to the variance of multiple FE models

The relationship between measurement uncertainty and distribution of multiple FE models is investigated in the space of the first two principal components that explain more than 80% of total variance. In Figure 4.14, every point represents each of multiple FE models in the subspace of the first two principal components. Color legend visualizes the perturbation of the measurement data that is normalized to the mean value using Eq. (3.6). In this case study, variation of the displacement can be related with the 1st principal component, a horizontal axis (Figures 4.14 (d) - (f)). On the other hand, pattern of natural frequency variation is not apparent. The effect of displacement uncertainties are concluded as more important than those of natural frequencies for the distribution of multiple FE models. Meanwhile, black vectors indicate contribution of structural parameters to the distribution of multiple models. The P2 and P3, stiffness of girders at span 1, contribute the most to the principal components, and thus are closely related to the

displacement variation. From the observation, reducing the uncertainty of displacement is expected to result in smaller variance of the P2 and P3, consequently, overall variability of updated FE models may be reduced.

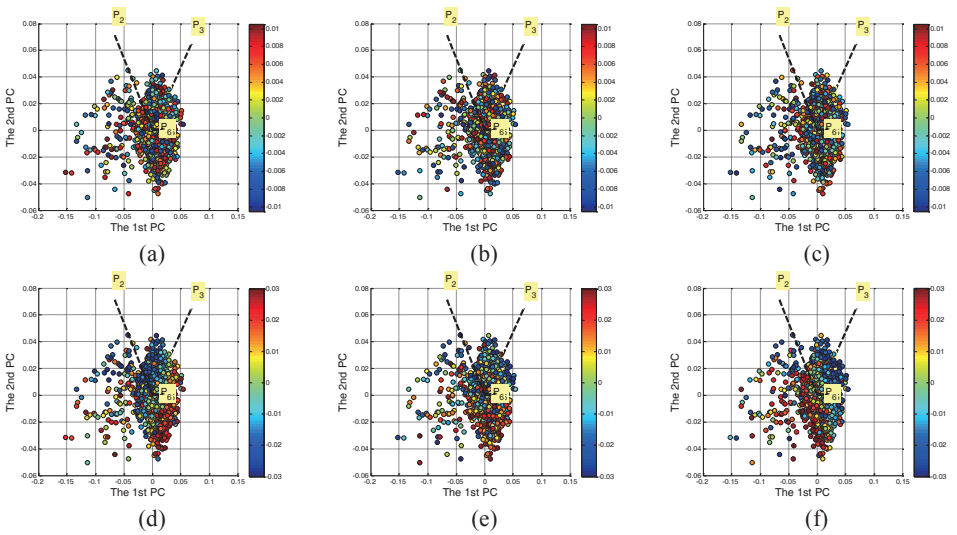

Figure 4.14 Characteristics of FE models with respect to the change rate of measurement data in case of (a) f_1, (b) f_2, (c) f_3, (d) δ_{11}, (e) δ_{12} and (f) δ_{13}

K-means method is then applied to the projected values of structural parameters in the principal subspace. According to the calculated scores (Figure 4.15), the multiple FE models are classified into two groups (Figure 4.16).

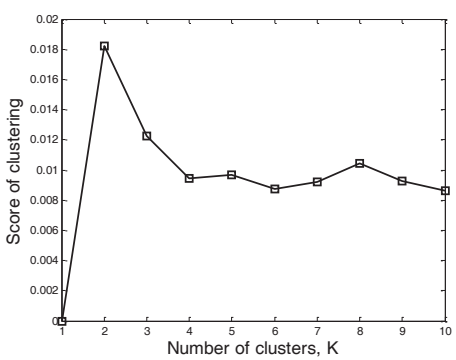

Figure 4.15 Scores of clustering for different number of clusters

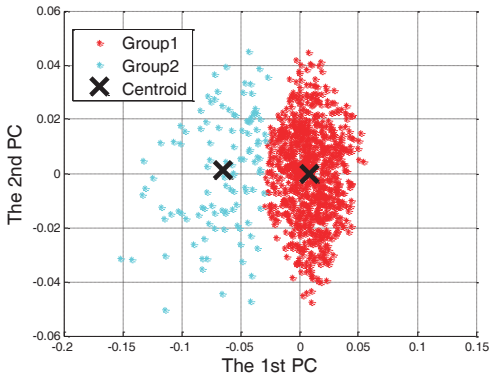

Figure 4.16 Classification of multiple FE models into two groups

Each group of FE models represents possible physical properties of the bridge. Engineer can select a purposed group of models based on both of the own judgment and the information about their characteristic obtained by applying PCA and *K*-means. The significance of specific cluster can be determined from the number of FE models belonged to the cluster. The compactness of the cluster (*WCD*), which can be related to the variability of the updated FE models, is also a good index to represent properties of cluster. In this example, clusters with more FE models and smaller *WCD* are preferred to assess the most probable condition of the bridge. Thus, Group 1 is selected by comparing the two clusters in terms of number of belonged FE models and *WCD* (Table 4.5).

Table 4.5 Properties of the groups in terms of number of FE models and *WCD*

	Group 1	Group 2
Number of FE models	887	113
WCD	0.0263	0.0514

In view of measurement uncertainty, average change rate of responses are smaller in case of the Group 1 (Table 4.6). It means that the FE models in the Group 1 are more suitable to represent typical condition of the bridge on average. The fact is also confirmed by comparing average change rate of the structural parameters for two groups. Table 4.7 summarizes mean values of the updated structural parameters in terms of change rate to the initial value.

Table 4.6 Average value of change rate of responses for the identified groups

	Average change rate (%)	
	Group 1	Group 2
f_1	0.0077	-0.0554
f_2	0.0059	-0.0483
f_3	0.0101	-0.1132
δ_{11}	0.0116	-0.0523
δ_{21}	0.0116	-0.0523
δ_{12}	0.0287	-0.1398
δ_{22}	0.0287	-0.1398
δ_{13}	-0.0412	0.2290
δ_{23}	-0.0412	0.2290

Table 4.7 Average value of change rate of structural parameters for the identified groups

Parameter number	Average change rate (%)	
	Group 1	Group 2
1	-6.345	-7.421
2	7.189	12.029
3	-9.907	-14.733
4	0.471	1.364
5	0.064	-1.792
6	0.083	-1.224
7	-0.031	-1.003
8	1.630	1.948
9	-0.842	-1.028

Next, Gaussin mixture model is fitted to the distribution of multiple FE models in the principal subspace. Regularization parameter is determined as 0.001 and added to the diagonal components of covariance matrices in order to avoid getting ill-conditioned covariance matrices. The number of component PDFs are determined same as the *K*-means application. Figure 4.17 illustrates the two Gaussian component PDFs, which are denoted as component PDF 1 and 2 from the left to the right. Mean vectors of the component PDFs are represented by yellow diamond markers. Contour describes covariance and density of component PDFs. Contour of component PDF 1 located at the left side the figure are not visible. That is accounted for by relative small probability of the component PDF 1. Furthermore, plotting on the multidimensional data onto 2-

D plane also make it difficult to be shown. Mixing coefficients and mean vectors of the two component PDFs are summarized in Table 4.8.

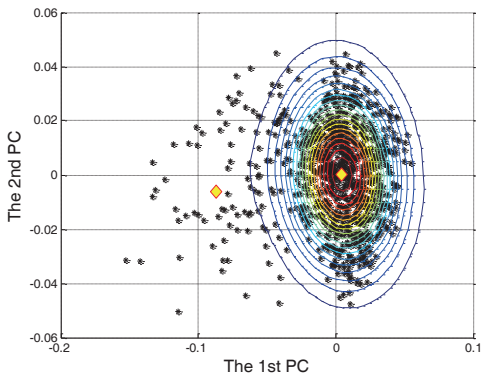

Figure 4.17 Gaussian mixture model to describe distribution of updated FE models

Table 4.8 Mean vectors and mixing coefficients of component PDFs

Component PDF 1		Component PDF 2	
$\boldsymbol{\mu}_1$(*)	π_1	$\boldsymbol{\mu}_2$(*)	π_2
-0.08693	0.050	0.00455	0.950
-0.00607		0.00032	
-0.01452		0.00076	

(*): Coordinate of mean vectors are expressed with respect to the first three principal components

The component PDF 2 is concluded as appropriate to represent condition of the bridge based on the highest mixing coefficient, and small perturbation of data and structural parameters. The selected group for the assessment is similar to that in case of *K*-means method application. The coverage of component PDF 2 is similar to the Group 1 identified by *K*-means method. Likewise, the component PDF 1 is also very similar to the Group 2. It indicates that the two different methods identify similar group of the FE models based on the similarity of FE models.

4.3.2 Case 2: Representation of measurement data uncertainty by the jointly normal distribution

In the case 2, uncertainty of natural frequency and displacement are represented by jointly normal distribution with C.O.Vs 0.01 of both responses. The uncertainty level of the probability model

is similar to that considered in case 1. Figure 4.18 shows the distribution of the 1,000 FE models updated by using measurement data sampled from the jointly normal distribution. Scattering and clustering of models are better revealed as consequence of PCA application likewise the previous case study. The first four principal components can expalin more than 95% of total variance (Figure 4.19), which means importance of the few principal component is emphasized than before.

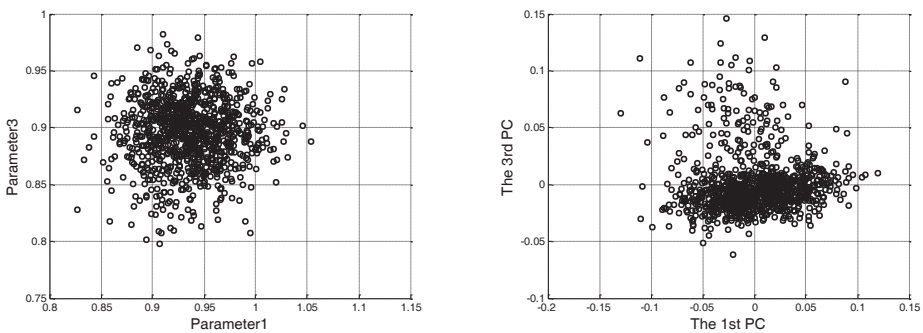

(a) The space of structural parameters (b) Principal subspace

Figure 4.18 Distribution of the updated multiple FE models

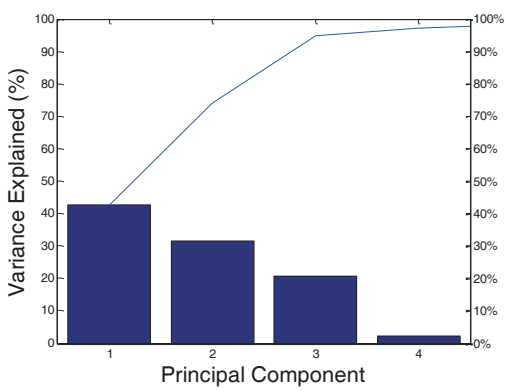

Figure 4.19 Contribution of each principal component to the variance of multiple FE models

The relationship between measurement uncertainty and distribution of multiple FE models is also investigated in the plane of the first two principal components (Figure 46). In contrast to the case 1, variations of the displacement and natural frequency are shown apparently. The different type of distribution model with slightly modified perturbation range cause the difference. Especially, variation of the natural frequency can be related to the perturbation of mass properties

(Figures 4.20 (a) - (c)), while that of the displacement account for the perturbation of stiffness of girders at the first span (Figures 4.20 (d) - (f)). Therefore, stiffness of the first span and mass properties may affect most to the following assessment in close relation to the uncertainty of displacement and natural frequency.

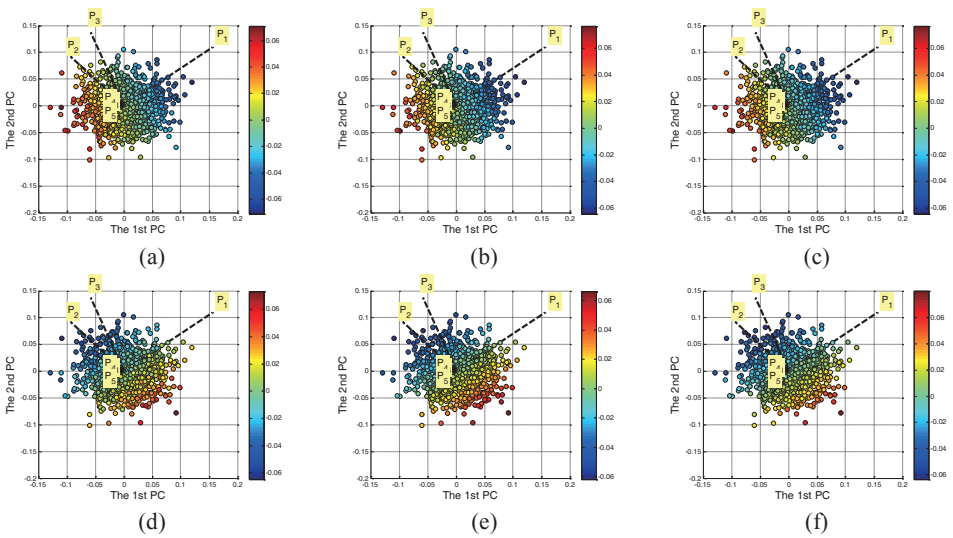

Figure 4.20 Characteristics of FE models with respect to the change rate of measurement data in case of (a) f_1, (b) f_2, (c) f_3, (d) δ_{11}, (e) δ_{12} and (f) δ_{13}

The multiple FE models are classified into three groups (Figure 4.21) based on the score function evaluation (Figure 4.22). In this case, combination of Group 2 and Group 3 is regarded to represent the typical condition of the bridge. The FE models of Group 1 can be considered as assemble of outliers, which is also supported by larger *WCD* (Table 4.9) and wider perturbation of structural parameters (Table 4.11). In the meantime, FE models in Group 2 and Group 3 represent more flexible and stiffer condition of structure, respectively, which are inferred from variation of the responses (Table 4.10) and the updated values of structural parameters (Table 4.11).

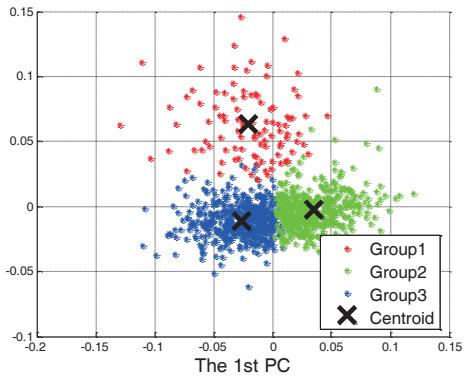

Figure 4.21 Classification of multiple FE models into three groups

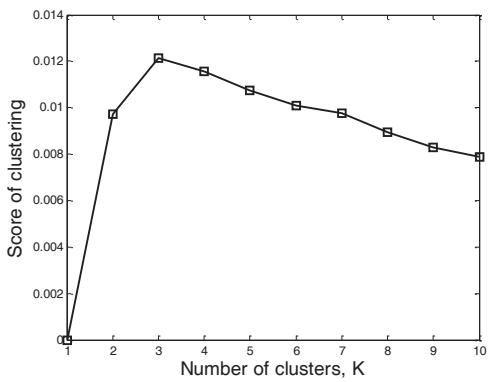

Figure 4.22 Scores of clustering for different number of clusters

Table 4.9 Properties of the groups in terms of number of FE models and *WCD*

	Group 1	Group 2	Group 3
Number of FE models	100	423	477
WCD	0.0613	0.0419	0.0415

Table 4.10 Average value of change rate of each responses for the identified groups

	Average change rate (%)		
	Group 1	Group 2	Group 3
f_1	0.430	-1.621	1.347
f_2	0.434	-1.629	1.355
f_3	0.393	-1.620	1.355
δ_{11}	-0.166	1.139	-0.973
δ_{21}	-0.121	1.182	-1.023
δ_{12}	-0.070	1.196	-1.046
δ_{22}	-0.019	1.193	-1.051
δ_{13}	0.114	1.154	-1.044
δ_{23}	0.209	1.078	-0.999

Table 4.11 Average value of change rate of structural parameters for the identified groups

Parameter number	Average change rate (%)		
	Group 1	Group 2	Group 3
1	-8.439	-3.764	-8.354
2	11.885	5.865	8.418
3	-14.800	-11.337	-8.690
4	1.587	-0.048	0.869
5	-1.987	-0.618	0.563
6	-1.287	-0.217	0.333
7	-1.353	-0.328	0.182
8	2.269	1.210	1.992
9	-0.913	-1.170	-0.581

Next, Gaussin mixture model is fitted to the distribution of multiple FE models in the principal subspace likewise the previous case study. The three component PDFs in Figure 4.23 are denoted as component PDF 1, 2 and 3 from the left to the right. Table 4.12 summarizes mixing coefficients and mean vectors of three component PDFs. It is obvious that component PDF 3 takes most of the reponsibility to describe distribution of FE models. FE models belonged to the component PDF 3 are also very similar to those of Group 2 and Group 3 identified by *K*-means method. The group of FE models can be regarded to indicate most probable structural condition. Remaining FE models can be considered as outliers, highly influence by noise or modeling error, rather than meaningful distribution.

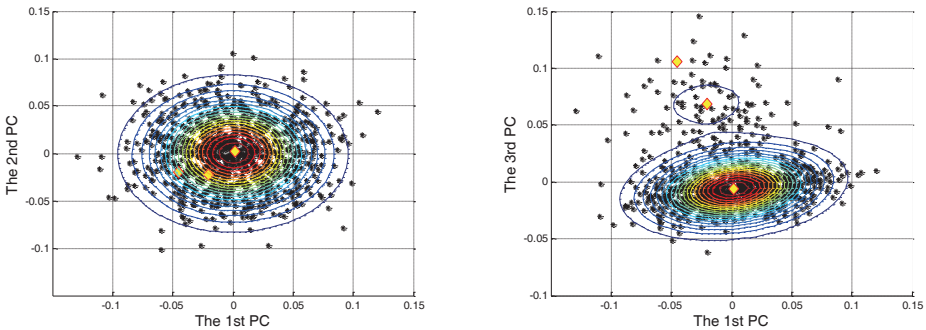

(a) In the plane of the 1st and the 2nd PCs (b) In the plane of the 1st and the 3rd PCs

Figure 4.23 Gaussian mixture model to describe distribution of updated FE models

Table 4.12 Mean vectors and mixing coefficients of component PDFs

Component PDF 1		Component PDF 2		Component PDF 3	
$\boldsymbol{\mu}_1$(*)	π_1	$\boldsymbol{\mu}_2$(*)	π_2	$\boldsymbol{\mu}_3$(*)	π_3
-0.0454	0.008	-0.0201	0.068	0.0019	0.924
-0.0195		-0.0222		0.0018	
0.1061		0.0685		-0.0059	

(*): Coordinate of mean vectors are expressed with respect to the first three principal components

4.3.3 Case 3: Representation of measurement data uncertainty by the jointly normal distribution

In the case 3, C.O.V of the jointly normal distribution corresponding to natural frequency is increased as 0.05 to consider higher level of uncertainty. Figure 4.24 shows the distribution of the 1,000 FE models in the space of structural parameters and principal subspace, respectively.

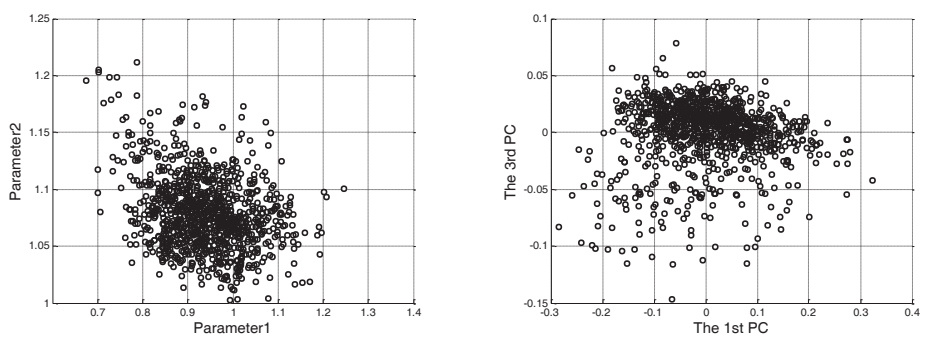

(a) The space of structural parameters (b) Principal subspace

Figure 4.24 Distribution of the updated multiple FE models

In this case, 95% of the distribution of multiple FE models can be described by using only the first three principal components (Figure 4.25).

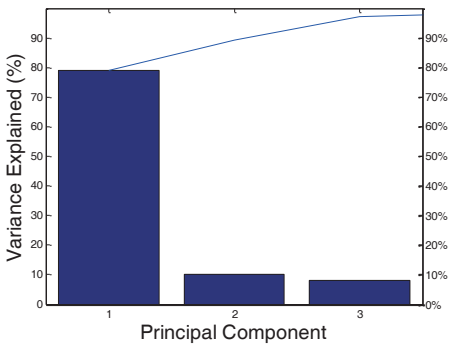

Figure 4.25 Contribution of each principal component to the variance of multiple FE models

The relationship between measurement uncertainty and distribution of multiple FE models is similar to the previous case (Figure 4.26). Variations of the natural frequency and displacement are related the first principal component and the second principal component, respectively. In addition, mass properties and stiffness of girders at the first span vary sensitively to the uncertainty of measurement data, same as before.

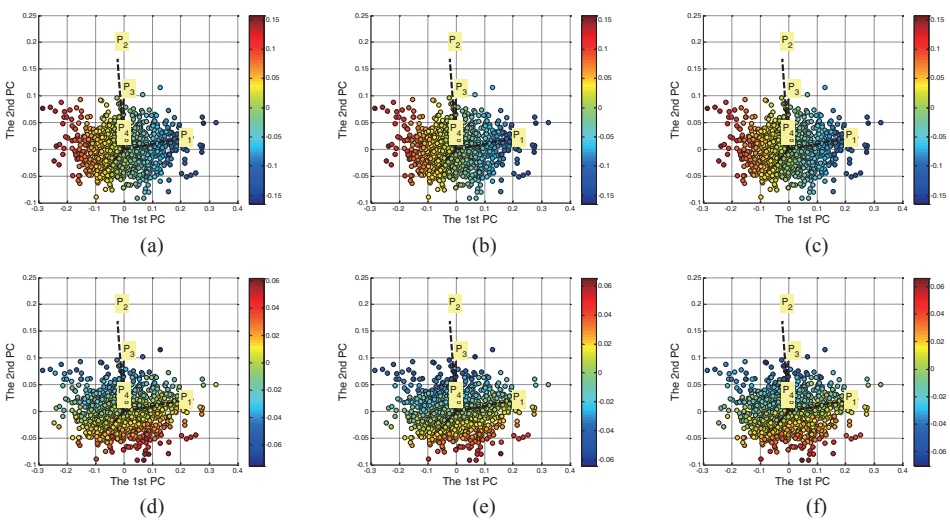

Figure 4.26 Characteristics of FE models with respect to the change rate of measurement data in case of (a) f_1, (b) f_2, (c) f_3, (d) δ_{11}, (e) δ_{12} and (f) δ_{13}

The multiple FE models are classified into two groups (Figure 4.27) based on the score function evaluation (Figure 4.28). Properties of the two groups are similar in terms of number of FE models and *WCD* (Table 4.13), while their structural properties contrast each other as either more flexible or stiffer, respectively (Tables 4.14 and 4.15).

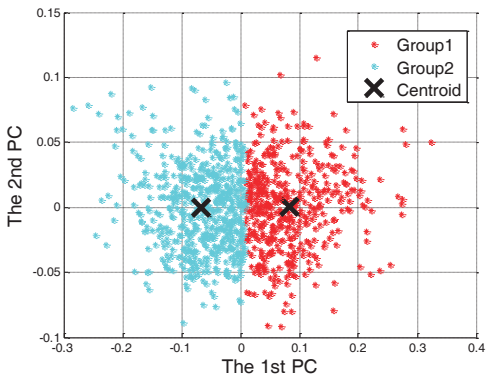

Figure 4.27 Classification of multiple FE models into two groups

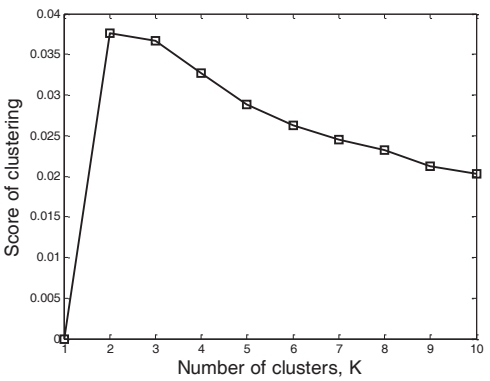

Figure 4.28 Scores of clustering for different number of clusters

Table 4.13 Properties of the groups in terms of number of FE models and *WCD*

	Group 1	Group 2
Number of FE models	446	554
WCD	0.0725	0.0747

Table 4.14 Average value of change rate of each responses for the identified groups

	Average change rate (%)	
	Group 1	Group 2
f_1	-4.389	3.532
f_2	-4.395	3.538
f_3	-4.409	3.551
δ_{11}	0.505	-0.407
δ_{21}	0.500	-0.403
δ_{12}	0.474	-0.381
δ_{22}	0.453	-0.364
δ_{13}	0.409	-0.330
δ_{23}	0.360	-0.291

Table 4.15 Average value of change rate of structural parameters for the identified groups

Parameter number	Average change rate (%)	
	Group 1	Group 2
1	1.658	-12.553
2	7.108	8.560
3	-10.724	-10.539
4	-0.246	1.190
5	-2.313	0.797
6	-0.853	0.402
7	-1.035	0.299
8	0.873	2.244
9	-1.269	-0.671

The Gaussian mixture model for the updated FE models are shown in the plane of PC 1 and PC 2 (Figure 4.29 (a)). For better visulization, the plane of PC 1 and PC 3 is also taken to plot the Gaussian mixture model along with distribution of updated FE models (Figure 4.29 (b)). The two component PDFs are denoted as component PDF 1 and 2 from the left to the right. Table 4.16 summarizes mixing coefficients and mean vectors of three component PDFs. The component PDF 2 takes most of the reponsibility to describe distribution of FE models while the component PDF 1 can be regarded to indicate outliers. In this case, classificaion of FE models by *K*-means method and Gaussian mixture model is quite different. It proves better performance of Gaussian mixture

model over the *K*-means method to classify ambigiously separated FE models.

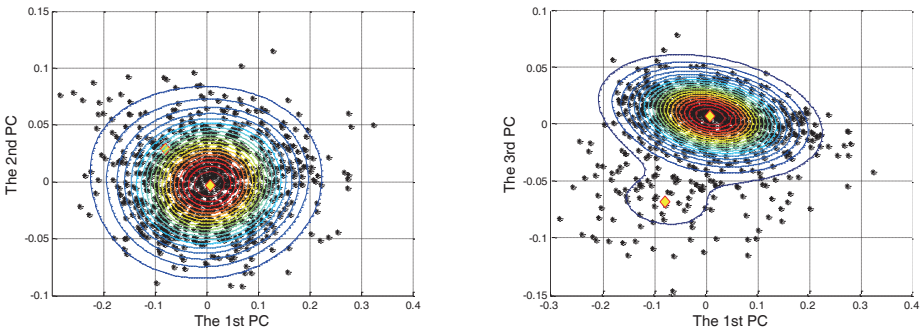

(a) In the plane of the 1st and the 2nd PCs (b) In the plane of the 1st and the 3rd PCs

Figure 4.29 Gaussian mixture model to describe distribution of updated FE models

Table 4.16 Mean vectors and mixing coefficients of component PDFs

Component PDF 1		Component PDF 2	
μ_1(*)	π_1	μ_2(*)	π_2
-0.0792	0.088	0.0077	0.912
0.0294		-0.0029	
-0.0683		0.0066	

(*): Coordinate of mean vectors are expressed with respect to the first three principal components

4.3.4 Case 4: Representation of measurement data uncertainty by the jointly normal distribution

In the case 4, C.O.V values of the displacement and natural frequency are increased as 0.05. The distribution of the 1,000 updated FE models is shown in the space of structural parameters and principal subspace, respectively (Figure 4.30). According to the increase of uncertainty level, structural parameters of several updated FE models became to lie on the constraints. The first three principal components can explaine more than 95% of the variance of multiple FE models (Figure 4.31). The relationship between measurement uncertainty and distribution of multiple FE models is similar to the previous case (Figure 4.32), which are more apparent than before according to the increase of uncertainty level for displacement.

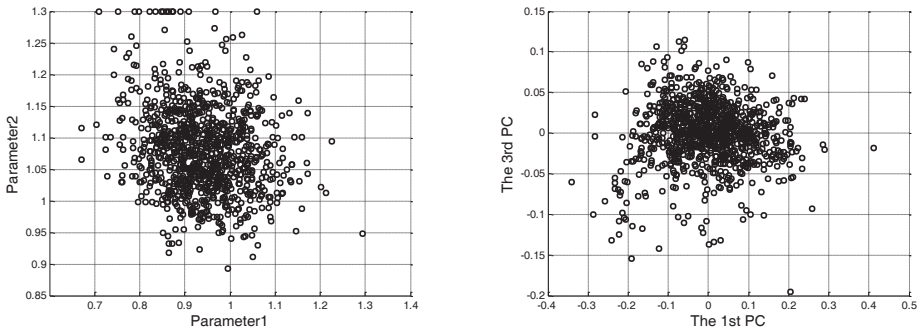

(a) The space of structural parameters (b) Principal subspace

Figure 4.30 Distribution of the updated multiple FE models

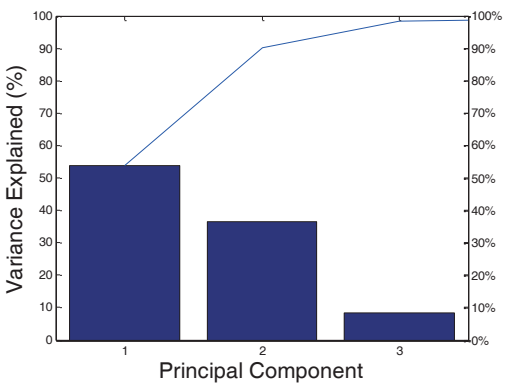

Figure 4.31 Contribution of each principal component to the variance of multiple FE models

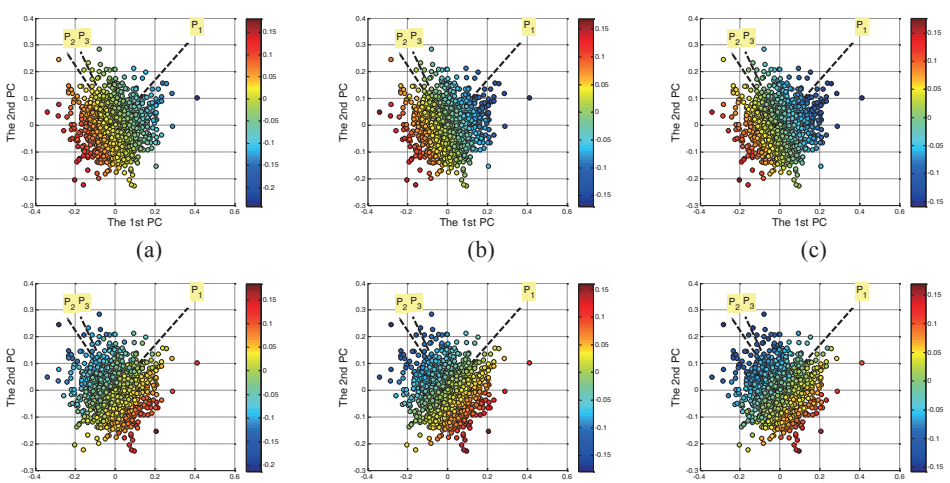

(a) (b) (c)

(d) (e) (f)

Figure 4.32 Characteristics of FE models with respect to the change rate of measurement data in case of (a) f_1, (b) f_2, (c) f_3, (d) δ_{11}, (e) δ_{12} and (f) δ_{13}

The multiple FE models are classified into three groups (Figure 4.33) based on the score function evaluation (Figure 4.34). Properties of the three groups are similar in terms of number of FE models and *WCD* (Table 4.17). FE models in Group 2 and Group 3 are featured by more flexible and stiffer structural conditions, respectively (Tables 4.18 and 4.19). Properties of FE models in Group 1 are similar to those in Group 3, except that more flexible spring supports are considered in order to allow larger displacements.

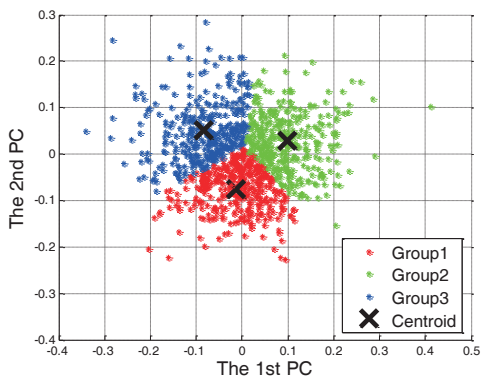

Figure 4.33 Classification of multiple FE models into three groups

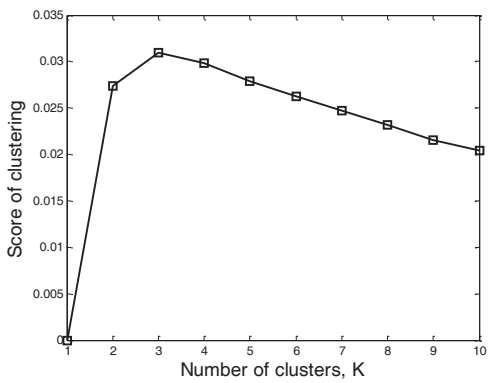

Figure 4.34 Scores of clustering for different number of clusters

Table 4.17 Properties of the groups in terms of number of FE models and *WCD*

	Group 1	Group 2	Group 3
Number of FE models	345	327	328
WCD	0.087	0.093	0.102

Table 4.18 Average value of change rate of each responses for the identified groups

	Average change rate (%)		
	Group 1	Group 2	Group 3
f_1	2.619	-5.299	2.512
f_2	2.474	-5.287	2.669
f_3	2.661	-5.310	2.496
δ_{11}	2.665	2.157	-4.967
δ_{21}	2.802	2.223	-5.164
δ_{12}	2.875	2.233	-5.255
δ_{22}	2.892	2.223	-5.259
δ_{13}	2.879	2.113	-5.132
δ_{23}	2.759	1.969	-4.863

Table 4.19 Average value of change rate of structural parameters for the identified groups

Parameter number	Average change rate (%)		
	Group 1	Group 2	Group 3
1	-11.726	2.819	-9.145
2	4.484	5.083	14.744
3	-13.817	-12.445	-4.237
4	0.333	-0.732	2.311
5	0.744	-2.708	0.517
6	0.336	-1.102	0.375
7	0.291	-1.230	0.168
8	1.600	0.450	3.271
9	-1.271	-1.589	0.357

The Gaussian mixture model for the updated FE models are shown in Figure 4.35. The three component PDFs are denoted as component PDF 1, 2 and 3 from the left to the right. Table 4.20 summarizes mixing coefficients and mean vectors of three component PDFs. The component PDF 2 takes most of the reponsibility to describe distribution of FE models while others can be regarded to indicate distribution of outliers. This example also shows better performance of Gaussian mixture model over the *K*-means method to classify ambigiously separated FE models.

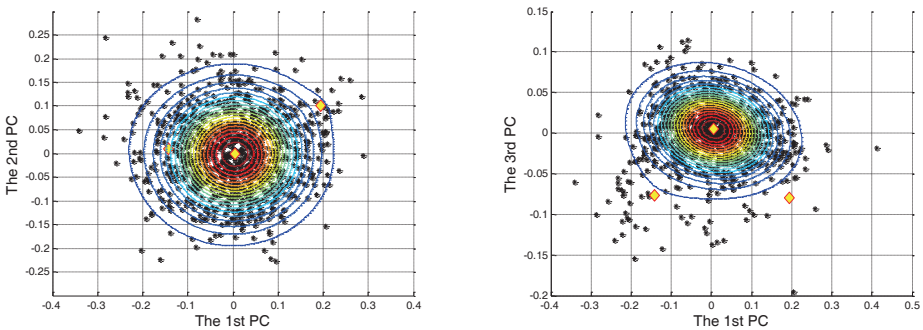

(a) In the plane of the 1st and the 2nd PCs (b) In the plane of the 1st and the 3rd PCs

Figure 4.35 Gaussian mixture model to describe distribution of updated FE models

Table 4.20 Mean vectors and mixing coefficients of component PDFs

Component PDF 1		Component PDF 2		Component PDF 3	
$\boldsymbol{\mu}_1$(*)	π_1	$\boldsymbol{\mu}_2$(*)	π_2	$\boldsymbol{\mu}_3$(*)	π_3
-0.142	0.048	0.005	0.942	0.194	0.010
0.009		-0.002		0.101	
-0.076		0.005		-0.079	

(*): Coordinate of mean vectors are expressed with respect to the first three principal components

4.3.5 Case 5: Representation of measurement data uncertainty by the jointly normal distribution

In case 5, much higher level of uncertainty is applied to the natural frequency with C.O.V 0.10. C.O.V of the displacement is reduced as 0.01. Severe non-linearity is shown in the distribution of the updated FE models (Figure 4.36).

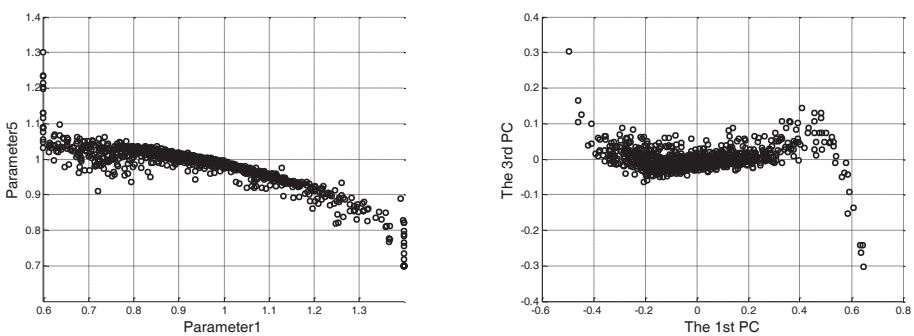

(a) The space of structural parameters (b) Principal subspace

Figure 4.36 Distribution of the updated multiple FE models

In this case, 95% of the distribution of multiple FE models can be described by using only the first three principal components (Figure 4.37). However, the first principal component take most of the responsibility of which contribution is almost 90%. Therefore, the first principal component is expected to be closely related with the variation of natural frequency. As expected, the relationship between variation of natural frequency and distribution of multiple FE models is revealed apparently along the first principal component, while that for the displacement is not (Figure 4.38). Mass properties are mainly related to the variation of natural frequency. Whereas, the non-linearity near the edge of figures can be associated with perturbation of parameter 2, 3, 5 and 7, which represent stiffness of girders at different spans (Table 4.2).

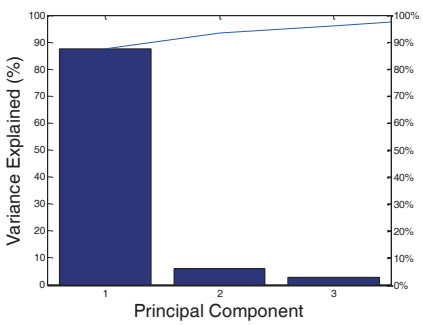

Figure 4.37 Contribution of each principal component to the variance of multiple FE models

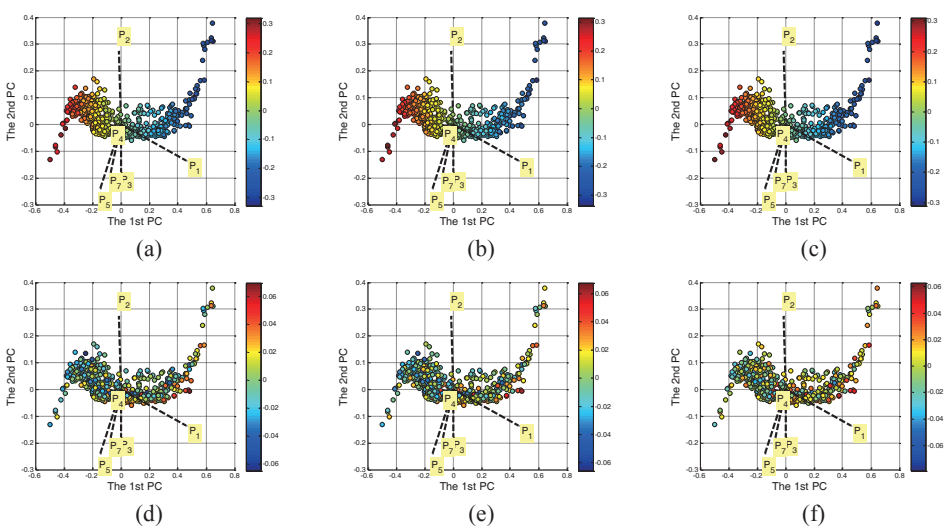

Figure 4.38 Characteristics of FE models with respect to the change rate of measurement data in case of (a) f_1, (b) f_2, (c) f_3, (d) δ_{11}, (e) δ_{12} and (f) δ_{13}

The multiple FE models are classified into six groups (Figure 4.39) based on the score function evaluation (Figure 4.40). In this case, any of the groups cannot be assured as dominant. Group 1, 4 and 5 are regarded to represent extreme structural conditions, which are supported by very large perturbation of measurement data and structural parameters (Table 4.21 and 4.22).

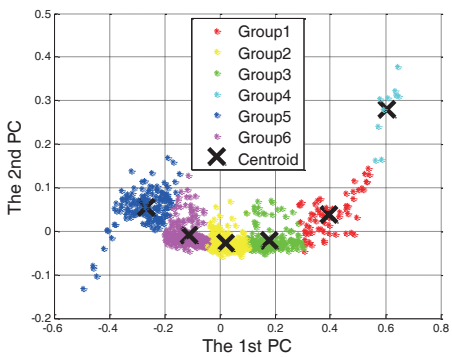

Figure 4.39 Classification of multiple FE models into six groups

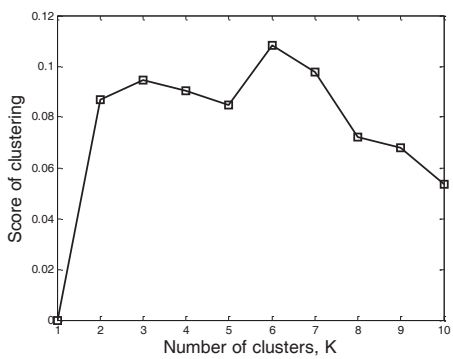

Figure 4.40 Scores of clustering for different number of clusters

Table 4.21 Properties of the groups in terms of number of FE models and *WCD*

	Group 1	Group 2	Group 3	Group 4	Group 5	Group 6
Number of FE models	64	296	197	11	163	269
WCD	0.107	0.059	0.071	0.151	0.099	0.064

Table 4.22 Average value of change rate of each responses for the identified groups

	Average change rate (%)					
	Group 1	Group 2	Group 3	Group 4	Group 5	Group 6
f_1	-17.229	-2.060	-9.617	-26.288	14.676	5.587
f_2	-17.315	-1.991	-9.647	-25.740	14.794	5.456
f_3	-17.368	-2.048	-9.672	-26.113	14.891	5.514
δ_{11}	0.760	0.193	0.504	0.833	-0.797	-0.310
δ_{21}	0.756	0.181	0.504	0.923	-0.789	-0.311
δ_{12}	0.711	0.158	0.488	1.064	-0.747	-0.291
δ_{22}	0.694	0.143	0.499	1.093	-0.733	-0.288
δ_{13}	0.688	0.105	0.533	1.073	-0.697	-0.300
δ_{23}	0.668	0.078	0.537	1.045	-0.643	-0.293

Table 4.23 Average value of change rate of structural parameters for the identified groups

Parameter number	Average change rate (%)					
	Group 1	Group 2	Group 3	Group 4	Group 5	Group 6
1	31.098	-2.664	11.972	40.000	-30.888	-15.760
2	11.727	7.321	7.629	17.250	13.136	8.211
3	-14.952	-10.278	-11.123	-15.106	-15.025	-10.427
4	-2.115	0.121	-1.082	-12.780	3.849	1.356
5	-16.043	-1.021	-5.822	-30.000	3.045	1.605
6	-5.439	-0.335	-2.254	-24.450	1.818	0.749
7	-5.938	-0.457	-2.432	-26.388	1.705	0.619
8	-1.318	1.296	-0.114	-15.813	4.824	2.476
9	-2.262	-1.090	-1.823	-7.789	0.071	-0.528

In spite of the complex distribution of FE models, the Gaussian mixture model successfully describes them by the superposition of six component PDFs (Figure 4.41). Table 4.24 summarizes mixing coefficients and mean vectors of the component PDFs. The component PDF 4 of highest mixing coefficient is thought as dominant one, while the component PDF 2 may also represent meaningful structural condition. Remaining component PDFs can be regarded as to indicate less probable structural conditions by the effect of extremely perturbed measurement data or the noise.

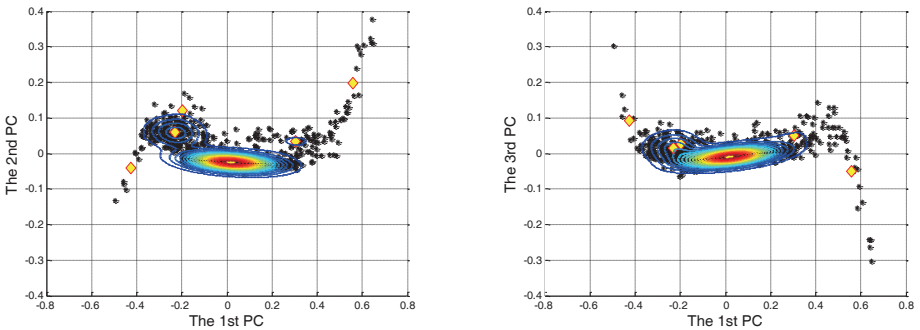

(a) In the plane of the 1st and the 2nd PCs (b) In the plane of the 1st and the 3rd PCs

Figure 4.41 Gaussian mixture model to describe distribution of updated FE models

Table 4.24 Mean vectors and mixing coefficients of component PDFs

Component PDF 1		Component PDF 2		Component PDF 3	
$\boldsymbol{\mu}_1$(*)	π_1	$\boldsymbol{\mu}_2$(*)	π_2	$\boldsymbol{\mu}_3$(*)	π_3
-0.426	0.010	-0.229	0.176	-0.197	0.007
-0.042		0.059		0.120	
0.093		0.014		0.027	
Component PDF 4		Component PDF 5		Component PDF 6	
$\boldsymbol{\mu}_4$(*)	π_4	$\boldsymbol{\mu}_5$(*)	π_5	$\boldsymbol{\mu}_6$(*)	π_6
0.018	0.717	0.304	0.069	0.559	0.021
-0.024		0.035		0.198	
-0.008		0.051		-0.050	

(*): Coordinate of mean vectors are expressed with respect to the first three principal components

4.3.6 Case 6: Representation of measurement data uncertainty by the jointly normal distribution

In case 6, C.O.V of displacement is increased as 0.05 compared to the previous case. Non-linear distribution of the updated FE models is also found (Figure 4.42). The first three principal components can explain more than 95% of the variance of multiple FE models (Figure 4.43).

The distribution of FE models is closely related to the variation of natural frequency and displacement, likewise the case 2, 3 and 4 (Figure 4.44). Mass properties and stiffness of girders at the first span are also the most sensitive parameters to the uncertainty of measurement data.

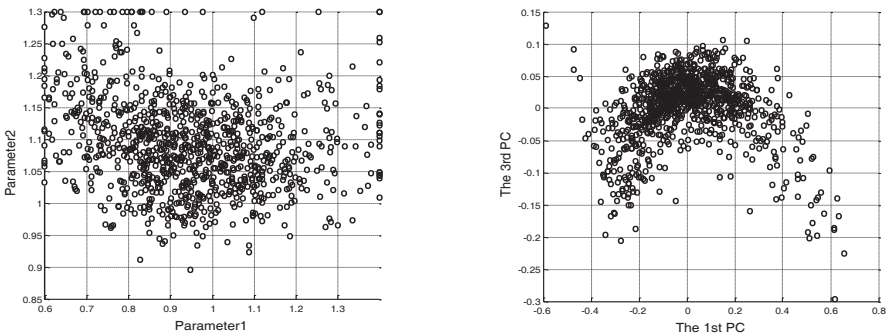

(a) The space of structural parameters (b) Principal subspace

Figure 4.42 Distribution of the updated multiple FE models

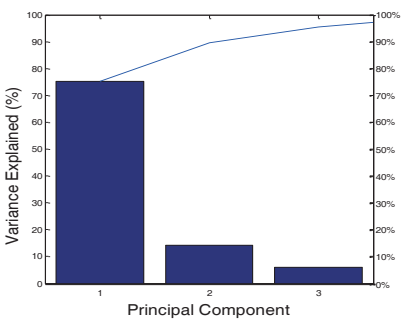

Figure 4.43 Contribution of each principal component to the variance of multiple FE models

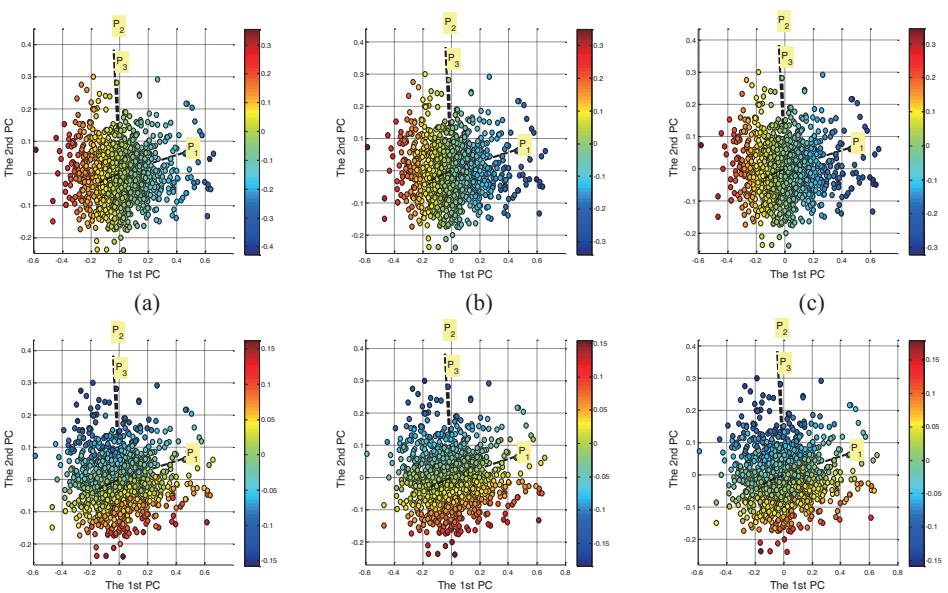

Figure 4.44 Characteristics of FE models with respect to the change rate of measurement data in case of (a) f_1, (b) f_2, (c) f_3, (d) δ_{11}, (e) δ_{12} and (f) δ_{13}

The multiple FE models are classified into three groups (Figure 4.45) based on the score function evaluation (Figure 4.46). Properties of the identified groups are summarized in Tables 4.25, 4.26 and 4.27. Properties of FE models in Group 1 and Group 2 contrast each other with respect to variation of measurement data and the structural parameters, which are either stiffer or more flexible structural condition. FE models in Group 3 indicate less probable condition of structures under rarely observable measurement data.

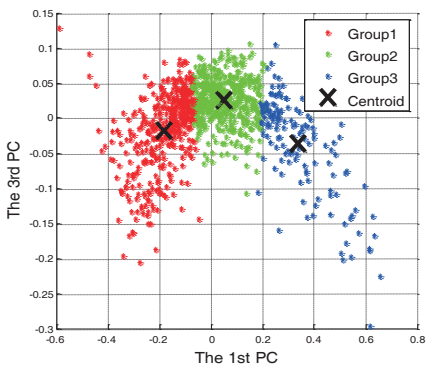

Figure 4.45 Classification of multiple FE models into three groups

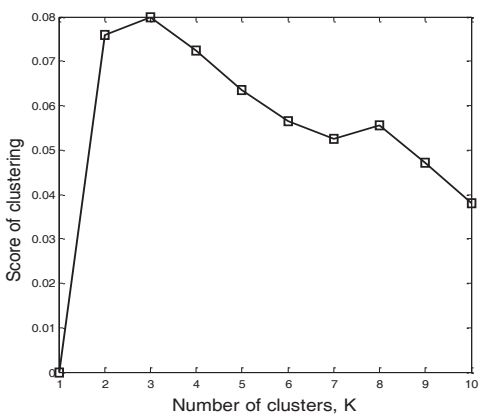

Figure 4.46 Scores of clustering for different number of clusters

Table 4.25 Properties of the groups in terms of number of FE models and *WCD*

	Group 1	Group 2	Group 3
Number of FE models	386	474	140
WCD	0.147	0.117	0.181

Table 4.26 Average value of change rate of each responses for the identified groups

	Average change rate (%)		
	Group 1	Group 2	Group 3
f_1	9.797	-3.349	-15.731
f_2	9.830	-3.398	-15.604
f_3	9.865	-3.362	-15.802
δ_{11}	-1.594	0.743	1.880
δ_{21}	-1.578	0.706	1.958
δ_{12}	-1.500	0.619	2.021
δ_{22}	-1.440	0.564	2.066
δ_{13}	-1.309	0.450	2.100
δ_{23}	-1.163	0.342	2.051

Distribution of the updated FE models are described by Gaussian mixture models with three component PDFs (Figure 4.47). Each of the component PDFs can be related rougly to the groups identified by applying *K*-means method, while coverage of them are somewhat different. The Gaussian mixture model shows better performance for classifying the updated FE models.

Table 4.27 Average value of change rate of structural parameters for the identified groups

Parameter number	Average change rate (%)		
	Group 1	Group 2	Group 3
1	-22.352	-0.181	25.061
2	11.972	6.897	8.974
3	-11.084	-10.395	-14.745
4	2.841	-0.079	-3.023
5	2.469	-1.883	-13.357
6	1.430	-0.695	-5.806
7	1.270	-0.840	-6.175
8	3.978	1.023	-2.100
9	0.131	-1.151	-2.744

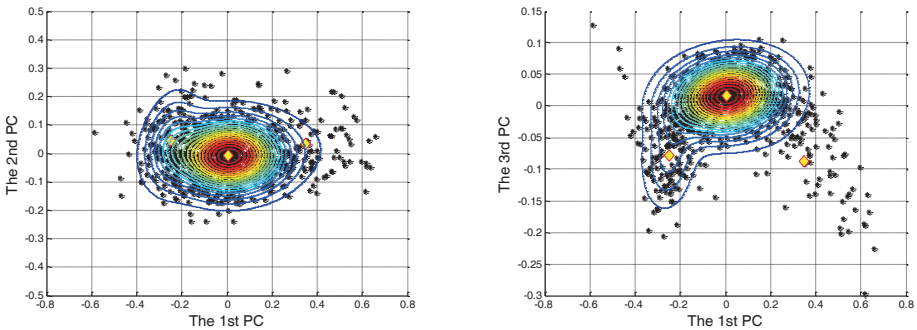

(a) In the plane of the 1st and the 2nd PCs (b) In the plane of the 1st and the 3rd PCs

Figure 4.47 Gaussian mixture model to describe distribution of updated FE models

Table 4.28 Mean vectors and mixing coefficients of component PDFs

Component PDF 1		Component PDF 2		Component PDF 3	
$\boldsymbol{\mu}_1$(*)	π_1	$\boldsymbol{\mu}_2$(*)	π_2	$\boldsymbol{\mu}_3$(*)	π_3
-0.250	0.106	0.006	0.834	0.347	0.061
0.047		-0.008		0.034	
-0.078		0.016		-0.087	

(*): Coordinate of mean vectors are expressed with respect to the first three principal components

4.3.7 Case 7: Representation of measurement data uncertainty by the jointly normal distribution

C.O.V values of both responses are assumed as 0.10 that may be very extreme measurement uncertainty conditions. As results of the highest level of measurement uncertainty, more of the updated FE models lie on the constraints. Nevertheless, most of the updated models are still found within the constraint.

Since the level of uncertainty for the two types of responses are same, discrepancy between the contribution of the first three principal components became smaller (Figure 4.49). In other words, distribution of the FE models cannot be expalined by single variables, but two or three variables are required.

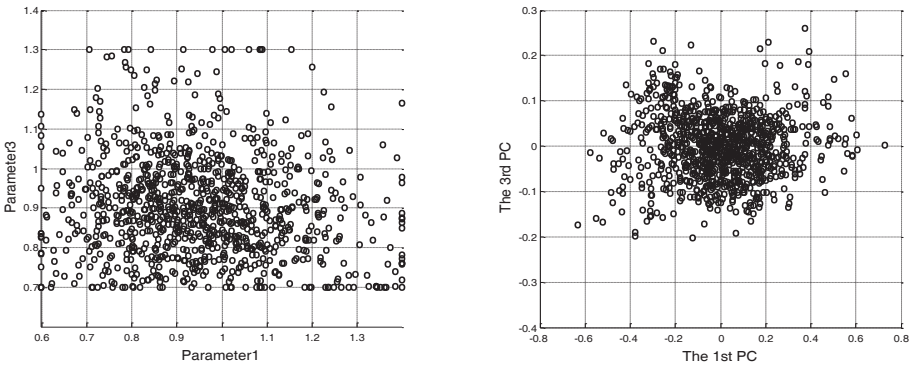

(a) The space of structural parameters (b) Principal subspace

Figure 4.48 Distribution of the updated multiple FE models

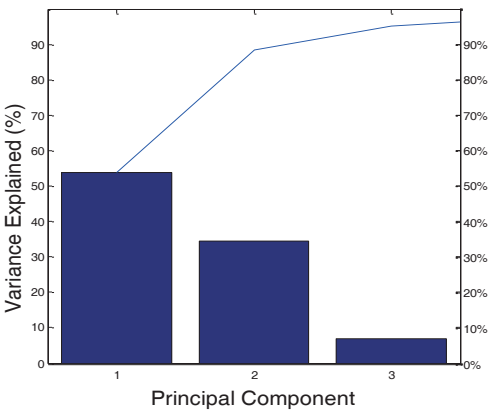

Figure 4.49 Contribution of each principal component to the variance of multiple FE models

The relationship between measurement data uncertainties and structural parameters is same as before (Figure 4.50).

The multiple FE models are classified into three groups (Figure 4.51) based on the score function evaluation (Figure 4.52). Features of the three identified groups are similar to those for case 4 in section 4.3.4.

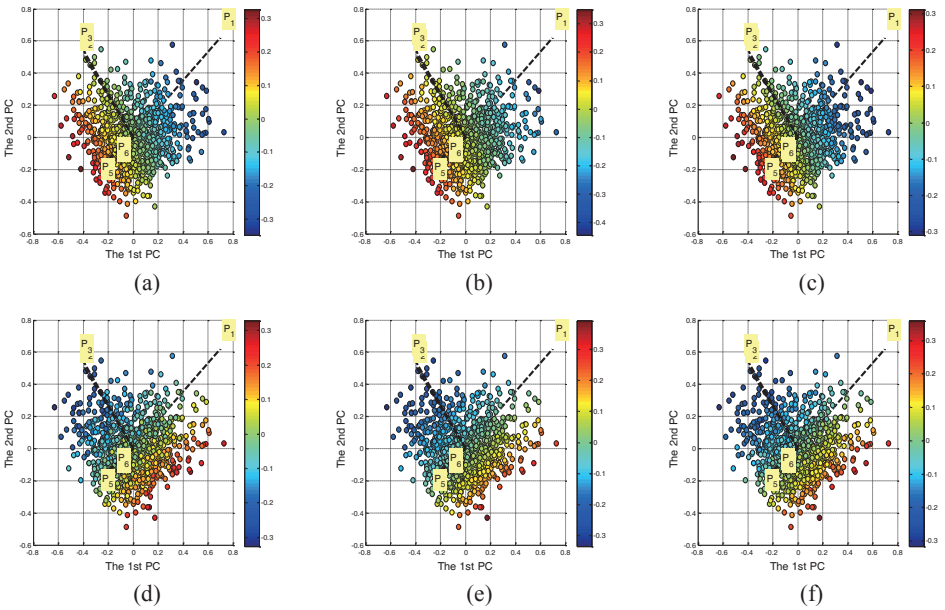

Figure 4.50 Characteristics of FE models with respect to the change rate of measurement data in case of (a) f_1, (b) f_2, (c) f_3, (d) δ_{11}, (e) δ_{12} and (f) δ_{13}

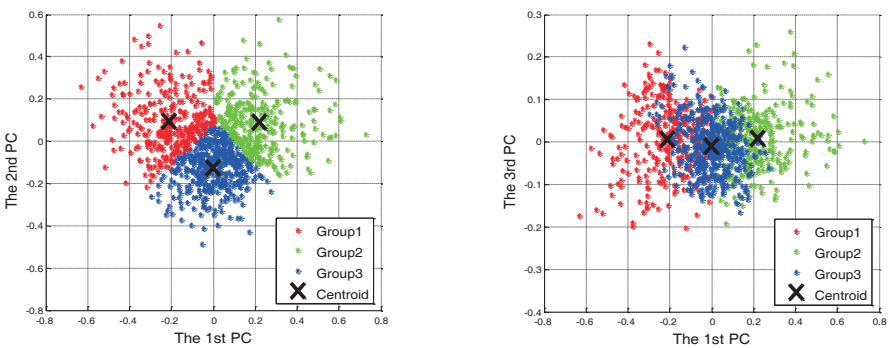

(a) In the plane of the 1st and the 2nd PCs (b) In the plane of the 1st and the 3rd PCs

Figure 4.51 Classification of multiple FE models into three groups

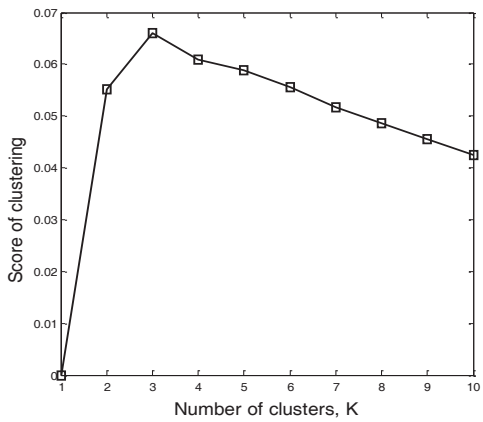

Figure 4.52 Scores of clustering for different number of clusters

Table 4.29 Properties of the groups in terms of number of FE models and *WCD*

	Group 1	Group 2	Group 3
Number of FE models	294	286	420
WCD	0.220	0.210	0.158

Table 4.30 Average value of change rate of each responses for the identified groups

	Average change rate (%)		
	Group 1	Group 2	Group 3
f_1	6.994	-11.619	3.007
f_2	7.199	-11.687	2.895
f_3	6.908	-11.718	3.144
δ_{11}	-10.539	3.365	5.085
δ_{21}	-10.960	3.515	5.271
δ_{12}	-11.100	3.590	5.340
δ_{22}	-11.097	3.670	5.278
δ_{13}	-10.815	3.723	5.046
δ_{23}	-10.159	3.676	4.628

Gaussian mixture model is plotted in Figure 4.53 along with distribution of the updated FE models. Separation of the updated FE models is less obvious, because the models are widely dispersed due to very large level of measurement uncertainty.

Table 4.31 Average value of change rate of structural parameters for the identified groups

Parameter number	Average change rate (%)		
	Group 1	Group 2	Group 3
1	-13.842	15.762	-12.833
2	22.763	5.500	2.070
3	3.529	-14.234	-15.882
4	7.102	-2.266	0.048
5	1.695	-8.252	0.656
6	1.449	-3.341	0.302
7	1.039	-3.583	0.270
8	8.073	-1.027	1.377
9	3.731	-2.558	-1.627

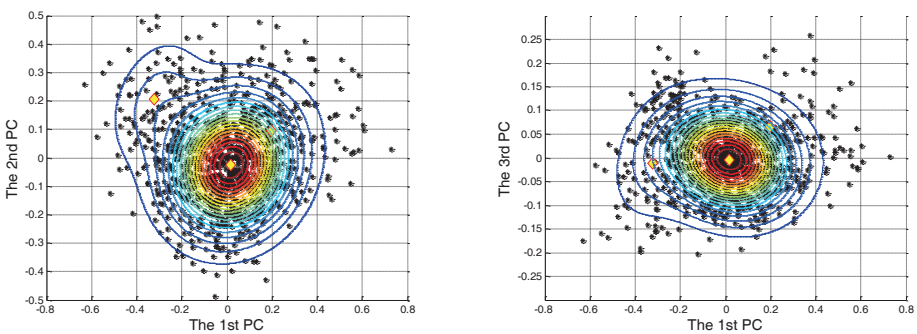

(a) In the plane of the 1st and the 2nd PCs (b) In the plane of the 1st and the 3rd PCs

Figure 4.53 Gaussian mixture model to describe distribution of updated FE models

Table 4.32 Mean vectors and mixing coefficients of component PDFs

Component PDF 1		Component PDF 2		Component PDF 3	
μ_1(*)	π_1	μ_2(*)	π_2	μ_3(*)	π_3
-0.321	0.078	0.015	0.860	0.195	0.061
0.206		-0.026		0.094	
-0.012		-0.004		0.065	

(*): Coordinate of mean vectors are expressed with respect to the first three principal components

4.4 Probabilistic Condition Assessment of Yeondae Bridge

4.4.1 Evaluation of Load Rating Factor (RF)

The rating factor (RF) is evaluated using the Eq. (3.12) in section 3.3.1 for the multiple FE models of each case. The condition factor φ_{cond} is taken 1.0 because previous inspection reports have assessed its condition as 'Fair or good'.

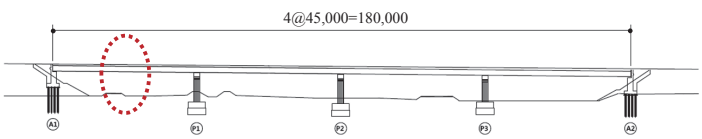

Figure 4.54 Location of critical section for rating factor evaluation

The 0.4L point from the support at the abutment in the first span is found to be subjected to the maximum positive flexure by a moving load analysis. The strength limit state I (MLTM, 2012), which is regarded as a typical load combination for a vehicle load, is examined for the basic load combination related to normal vehicular use of the bridge. Detailed information about vehicle loading condition and corresponding maximum responses are introduced in previous research (Kim *et al*., 2013).

In the case of Yeondae bridge, exact physical properties of the bridge is unknown. Therefore, to verify the effectiveness of the proposed method, comparative FE models are also generated by using two approaches. The first approach is random generation of candidate models from the baseline FE model within a threshold, by which the level of uncertainty is considered (Goulet *et al*., 2010). Errors of candidate models are calculated with Eq. (4.3), and compared with the threshold to determine acceptance of the models. In this example, the threshold is set as 5%. The second approach is sampling of candidate models by using the properly assumed PDF for structural parameters (Catbas *et al*., 2012). The probability model for design purpose is referred from literatures (Tabsh *et al*., 1991; Kulicki *et al.*, 2007), and then applied to a FE model that is

updated using the single set of measurement data. Table 4.33 summarizes the adopted probability models for the second approach.

Table 4.33 Probability models for design purpose

	Bias factor (λ)	C.O.V (c_v)	Distribution type
Young's modulus (E)	1.00	0.06	Lognormal
Section properties (I, J)	1.07	0.08	Lognormal
Stiffness of spring supports (k)	1.00	0.05	Uniform
Mass (m)	1.03	0.08	Normal

1,000 FE models are obtained by two approaches, and utilized to estimate distribution of rating factors (Table 4.34).

Table 4.34 Mean and standard deviation of RFs estimated by two previous approaches

	Approach 1 (Random models)	Approach 2 (Sampled models from PDF)
Mean value (μ_{RF})	2.27	2.27
Standard deviation (σ_{RF})	0.462	0.405

The multiple FE models updated for each case study are also utilized to evaluate distribution of RFs. Table 4.35 summarizes the statistical properties of RFs in terms of mean and standard deviation when all the identified models are used. Mean values of RF obtained by the proposed method are always smaller than the results obtained by two previous approaches. In addition, standard deviation of RF is greatly reduced by the proposed method. The observation indicates the conservativeness of the two previous approaches. On the contrary, the proposed method can estimate probable variability of the structural condition from the uncertainty of measurement data quantitatively through FE model update process, and thus the conservativeness of numerical model could be reduced.

Meanwhile, the mean values of RFs decreases with larger variance according to the increase

of the level of uncertainty. Wider dispersion of the updated FE models due to higher level of uncertainty cause the results. Since the exact condition of the bridge is unknown, we cannot estimate accuracy of the estimated RFs unlike previous idealized example. A certain fact is that the RFs are highly influenced by the uncertainty level. Comparing the Case 1 and 2, the type of distribution model is less influential to the mean value and standard deviation of RF.

Table 4.35 Mean and standard deviation of RFs estimated by using all updated FE models

	Case 1	Case 2	Case 3	Case 4	Case 5	Case 6	Case 7
Mean value (μ_{RF})	2.13	2.13	2.11	2.12	2.07	2.07	2.07
Standard deviation (σ_{RF})	0.090	0.088	0.118	0.131	0.212	0.232	0.244

The variation ranges of RF are depicted between $\mu_{RF}\pm1\sigma_{RF}$ in Figure 4.55 (a). Noticeable increase of the variance of RF is observed as the level of uncertainty increases, especially when the level of natural frequency uncertainty is increased at case 3 and 5. Accordingly, level of natural frequency uncertainty is concluded as more influential than that of displacement on the distribution of multiple models in case of Yeondae bridge.

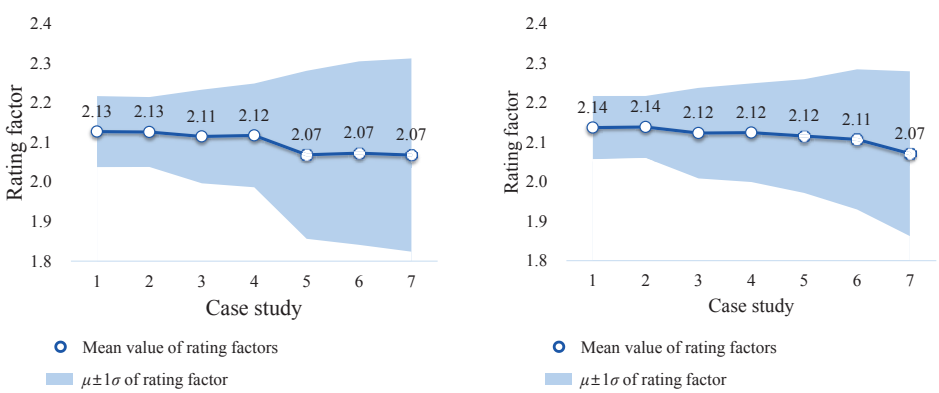

(a) Using all the updated models (b) Selecting a couple of groups

Figure 4.55 Range of RF distribution

Next, the rating factor is evaluated by selecting proper FE models in a couple of groups. The multiple FE models are classified into groups based on the posterior probability calculated by using the Gaussian mixture model that performs better classification than *K*-means method does in the higher uncertainty level. Then, groups of which mixing coefficients are larger than 10% are selected to estimate RF. As shown by Figure 4.55 (b) and Table 4.36, mean values of RF became less sensitive to the uncertainty level. Mean values of RF mostly coincide except the last case. Furthermore, variance of RF is also greatly reduced. Selecting several groups of probable FE models enables to refine the multiple FE models and following assessments even for the higher uncertainty level.

Table 4.36 Mean and standard deviation of RFs estimated by selected groups

	Case 1	Case 2	Case 3	Case 4	Case 5	Case 6	Case 7
Mean value (μ_{RF})	2.14	2.14	2.12	2.12	2.12	2.11	2.07
Standard deviation (σ_{RF})	0.080	0.079	0.115	0.125	0.144	0.177	0.209

4.4.2 Structural reliability analysis

Structural reliability analysis is carried out with respect to the first span of the bridge. Maximum bending moment induced by the design truck at the critical section, which is same as in the load rating, is considered. The limit state function for the positive bending moment is expressed as Eq. (4.6) that implies failure of the composite section by bending moment owing to the vehicle load.

$$g_M = M_n - M_{LL}(1 + IM) - M_{DW} - M_{DC} \tag{4.6}$$

The identified Gaussian mixture models provide probabilistic information about variability of structural parameters. However, probability models for yield stress and truck load are not identifiable by the proposed method, thus, they are referred from the literatures (Catbas *et al.*, 2013). Properties of the implemented probability models are listed in Table 4.37. Reliability index

of Yeondae bridge is calculated by using FORM with obtained probability models.

Table 4.37 Statistical parameters for structural reliability analysis

	Bias factor (λ)	C.O.V (c_v)	Distribution type
Yield stress (F_y)	1.05	0.10	Lognormal
Truck load (P)	1.00	0.20	Lognormal

Reliability indices are also obtained by two other approaches likewise to the load rating evaluation. In the first approach, the candidate models randomly generated within the threshold are utilized. A multivariate Gaussian distribution is fitted to the distribution of random models, and utilized for structural reliability analysis. In the second approach, the probability models of design purpose that was applied for the single updated model (Table 4.33) is utilized for structural reliability.

Table 4.38 compares the reliability indices and probability of failure calculated by two previous approaches. Next, the evaluation results obtained by the proposed method are also summarized in Table 4.39. Reliability index decreases according to the increase of uncertainty level, which is in accordance with common sense. Meanwhile, reliability indices obtained for case 1, 2 and 3 are higher than the values obtained by previous methods. On the other hand, lower reliability indices are obtained for the case 4 - 7. The observation indicates that reliability index estimated based on design philosophy and conservative assumptions does not guarantee the conservativeness in case that actual structural variability is much larger. On contrary, the proposed method can quantify the effect of the uncertainty of measurement data onto the reliability index and probability of failure. Variation of the reliability indices in Table 4.39 are also presented in Figure 4.56 as blue line. Remarkable decrease of reliability index is found in case 4, for which C.O.V of both responses are defined as 0.05.

Table 4.38 Reliability index and probability of failure calculated by previous approaches

	Approach 1 (Random models)	Approach 2 (PDF for design purpose)
Reliability index (β)	6.87	6.80
Probability of failure ($\times 10^{-13}$)	31.48	51.34

Table 4.39 Reliability index and probability of failure calculated by using all updated FE models

	Case 1	Case 2	Case 3	Case 4	Case 5	Case 6	Case 7
Reliability index (β)	7.18	7.19	7.15	5.47	3.23	3.30	2.76
Probability of failure ($\times 10^{-13}$)	3.58	3.13	4.50	2.26E+5	6.14E+9	4.78E+9	2.85E+10

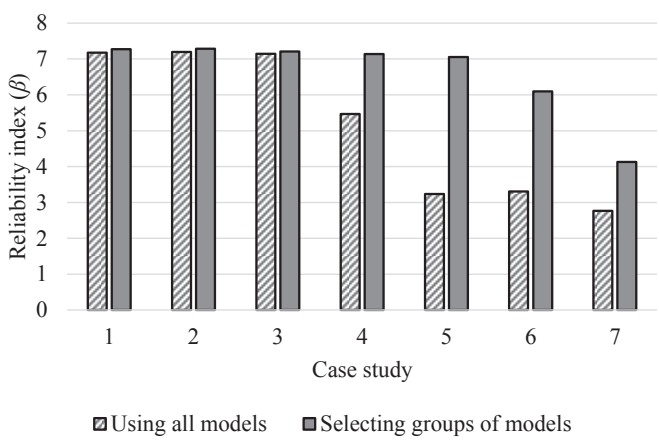

Figure 4.56 Variation of reliability indices according to the uncertainty level

Next, component PDFs of which mixing coefficients are larger than 10% are selected. In this case, reliability index is calculated by using Eqs. (3.17) and (3.18). The obtained reliability indices are plotted in Figure 4.56 as red line, comparatively. The effect of the clustering-based model selection procedure is obviously shown by the variation of reliability index, which are less sensitive to the increase of uncertainty level. The effect of higher level of measurement uncertainty could be mitigated, and more consistent reliability index could be obtained clustering-based model selection procedure. Table 4.40 summarizes the reliability indices and probability of

failures refined by selecting several component PDFs of probable FE models.

Table 4.40 Reliability index and probability of failure calculated by selected component PDFs

	Case 1	Case 2	Case 3	Case 4	Case 5	Case 6	Case 7
Reliability index (β)	7.27	7.28	7.21	7.14	7.06	6.09	4.13
Probability of failure ($\times 10^{-13}$)	1.78	1.62	2.89	4.83	8.50	5.50E+03	1.83E+08

4.5 Robustness to Numerical Instability of FE model Update

In the section 4.2.3, nine effective optimization parameters are selected to avoid rank-deficiency. However, in actual applications to civil structures, the number of structural parameters cannot always be maintained as less than or equal to those of measurement data. In this chapter, the proposed method is verified whether the multiple FE models can still be found properly in spite of rank-deficiency. In addition, the unregularized objective function is considered to check numerical stability of the modified BFGS method in dealing with ill-posed characteristic.

4.5.1 Formulation of optimization problem

The preliminary structural parameters are classified and grouped into 37 parameters based on engineer's judgment. Table 4.41 summarizes the newly considered structural parameters and their allowable bounds. For updating of the structural parameters, the unregularizad objective function in Eq. (4.3) is taken. As a result, problem of ill-posedness and rank-deficiency may be occurred. Nevertheless, the implemented modified BFGS is expected to find local optimal solution stably.

Table 4.41 Structural parameters and their allowable bounds considered in the optimization

# of parameter	Structural parameters	Allowable bounds (%)
1 ~ 5	Coefficients of spring support elements in translation and rotational direction	±40
6, 8, 10, 12, 14	Mass of girders (span 1, 2, 3 and 4), cross frame	±10
7, 9, 11, 13, 15, 16	Young's modulus of girders (span 1, 2, 3 and 4), cross frame, and slab	±20
17, 20, 23, 26, 29, 32	Torsional stiffness of girders (span 1, 2, 3 and 4), cross frame, and slab	±25
18, 21, 24, 27, 30, 33	Moment of inertia (I_{yy})of girders (span 1, 2, 3 and 4), cross frame, and slab	±10
19, 22, 25, 28, 31, 34	Moment of inertia (I_{zz})of girders (span 1, 2, 3 and 4), cross frame, and slab	±10
35	Area of transverse slab	±30
36, 37	Mass of substructural member (vertical, rotational)	±30

4.5.2 Verification of optimal solutions

Before finding multiple FE models, a single model is updated with different constraints using a set of measurement data to check its convergence. The applied constraints are (1) normal range given in Table 4.41, (2) doubled range, (3) halved range, and (4) unconstrained case. The updated values corresponding to the four constraint conditions are compared in Figure 4.57. Structural parameters with meaningful variations are selected for comparison. Updated values are close each other in most parameters even though different constraints are applied.The effect of constraint variation is also represented in terms of average and maximum error of updated values (Table 4.42).

The convergence properties are also verified. First-order optimality, which indicates KKT condition regarding the gradient of Lagrangian function, is investigated to check convergency. In addition, optimized value of the objective function is also considered. Figure 4.58 compares the two values for the four constraint conditions. Unconstrained case shows the most optimal solution, but the differences are not significant. The results prove that the formulated optimization problem and implemented algorithm is able to deal with the rank-deficiency and ill-posed characteristic, and find a local optimal solution.

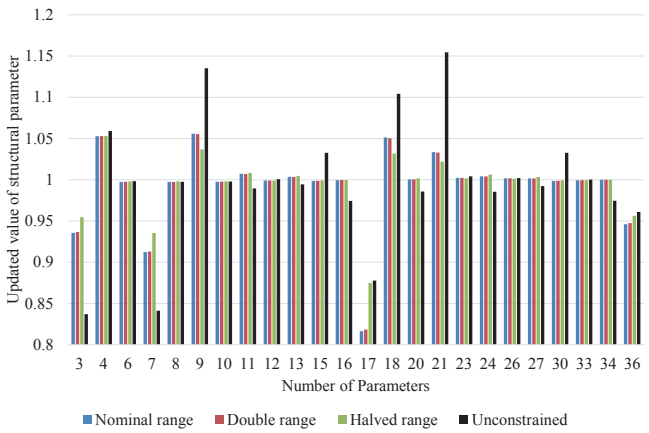

Figure 4.57 Comparison of the updated values of structural parameters

Table 4.42 Change rate of updated values compared to the case of normal range

	Doubled range	Halved range	Unconstrained
Average change rate (%)	0.02	0.5	2
Maximum change rate (%)	0.2	7	12

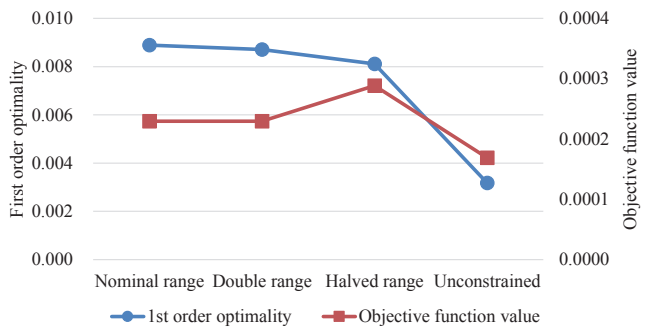

Figure 4.58 Comparison of convergency for various constraint conditions

4.5.3 Probability models for uncertainty of measurement data

The four case studies are considered to investigate effect of various probability models for the uncertainty of measurement data. Distribution types and the statistical parameters for the case studies are summarized in Table 4.43. Thousand sets of measurement data are sampled from

uniform distribution and jointly normal distributions, respectively.

Table 4.43 Distribution types and the statistical parameters for the 4 case studies

	Distribution type	Natural frequency		Static displacement	
		C.O.V	Perturbation	C.O.V	Perturbation
Case 1	Jointly normal	0.01	±2%	0.01	±2%
Case 2	Jointly normal	0.05	±10%	0.01	±2%
Case 3	Jointly normal	0.01	±2%	0.05	±10%
Case 4	Jointly normal	0.05	±10%	0.05	±10%

4.5.4 Distribution of updated FE models

The updated FE models for four case studies are analyzed by applying PCA, *K*-means and Gaussian mixture model, same as before.

(1) Case 1

The 1,000 updated FE models for case 1 is shown in Figure 4.59. Same as before, scattering and clustering of models are better revealed as consequence of PCA application.

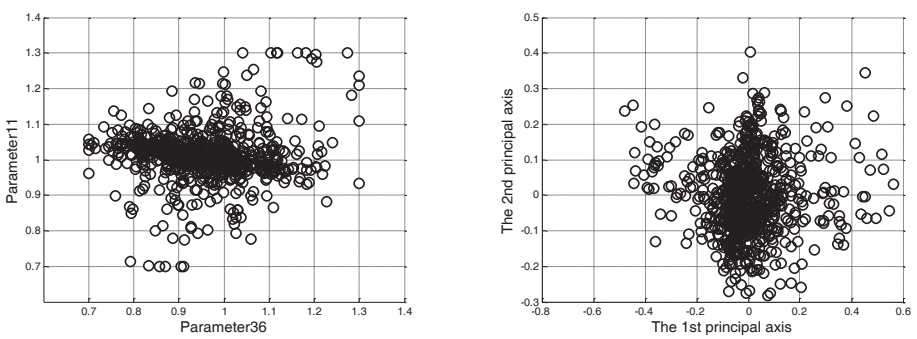

(a) The space of structural parameters (b) Principal subspace

Figure 4.59 Distribution of the updated multiple FE models

The updated models are investigated regarding constraint violation. As shown in Figure 4.60 (a), 86% of total updated models do not violate the constraint at all. In addition, average change rate of structural parameter values are about 2.9%. This result shows that the multiple models are

converged to local optimal solutions. Therefore, distribution of the updated models can be accounted for by the effect of uncertainty of measurement data, not by numerical instability.

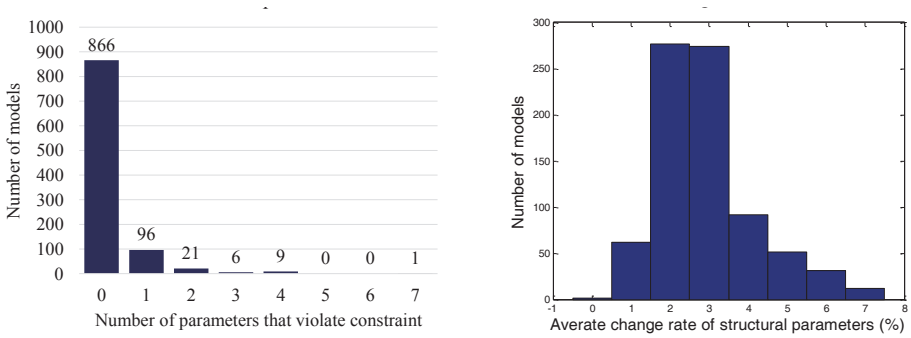

(a) Constraint violation check (b) Average change rate of structural parameters

Figure 4.60 Properties of the updated FE models in relation to constraint violation

The relationship between the distribution of structural parameters and uncertainty conditions of the measurement data is investigated by using the two largest principal components. In this case, the effect of natural frequency variation is well revealed along the second principal component, a vertical axis. On the other hand, effect of displacement variations are not noticeable, but are weakly observed along the seventh principal component. The effect of natural frequency uncertainties are concluded as more crucial than those of displacement uncertainties for the distribution of multiple FE models. The principal component coefficients, the black vectors in the figure, inform that contribution of Young's modulus and moment of inertia mostly coincide each other, which determine the stiffness of girders. This result is in accordance with the grouping of the two parameters in the previous example. Mass properties are especially sensitive to the uncertainty of the natural frequency, which is also similar to the previous results.

Next, Gaussian mixture model is applied based on outcomes of *K*-means application. Figure 4.62 illustrates the four Gaussian component PDFs. Mean vectors of the component PDFs are represented by yellow diamond markers. Contour describes covariance and density of component PDF.

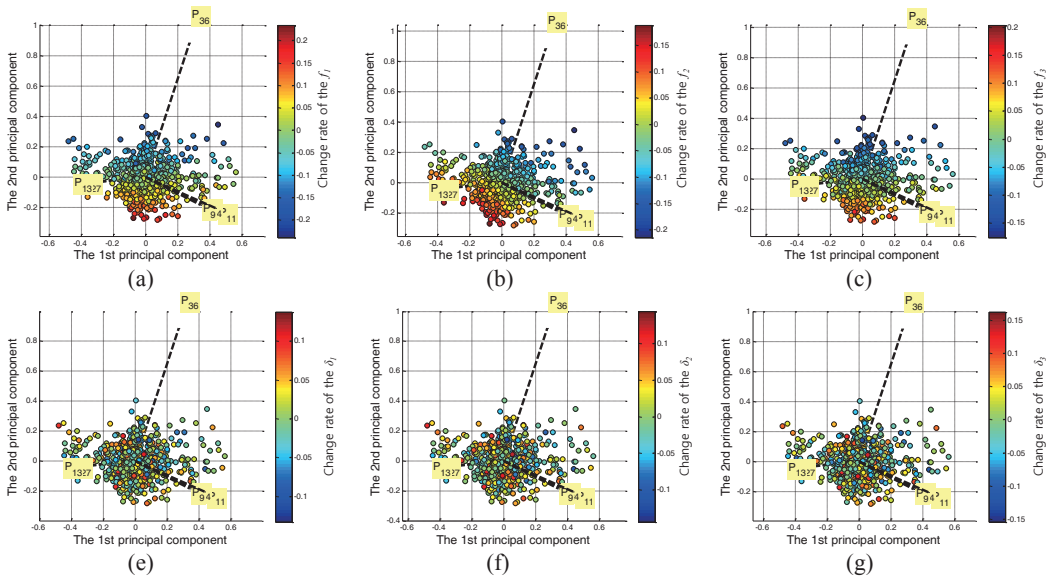

Figure 4.61 Characteristics of FE models with respect to the change rate of measurement data in case of (a) f_1, (b) f_2, (c) f_3, (d) δ_1, (e) δ_2 and (f) δ_3

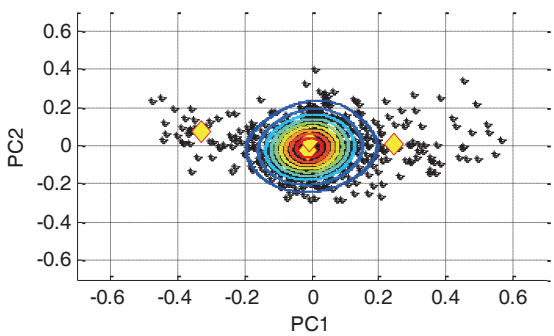

Figure 4.62 Gaussian mixture model to describe distribution of updated FE models

(2) Case 2

The 1,000 updated FE models for case 2 is shown in Figure 4.63. According to increased uncertainty level, more FE models lie on the constraint. Separation of the multiple FE models in the principal subspace became more apparent.

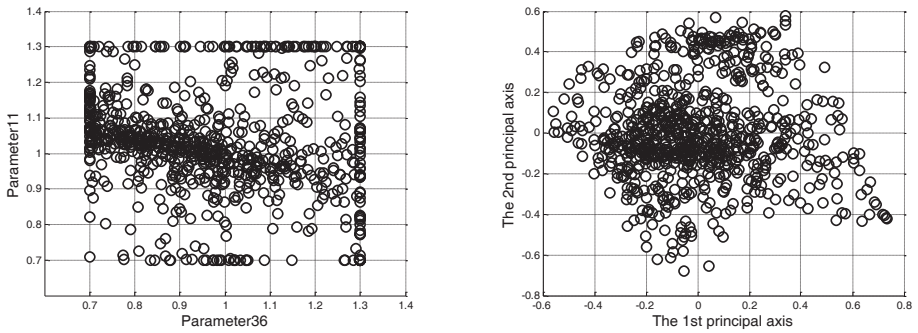

(a) The space of structural parameters (b) Principal subspace

Figure 4.63 Distribution of the updated multiple FE models

The updated models are investigated regarding constraint violation. As shown in Figure 4.64 (a), 52% of total updated models do not violate the constraint. Average change rate of structural parameter values are about 4.6%. Even though the FE models with parameters on the constraints are increased, the local optimal solutions are found stably by using the employed optimization algorithm.

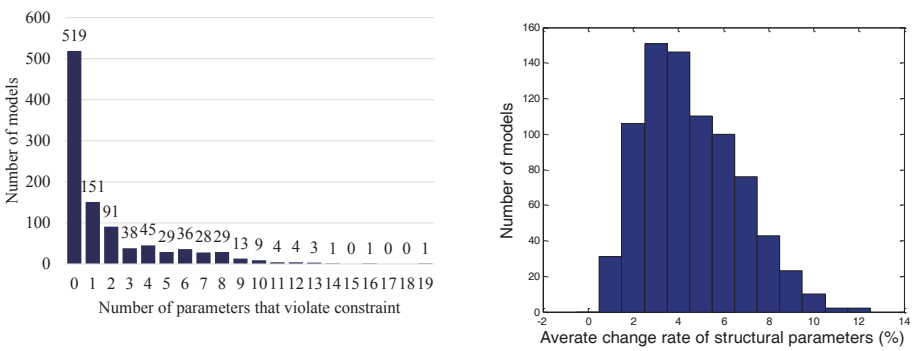

(a) Constraint violation check (b) Average change rate of structural parameters

Figure 4.64 Properties of the updated FE models in relation to constraint violation

The effect of natural frequency variation is well revealed along the first principal component. On the other hand, effect of displacement variations are not noticeable as before. Same conclusion can also be inferred regarding the similarity of Young's modulus and moment of inertia for each span, and significance of mass properties.

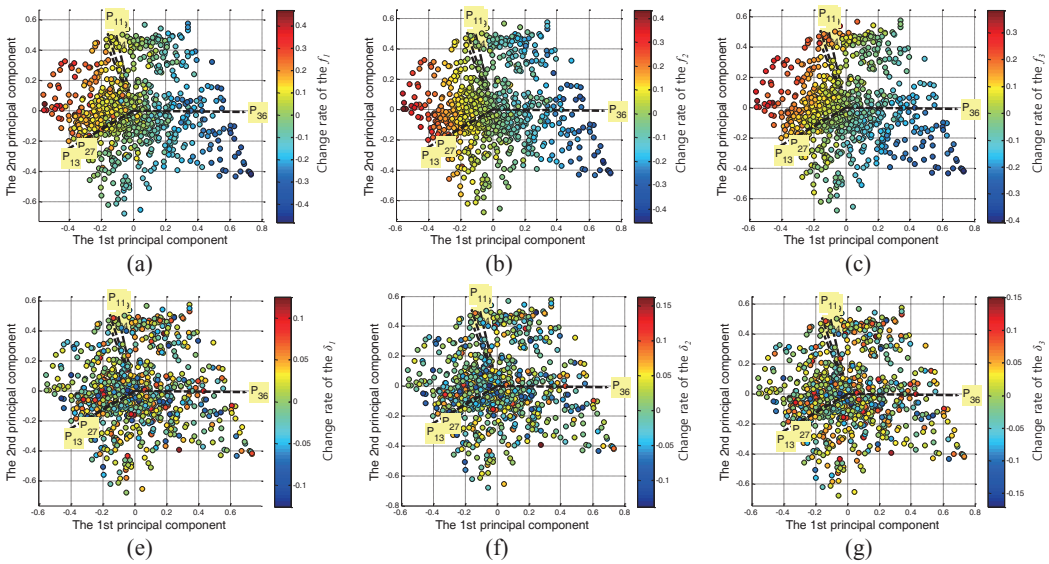

Figure 4.65 Characteristics of FE models with respect to the change rate of measurement data in case of (a) f_1, (b) f_2, (c) f_3, (d) δ_1, (e) δ_2 and (f) δ_3

Gaussian mixture model is found by superposition of three component PDFs based on the outcomes of *K*-means application (Figure 4.66).

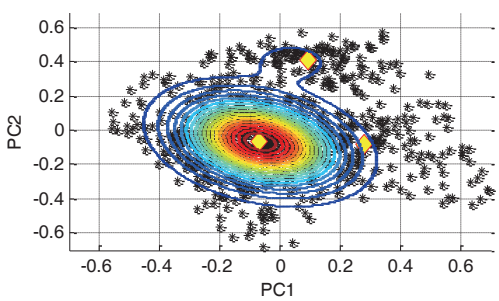

Figure 4.66 Gaussian mixture model to describe distribution of updated FE models

(3) Case 3

The 1,000 updated FE models for case 3 is shown in Figure 4.67. The updated models are less scattered according to the decreased level of uncertainty of natural frequency.

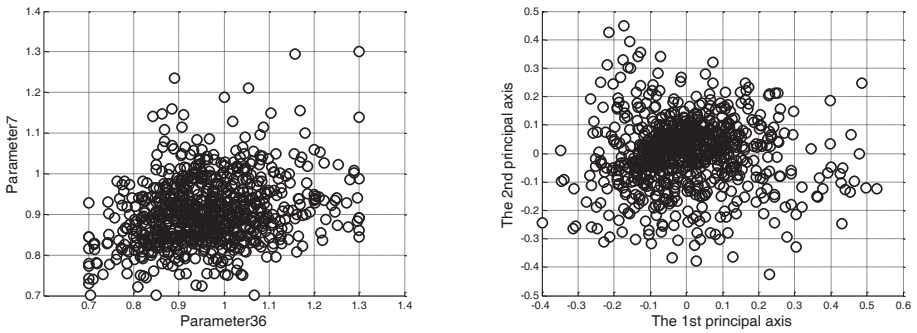

(a) The space of structural parameters (b) Principal subspace

Figure 4.67 Distribution of the updated multiple FE models

The updated models are investigated regarding constraint violation. Figure 4.68 shows that 84% of total updated models do not violate the constraint at all. Average change rate of structural parameter values are about 3.0%. Comparing these results with those of case 2, the effect of natural frequency uncertainty can be concluded as more influential than the effect of displacement uncertainty.

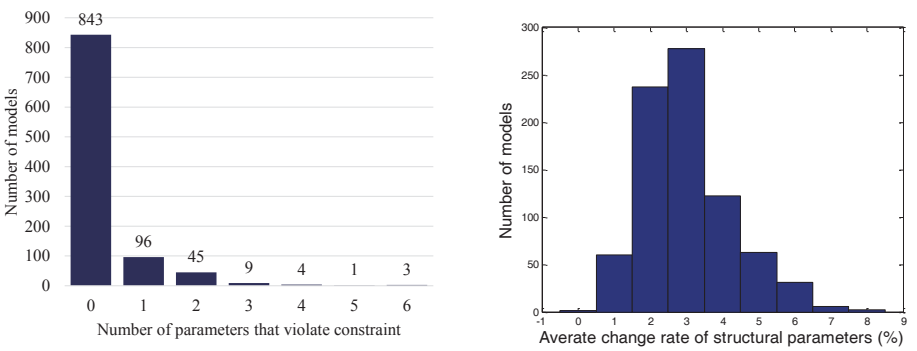

(a) Constraint violation check (b) Average change rate of structural parameters

Figure 4.68 Properties of the updated FE models in relation to constraint violation

As a result, in contrast to previous cases, effect of displacement variations is now observed in the plane of two principal components. The reduced uncertainty level of natural frequency may be the reason for similar influence of natural frequency and displacement. As a result, the contributions of stiffness properties are emphasized than before.

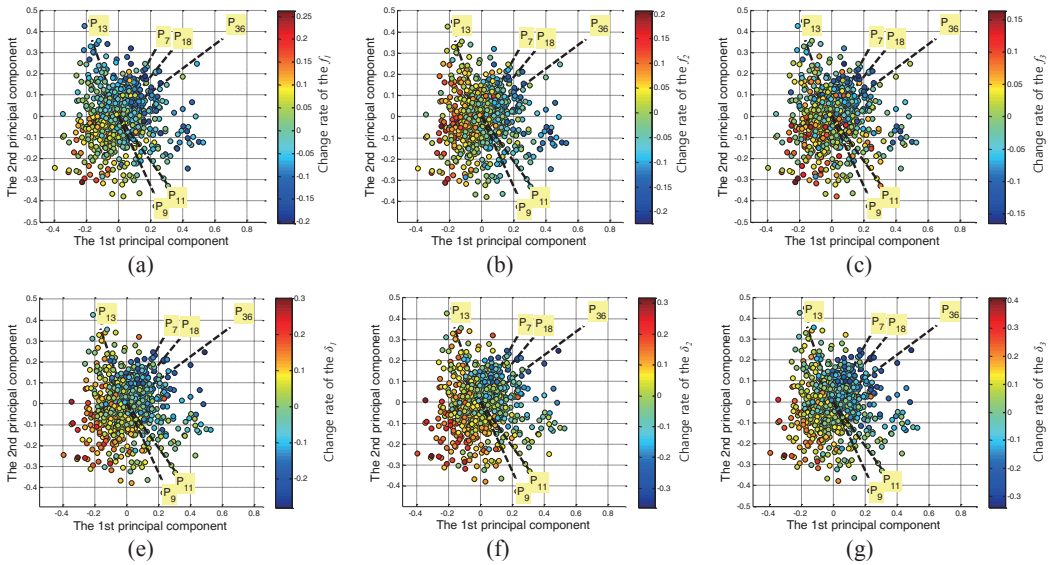

Figure 4.69 Characteristics of FE models with respect to the change rate of measurement data in case of (a) f_1, (b) f_2, (c) f_3, (d) δ_1, (e) δ_2 and (f) δ_3

Gaussian mixture model is constructed by superposition of four component PDFs based on the outcomes of *K*-means application (Figure 4.70).

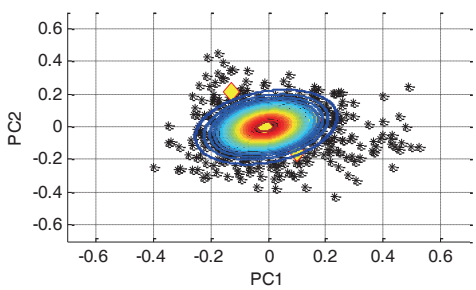

Figure 4.70 Gaussian mixture model to describe distribution of updated FE models

(4) Case 4

The 1,000 updated FE models for case 4 is shown in Figure 4.71. Large non-linearity and separation are observed in the distribution of multiple FE models due to the highest uncertainty levels for both type of measurements.

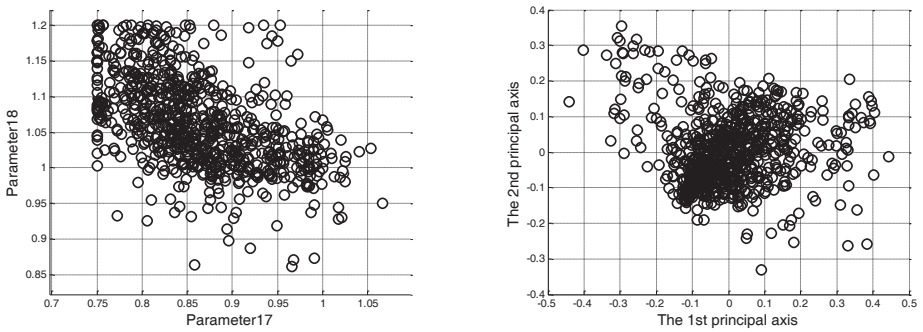

(a) The space of structural parameters (b) Principal subspace

Figure 4.71 Distribution of the updated multiple FE models

The updated models are investigated regarding constraint violation. Figure 4.72 shows that 44% of total updated models do not violate the constraint. Average change rate of structural parameter values are about 4.8%. The large variability of the updated FE models cause more parameters lie on the constraints. Nevertheless, most of the updated parameters are still within the constraints by the virtue the implemented optimization algorithm.

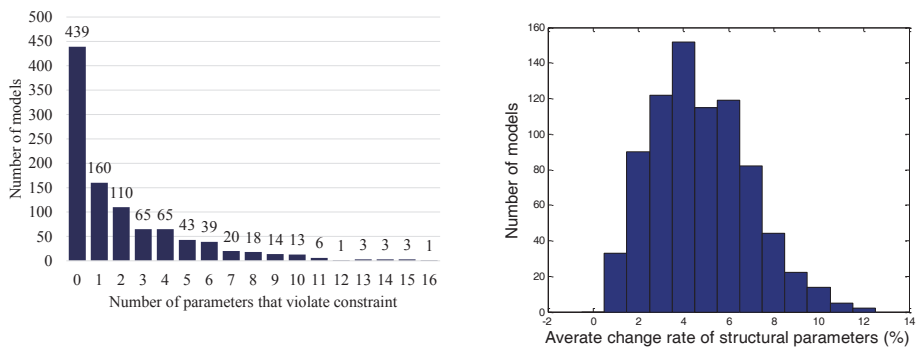

(a) Constraint violation check (b) Average change rate of structural parameters

Figure 4.72 Properties of the updated FE models in relation to constraint violation

The relationship between measurement uncertainty and structural parameters is similar as before (Figure 4.73).

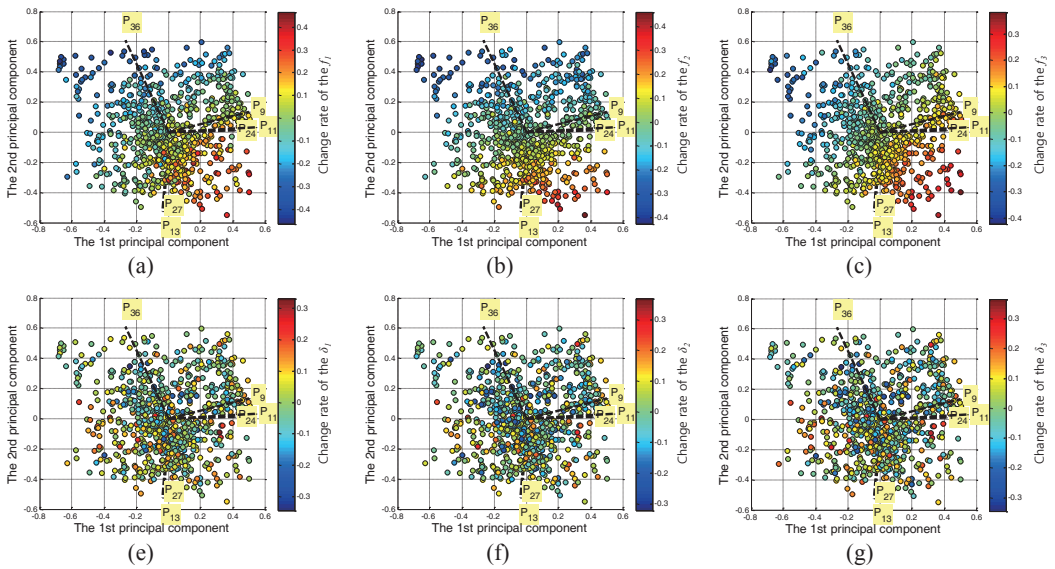

Figure 4.73 Characteristics of FE models with respect to the change rate of measurement data in case of (a) f_1, (b) f_2, (c) f_3, (d) δ_1, (e) δ_2 and (f) δ_3

Gaussian mixture model is constructed by superposition of three component PDFs based on the outcomes of *K*-means application (Figure 4.74).

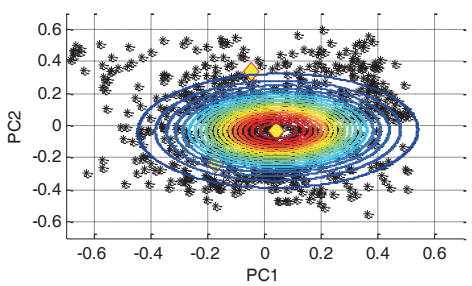

Figure 4.74 Gaussian mixture model to describe distribution of updated FE models

4.5.5 Structural reliability analysis

The Gaussian mixture models are utilized to assess condition of Yeondae bridge in terms of reliability index. Same limit state and critical section specified in section 4.4.2 are considered. The reliability indices and probability of failures obtained by the updated FE models are also summarized in Table 4.44. Reliability index decreases according to the increase of uncertainty

level, which is in accordance with common sense. The updated FE models for case 2 and 4, which are featured by higher level of natural frequency uncertainty, estimate especially smaller reliability indices. It is concluded the level of natural frequency uncertainty is more influential to the reliability index than that of displacement.

Table 4.44 Reliability index and probability of failure calculated by using all updated FE models

	Case 1	Case 2	Case 3	Case 4
Reliability index (β)	6.90	6.49	6.85	6.54
Probability of failure ($\times 10^{-13}$)	26.38	418.15	36.63	312.34

Next, component PDFs of which mixing coefficients are larger than 10% are selected. The reliability indices are plotted in Figure 4.75 as red line comparing with the previously obtained values. The variation of reliability index became less sensitive to the increase of uncertainty level by the effect of the clustering-based model selection procedure. The effect of higher uncertainty of measurement data could be mitigated, and reliability index is estimated stably by the proposed clustering-based method. Table 4.45 summarizes the reliability indices and probability of failures that are refined by selecting several component PDFs of probable FE models.

Table 4.45 Reliability index and probability of failure calculated by selected component PDFs

	Case 1	Case 2	Case 3	Case 4
Reliability index (β)	7.11	7.13	7.12	6.54
Probability of failure ($\times 10^{-13}$)	5.98	5.11	5.48	304.44

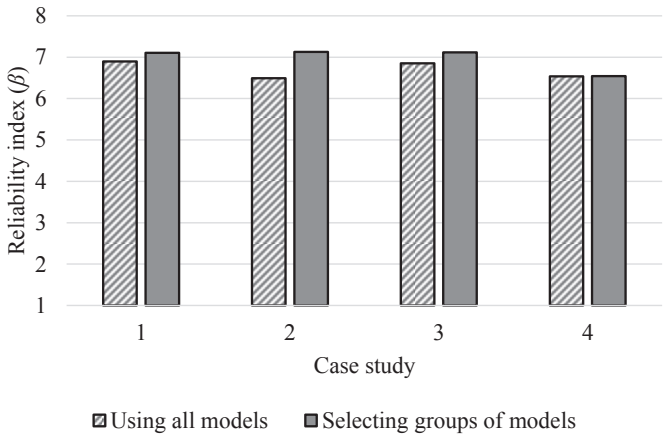

Figure 4.75 Variation of reliability indices according to the uncertainty level

4.6 Summary

In this chapter, the proposed method for probabilistic assessment of structural condition through clustering-based FE model update is verified by applying to Yeondae bridge. In section 4.1, general descriptions on the bridge and field measurements are introduced. In section 4.2, a procedure of optimization to update multiple FE models is introduced. The most effective structural parameters for optimization are selected systematically by applying PCA. As a result, problems of rank-deficiency and ill-posed properties could be avoided. In addition, seven case studies are considered implementing various probability models for measurement uncertainties. The measurement uncertainties are modeled with uniform distribution and jointly normal distributions. The values of C.O.V the jointly normal distributions are varied to reflect various levels of measurement uncertainty, of which perturbation ranges are approximately ±1% ~ ±20%.

In section 4.3, distribution features of the updated FE models for the seven case studies are analyzed by implementing Principal Component Analysis (PCA), *K*-means method and Gaussian mixture model. In all cases, multimodal distribution of FE models are observed, which became to be revealed better in the principal subspace. The relationship between measurement data

uncertainty and perturbation of structural parameters can be identified in the principal subspace. The multimodal distribution of the updated FE models is classified into several groups by using *K*-means method and Gaussian mixture model. Each of the classified groups or component PDFs represents specific physical properties in relation to variation of measurement data. As level of measurement data uncertainty increases with larger C.O.V, separation of FE models is less apparent. Nevertheless, the Gaussian mixture model shows good performance in classifying meaningful FE models that can represent physical properties of the bridge. The identified Gaussian mixture models and updated FE models are utilized for further probabilistic assessment with respect to load rating and structural reliability analysis. Higher level of measurement uncertainty causes wider dispersion of the updated FE models, and results in smaller reliability index. The reliability indices estimated by the proposed method are more appropriate to represent structural condition according to the measurement uncertainty in contrast to the previous approaches that are based on design assumption or arbitrary criteria. In addition, reliability index is more appropriate to fully reflect the probabilistic feature of the updated FE models. Especially, the clustering-based model selection procedure could lower the effect of higher uncertainty level, thus more accurate rating factor and reliability index could be obtained.

In section 4.5, robustness of the proposed method to the numerical issues is investigated by considering more structural parameters. Numerical application shows that rank-deficiency and ill-posedness problems in the optimization process are well handled by the modified BFGS, which attribute to obtaining multiple FE models stably. The updated FE models and the estimated reliability indices prove that the proposed method still works well even for the model update problem with rank-deficiency and ill-posedness.

Chapter 5. Conclusions

In this study, a new procedure for probabilistic assessment of structural condition based on multiple FE model update and clustering has been proposed. Multiple FE models are updated by successive optimization using sets of measurement data that are sampled from the Probability Density Function. Multimodal distribution property of the updated multiple FE models is revealed better as consequence of PCA application. In addition, the relationship between measurement uncertainty and the updated structural parameters is also identified in the principal subspace. Applying *K*-means method and Gaussian mixture model can classify the multiple FE models into several groups. Each of the classified groups represents distinct physical properties of structure in relation to variation of measurement data. The Gaussian mixture model shows better performance than *K*-means method in classifying meaningful FE models that can represent the structural condition.

The identified Gaussian mixture models and updated FE models are utilized for probabilistic assessment with respect to load rating and structural reliability analysis. The proposed method is capable to assess structural condition probabilistically according to variation of measurement uncertainty levels. Especially, clustering-based model selection procedure can reduce the possibility of inaccurate condition assessment caused by a high level of measurement error, thus can provide more consistent rating factor and reliability index.

An illustrative example of 3-span continuous bridge shows validity of the proposed method. In an idealized condition utilizing measurement data without noise, the actual structural condition can be identified by the proposed method. Multimodal properties of the updated FE models tend to appear more apparently according to increase in level of measurement uncertainty. Discrepancy between the estimated structural conditions by the multiple FE models to the actual ones increases as higher level of measurement uncertainty is considered. However, the proposed clustering-based model selection procedure can estimate reliability index accurately in spite of high levels of noise.

In the application example of Yeondae bridge, the proposed procedure can effectively update multiple FE models that correspond to the properly assumed probability models for uncertainty of measurement data. Findings in the numerical example are as follows:

- Applying PCA to sensitivity matrix of preliminary parameters is very useful approach to identify effective parameters and reduce the number of parameters systematically.
- The measurement uncertainties are modeled with uniform distribution and jointly normal distributions with varying C.O.V values for natural frequency and static displacement. Effect of different type of distribution model to the estimated rating factors and reliability index is insignificant as far as their perturbation ranges are similar. Whereas, level of uncertainty affect significantly to the distribution features as well as estimated structural conditions, which can be captured accurately by the proposed method.
- The effect of natural frequency uncertainty is closely related to the variation of mass properties. Similarly, static displacement uncertainty affect mostly the calibration of stiffness properties. The effects of two different responses to the distribution of multiple FE models are contrasted with each other. Therefore, FE model updating is desirable to consider both static and dynamic responses simultaneously to obtain appropriate model.
- *K*-means method shows unsatisfactory performance for classifying multiple FE models corresponding to high level of measurement uncertainty. Whereas, Gaussian mixture model is capable to describe and capture multimodal properties of multiple FE models consistently. Furthermore, mixing coefficients provided by the Gaussian mixture model are helpful to select appropriate groups of FE models to represent physical properties of concerned structure.
- The load Rating Factor is less sensitive to the variation of measurement uncertainty comparing to reliability index. Furthermore, making a decision with the mean and variance of the rating factor has a certain limit. Whereas, structural reliability analysis is more suitable to assess structural condition probabilistically reflecting probabilistic feature of multiple FE

models.

- Robustness of the proposed method to the numerical instability of FE model update is also investigated. Rank-deficiency and ill-posedness problems in the optimization process are well handled by the modified BFGS, which attribute to obtaining multiple FE models stably.

The proposed method can evaluate variability of structural condition quantitatively from the uncertainty of measurement data. The estimated probabilistic information about the current structural condition by the proposed procedure can provide useful and efficient information for optimizing repair and maintenance plan in terms of lifetime cost and safety. In the meantime, the proposed method needs improvement regarding optimization algorithm. Adopting concept of evolutionary optimization algorithms and parallel computing can obtain multiple FE models more efficiently. In addition, incorporating modeling uncertainty as well as measurement uncertainty can revise the proposed method to assess probabilistic condition more accurately. Finally, applying the proposed method for the assessment of cable-supported bridges using long-term monitored data will be very challenging and beneficial.

References

AASHTO LRFR (2011). *The Manual For Bridge Evaluation*. American association of state highways transportation officials, DC, Washington.

Beck, J. L., & Au, S. K. (2002). Bayesian updating of structural models and reliability using Markov chain Monte Carlo simulation. *Journal of Engineering Mechanics*, *128*(4), 380-391.

Beck, J. V., & Murio, D. A. (1986). Combined function specification-regularization procedure for solution of inverse heat conduction problem. *AIAA journal*, *24*(1), 180-185.

Bishop, C. M. (2006). *Pattern recognition and machine learning*. New York: springer.

Catbas, N., Gokce, H. B., & Frangopol, D. M. (2011). Predictive analysis by incorporating uncertainty through a family of models calibrated with structural health-monitoring data. *Journal of Engineering Mechanics*, *139*(6), 712-723.

Christodoulou, K., Ntotsios, E., Papadimitriou, C., & Panetsos, P. (2008). Structural model updating and prediction variability using Pareto optimal models. *Computer Methods in Applied Mechanics and Engineering*, *198*(1), 138-149.

Der Kiureghian, A. (2005). First- and second-order reliability methods. Chapter 14, in *Engineering design reliability handbook,* edited by E. Nikolaidis *et al*., CRC Press, Boca Raton, FL.

Doebling, S. W., Farrar, C. R., & Prime, M. B. (1998). A summary review of vibration-based damage identification methods. *Shock and vibration digest*, 30(2), 91-105.

Dubot, F., Favennec, Y., Rousseau, B., & Rousse, D. (2003). Regularization opportunities for the Gauss-Newton and BFGS algorithms: application to the diffuse optical tomography problem. *International Journal of Thermal Sciences*.

Erdogan, Y. S., Gul, M., Catbas, F. N., & Bakir, P. G. (2013). Quantification of Parametric Model Uncertainties in Finite Element Model Updating Problem via Fuzzy Numbers. In *Topics in Model Validation and Uncertainty Quantification, Volume 5* (pp. 67-74). Springer New York.

Farrar, C. R., & Worden, K. (2007). An introduction to structural health monitoring. *Philosophical Transactions of the Royal Society A: Mathematical, Physical and Engineering Sciences*, *365*(1851), 303-315.

Gokce, H. B., Catbas, F. N., Gul, M., & Frangopol, D. M. (2012). Structural Identification for Performance Prediction Considering Uncertainties: Case Study of a Movable Bridge. *Journal of Structural Engineering*, *139*(10), 1703-1715.

Goulet, J. A., Kripakaran, P., & Smith, I. F. (2010). Multimodel structural performance monitoring. *Journal of Structural Engineering*, *136*(10), 1309-1318.

Govers, Y., & Link, M. (2010). Stochastic model updating—Covariance matrix adjustment from uncertain experimental modal data. *Mechanical Systems and Signal Processing*, *24*(3), 696-706.

Haralampidis, Y., Papadimitriou, C., & Pavlidou, M. (2005). Multi-objective framework for structural model identification. *Earthquake engineering & structural dynamics*, *34*(6), 665-685.

Jung, S., Ok, S. Y., & Song, J. (2010). Robust structural damage identification based on multi-objective optimization. *International Journal for Numerical Methods in Engineering*, *81*(6), 786-804.

Katafygiotis, L. S., Papadimitriou, C., & Lam, H. F. (1998). A probabilistic approach to structural model updating. *Soil Dynamics and Earthquake Engineering*, *17*(7), 495-507.

KCI (2010). *Guide Specification for Assessment of Concrete bridges*, Korea Concrete Institute, Seoul, Korea.

Kim, H. J., Kim, H. K., & Park, J. Y. (2013). Reliability-based evaluation of load carrying capacity for a composite box girder bridge. *KSCE Journal of Civil Engineering*, *17*(3), 575-583.

Kim, H. J., Park, W., Koh, H. M., & Choo, J. F. (2013). Identification of Structural Performance of a Steel-Box Girder Bridge Using Machine Learning Technique. In *IABSE Symposium Report*, 99(12), 1313-1320, International Association for Bridge and Structural Engineering.

Kim, H. J., Park, W., & Koh, H. M. (2014). Probabilistic Performance Assessment of Highway Bridges Using Operational Monitoring Data. In *IABSE Symposium Report*, International Association for Bridge and Structural Engineering.

Koh, H. M., Lee, H. S., Kim, S., & Choo, J. F. (2009). Monitoring of bridges in Korea. *Encyclopedia of Structural Health Monitoring*, Chapter 124, John Wiley and Sons, Inc., 2009.

Kripakaran, P., & Smith, I. F. (2009). Configuring and enhancing measurement systems for damage identification. *Advanced engineering informatics*, *23*(4), 424-432.

Kulicki, J. M., Prucz, Z., Clancy, C. M., Mertz, D. R., & Nowak, A. S. (2007). Updating the calibration report for AASHTO LRFD code. *Report of NCHRP Project*, 20-7.

Kurtz, N., & Song, J. (2013). Cross-entropy-based adaptive importance sampling using Gaussian mixture. *Structural Safety*, *42*, 35-44.

Lee, H. S., Kim, Y. H., Park, C. J., & Park, H. W. (1999). A new spatial regularization scheme for the identification of the geometric shape of an inclusion in a finite body. *International journal for numerical methods in engineering*, *46*(7), 973-992.

Mares, C., Mottershead, J. E., & Friswell, M. I. (2006). Stochastic model updating: part 1—theory and simulated example. *Mechanical Systems and Signal Processing*, *20*(7), 1674-1695.

MLTM (2012). *Highway Bridge Design Code*, Korea Ministry of Land, Transportation and Maritime Affairs, Seoul, Korea.

Moens, D., & Vandepitte, D. (2005). A survey of non-probabilistic uncertainty treatment in finite element analysis. *Computer methods in applied mechanics and engineering*, *194*(12), 1527-1555.

Moon, F. L., & Aktan, A. E. (2006). Impacts of epistemic (bias) uncertainty on structural identification of constructed (civil) systems. *Shock and Vibration Digest*, *38*(5), 399-422.

Moses, F. (2001). *Calibration of load factors for LRFR bridge evaluation* (No. Project C12-46 FY'97).

Mottershead, J. E., Mares, C., James, S., & Friswell, M. I. (2006). Stochastic model updating: part 2—application to a set of physical structures. *Mechanical Systems and Signal Processing*, *20*(8), 2171-2185.

Mottershead, J. E., Link, M., & Friswell, M. I. (2011). The sensitivity method in finite element model updating: a tutorial. *Mechanical systems and signal processing*, *25*(7), 2275-2296.

Mottershead, J. E. & Friswell, M. I. (1995). *Finite Element Model Updating in Structural Dynamics*, Kluwer Academic Publishers, Norwell.

Mukhopadhyay, S., Luş, H., & Betti, R. (2014). Modal parameter based structural identification using input–output data: Minimal instrumentation and global identifiability issues. *Mechanical Systems and Signal Processing*, *45*(2), 283-301.

Neuman, S. P., Fogg, G. E., & Jacobson, E. A. (1980). A statistical approach to the inverse problem of aquifer hydrology: 2. Case study. *Water Resources Research*, *16*(1), 33-58.

Park, I., Amarchinta, H. K., & Grandhi, R. V. (2010). A Bayesian approach for quantification of model uncertainty. *Reliability Engineering & System Safety*,*95*(7), 777-785.

Park, W., Kim, H. K., & Jongchil, P. (2012). Finite element model updating for a cable-stayed bridge using manual tuning and sensitivity-based optimization. *Structural Engineering International*, *22*(1), 14-19.

Raphael, B., & Smith, I. (1998). Finding the right model for bridge diagnosis. *Artificial intelligence in structural engineering,* 308-319.

Robert-Nicoud, Y., Raphael, B., & Smith, I. F. C. (2000). Decision support through multiple models and probabilistic search. *Proceedings of Construction Information Technology*, 765-779.

Robert-Nicoud, Y., Raphael, B., & Smith, I. F. (2005). System identification through model composition and stochastic search. *Journal of computing in civil engineering*, *19*(3), 239-247.

Saitta, S., Raphael, B., & Smith, I. F. (2007). A bounded index for cluster validity. In *Machine Learning and Data Mining in Pattern Recognition,* 174-187.

Saitta, S., Kripakaran, P., Raphael, B., & Smith, I. F. (2008). Improving system identification using clustering. *Journal of Computing in Civil Engineering*, *22*(5), 292-302.

Schnur, D. S., & Zabaras, N. (1990). Finite element solution of two-dimensional inverse elastic problems using spatial smoothing. *International Journal for Numerical Methods in Engineering*, *30*(1), 57-75.

Schuëller, G. I., & Jensen, H. A. (2008). Computational methods in optimization considering uncertainties–an overview. *Computer Methods in Applied Mechanics and Engineering*, *198*(1), 2-13.

Smith, I. F., & Saitta, S. (2008). Improving knowledge of structural system behavior through multiple models. *Journal of structural engineering*, *134*(4), 553-561.

Soize, C., Capiez-Lernout, E., Durand, J. F., Fernandez, C., & Gagliardini, L. (2008). Probabilistic model identification of uncertainties in computational models for dynamical systems and experimental validation. *Computer Methods in Applied Mechanics and Engineering*, *198*(1), 150-163.

Soyoz, S., & Feng, M. Q. (2009). Long-Term Monitoring and Identification of Bridge Structural Parameters. *Computer-Aided Civil and Infrastructure Engineering*, *24*(2), 82-92.

Steenackers, G., & Guillaume, P. (2006). Finite element model updating taking into account the uncertainty on the modal parameters estimates. *Journal of Sound and vibration*, *296*(4), 919-934.

Tabsh, S. W., & Nowak, A. S. (1991). Reliability of highway girder bridges. *Journal of Structural Engineering*, *117*(8), 2372-2388.

Yeo, I., Shin, S., Lee, H. S., & Chang, S. P. (2000). Statistical damage assessment of framed structures from static responses. *Journal of Engineering Mechanics*, *126*(4), 414-421.

Zárate, B. A., & Caicedo, J. M. (2008). Finite element model updating: Multiple alternatives. *Engineering Structures*, *30*(12), 3724-3730.

초 록

이 논문에서는 다중 유한요소모델 업데이트를 통한 구조물의 확률론적 성능평가 방법을 제안한다. 계측 데이터의 불확실성을 반영한 모델 업데이트를 위해 다수의 계측 데이터 집합을 구성한다. 추출된 각각의 응답에 대해 독립적인 유한요소모델 업데이트 문제가 구성되며, 최적화 과정을 통해 업데이트된 유한요소 모델의 집합을 얻게 된다. 각각의 업데이트 된 유한요소 모델은 추출된 계측데이터에 대응되는 구조물의 상태를 나타내며, 전체 모델의 분포를 통해 계측데이터의 불확실성에 대응되는 구조물의 성능 변화를 추정할 수 있다. 또한, 업데이트된 다중 유한요소모델을 클러스터로 구분하고 확률 모형으로 표현하기 위해 기계학습 (machine learning) 기법을 사용하였다. 먼저 Principal Component Analysis (PCA) 기법을 적용하여 다중 유한요소 모델을 분포 특징이 가장 잘 드러나는 principal subspace로 선형변환시킨다. 이를 통해 계측 데이터의 불확실성과 구조변수의 변동성간의 상관관계를 분석할 수 있게 되며, 몇 개의 principal component를 이용하여 분포 특성을 효율적으로 나타낼 수 있게 된다. 다음으로, 변환된 다중 유한요소 모델에 대해 *K*-means 클러스터링 기법을 적용하여 몇 개의 그룹으로 구분한다. 또한 Gaussian mixture modeling 을 통해 업데이트된 유한요소모델의 분포가 갖는 확률적 특성을 추출한다. 이렇게 클러스터링 된 모델들과 그에 대응되는 확률 모델을 이용하여 구조물의 현재 상태에 대한 확률적인 정보를 얻게 된다. 제안된 방법을 강상자형 거더 교량인 연대교에 적용하여 검증하였다. 내하율의 통계적 분포 특성 및 교량의 파괴확률에 대한 신뢰도 지수를 계산하여 연대교의 구조적 성능에 대한 확률적인 정보를 도출하였다. 또한 클러스터링에 기반한 모델 선택 절차를 통해 계측데이터의 불확실성이 큰 경우에도 안정적으로 성능 평가를 할 수 있게 된다.

주요어: 구조성능평가, 모델 업데이트, 데이터불확실성, 클러스터링, 구조신뢰성평가

학 번: 2009-30227